NASA Technical Memorandum 74058

Transonic Static and Dynamic Stability Characteristics of a Finned Projectile Configuration

Richmond P. Boyden, Cuyler W. Brooks, Jr., and Edwin E. Davenport

APRIL 1978

NASA

LM156392E

M78-12885

NASA Technical Memorandum 74058

Transonic Static and Dynamic Stability Characteristics of a Finned Projectile Configuration

Richmond P. Boyden, Cuyler W. Brooks, Jr.,
and Edwin E. Davenport
Langley Research Center
Hampton, Virginia

SUMMARY

Static and dynamic stability tests have been made of a finned projectile configuration with aft-mounted fins arranged in a cruciform pattern. The tests were made at free-stream Mach numbers of 0.7, 0.9, 1.1, and 1.2 in the Langley 8-foot transonic pressure tunnel. Some of the parameters measured during the tests were lift, drag, pitching moment, pitch damping, and roll damping. Configurations tested include the basic configuration with (1) fins deployed, (2) fins deflected for control, and (3) fins removed to simulate the projectile with the fins folded within the body. The finned projectile was statically stable at low angles of attack, but the stability decreased and became neutral or slightly unstable as the angle of attack was increased. The model had positive damping in pitch for a free-stream Mach number of 0.7, but there were regions of negative damping at the other Mach numbers for the various model roll orientations. The finned projectile generally had positive damping in roll. Theoretical estimates showed a lack of agreement with experimental pitching-moment and normal-force derivatives for the fins-on configuration; however, good agreement was obtained for the roll damping case.

INTRODUCTION

In cooperation with the U.S. Navy, the NASA Langley Research Center has measured experimentally the static and dynamic stability characteristics of a finned projectile in the transonic speed range. The projectile was designed to be gun launched with the fins folded within the body. After the projectile is launched, the fins fold out and damp out the rolling motion which is imparted to the projectile by the helical grooves in the gun barrel. The fins are then used as control surfaces to correct the flight of the projectile as the projectile is guided toward the intended target.

Tests were made at free-stream Mach numbers of 0.7, 0.9, 1.1, and 1.2 to measure lift, drag, and pitching moment; tests for pitch damping and roll damping followed. Other parameters measured during the tests include the oscillatory longitudinal-stability parameter, the rolling moment due to roll displacement parameter, the normal force due to pitch rate parameter, and the normal force due to pitch displacement parameter. Configurations tested include the basic configuration with (1) fins deployed, (2) fins deflected for control, and (3) fins removed to simulate the projectile with the fins folded within the body. A full-scale model was used for these tests.

SYMBOLS

The aerodynamic parameters are referred to the body system of axes as shown in figure 1 except for the lift and drag coefficients which are referred to the stability axes. The axes originate at the assumed center of gravity which was

located 0.381 meter aft of the model nose. The reference length used to non-dimensionalize all of the aerodynamic parameters was the body diameter of 0.127 meter, and the reference area was the model base area of 0.01267 meter^2.

C_D drag coefficient, $\dfrac{\text{Drag force}}{q_\infty S}$

C_L lift coefficient, $\dfrac{\text{Lift force}}{q_\infty S}$

C_l rolling-moment coefficient, $\dfrac{\text{Rolling moment}}{q_\infty S l}$

C_{l_p} $= \dfrac{\partial C_l}{\partial \left(\dfrac{pl}{2V}\right)}$, per radian

$C_{l_{\dot p}}$ $= \dfrac{\partial C_l}{\partial \left(\dfrac{\dot p l^2}{4V^2}\right)}$, per radian

$C_{l_p} + C_{l_{\dot \beta}} \sin \alpha$ damping-in-roll parameter, per radian

C_{l_β} $= \dfrac{\partial C_l}{\partial \beta}$, per radian

$C_{l_{\dot \beta}}$ $= \dfrac{\partial C_l}{\partial \left(\dfrac{\dot \beta l}{2V}\right)}$, per radian

$C_{l_\beta} \sin \alpha - k^2 C_{l_{\dot p}}$ rolling moment due to roll displacement parameter, per radian

C_m pitching-moment coefficient, $\dfrac{\text{Pitching moment}}{q_\infty S l}$

C_{m_q} $= \dfrac{\partial C_m}{\partial \left(\dfrac{q l}{2V}\right)}$, per radian

$C_{m_{\dot q}}$ $= \dfrac{\partial C_m}{\partial \left(\dfrac{\dot q l^2}{4V^2}\right)}$, per radian

$C_{m_q} + C_{m_{\dot \alpha}}$ damping-in-pitch parameter, per radian

C_{m_α} $= \dfrac{\partial C_m}{\partial \alpha}$, per radian

$C_{m_{\dot\alpha}}$ $= \dfrac{\partial C_m}{\partial \left(\dfrac{\dot\alpha \ell}{2V}\right)}$, per radian

$C_{m_\alpha} - k^2 C_{m_{\dot q}}$ oscillatory longitudinal-stability parameter, per radian

C_N normal-force coefficient, $\dfrac{\text{Normal force}}{q_\infty S}$

C_{N_q} $= \dfrac{\partial C_N}{\partial \left(\dfrac{q \ell}{2V}\right)}$, per radian

$C_{N_{\dot q}}$ $= \dfrac{\partial C_N}{\partial \left(\dfrac{\dot q \ell^2}{4V^2}\right)}$, per radian

$C_{N_q} + C_{N_{\dot\alpha}}$ normal force due to pitch rate parameter, per radian

C_{N_α} $= \dfrac{\partial C_N}{\partial \alpha}$, per radian

$C_{N_{\dot\alpha}}$ $= \dfrac{\partial C_N}{\partial \left(\dfrac{\dot\alpha \ell}{2V}\right)}$, per radian

$C_{N_\alpha} - k^2 C_{N_{\dot q}}$ normal force due to pitch displacement parameter, per radian

C_n yawing-moment coefficient, $\dfrac{\text{Yawing moment}}{q_\infty S \ell}$

C_Y side-force coefficient, $\dfrac{\text{Side force}}{q_\infty S}$

f   frequency of oscillation, hertz

k   reduced frequency parameter, $\omega \ell /2V$ in pitch and roll, radians

ℓ reference length, body diameter, meters

M_∞ free-stream Mach number

p   angular velocity of model about X-axis, radians/second

q   angular velocity of model about Y-axis, radians/second

q_∞ free-stream dynamic pressure, pascals

3

R	Reynolds number, based on reference length ℓ

R   Reynolds number, based on reference length ℓ

S   reference area, body base area, meters^2

T   tunnel stagnation temperature, K

V   free-stream velocity, meters/second

X,Y,Z   body reference axes

α angle of attack, degrees or radians

β angle of sideslip, radians

δ_p deflection of pitch fins, positive when trailing edge is down for $\phi = 0^o$, degrees

δ_y deflection of yaw fins, positive when trailing edge is to left for $\phi = 0^o$, degrees

ϕ model roll angle, degrees

ω angular velocity, $2\pi f$, radians/second

     Dot over quantity indicates derivative with respect to time.

MODEL AND APPARATUS

     A drawing of the model used in the investigation and some details of the fin design are presented in figure 2. Although the model layout is similar in the plan and side views for a roll angle of 0°, the fin pair in the horizontal plane (pitch fins) is 1.78 cm farther rearward than the fin pair in the vertical plane (yaw fins). The body of the model was made of aluminum alloy and the fins were made of steel. A steel balance adapter was used to transfer the loads from the model to the internally mounted static and dynamic balances.

     Both the static and the dynamic tests were conducted in the Langley 8-foot transonic pressure tunnel. The operating characteristics of the wind tunnel are given in reference 1. A photograph of the model mounted in the tunnel for the forced-oscillation dynamic stability tests is presented in figure 3, and a description of the technique and the apparatus used for the small-amplitude forced-oscillation dynamic tests is presented in reference 2. The diameter of the sting used for the static stability tests was 3.49 cm in the vicinity of the model while the sting used for the dynamic stability tests was 5.59 cm in diameter.

TESTS

     The static force and moment tests were conducted to determine the lift, drag, and pitching-moment characteristics of the basic finned projectile as

well as the effectiveness of the fins when used as control devices. Both the static and dynamic tests were conducted over an angle-of-attack range from about -4° to 22°. For the static tests, the angles of attack have been corrected for the effects of balance and sting deflection occurring upstream of the accelerometer used to measure angle of attack. All drag measurements were corrected to a condition of free-stream static pressure acting on the base of the model.

The test conditions for both the static and dynamic tests were

Free-stream Mach number, M_∞	Free-stream dynamic pressure, q_∞, kPa	Free-stream velocity, V, m/sec	Stagnation temperature, T, K	Reynolds number, R
0.70	18.82	240	322	1.10×10^6
.90	25.52	300		1.24
1.10	30.20	355		1.31
1.20	31.64	380		1.32

The stagnation pressure was held constant at 76.13 kPa.

The small-amplitude forced-oscillation dynamic stability tests were made primarily to determine the damping in pitch $C_{m_q} + C_{m_{\dot\alpha}}$ and the damping in roll $C_{l_p} + C_{l_{\dot\beta}} \sin \alpha$. Other parameters determined during the course of the investigation include the oscillatory longitudinal stability $C_{m_\alpha} - k^2 C_{m_{\dot q}}$, the normal force due to pitch rate $C_{N_q} + C_{N_{\dot\alpha}}$, the normal force due to pitch displacement $C_{N_q} - k^2 C_{N_{\dot q}}$, and the rolling moment due to roll displacement $C_{l_\beta} \sin \alpha - k^2 C_{l_{\dot p}}$. The values of the nominal amplitude of the oscillation and of the range of the reduced frequency parameter were:

Oscillation axis	Amplitude of oscillation, deg	Reduced frequency parameter, k, rad
Pitch	1.0	0.0031 to 0.0121
Roll	2.5	0.0093 to 0.0151

No roughness was applied to the model to trip the boundary layer because the model was a full-scale replica and the test conditions were near full scale.

PRESENTATION OF RESULTS

The experimental results are presented for the various parameters by figure number as follows:

Parameters	Effect of -					
	Fins on and off at -	Model roll angle	Deflection of pitch fins at -	Deflection of yaw fins at -		Deflection of pitch and yaw fins at -
	$\phi = 0^{\circ}$		$\phi = 0^{\circ}$	$\phi = 0^{\circ}$	$\phi = 90^{\circ}$	$\phi = 45^{\circ}$
C_L, C_D, C_m	4	5	6	7	8	9
C_l, C_n, C_Y				10		
$C_{m_q} + C_{m_{\dot\alpha}}$, $C_{m_\alpha} - k^2 C_{m_{\dot q}}$ . . .	11	12	13			
$C_{N_q} + C_{N_{\dot\alpha}}$, $C_{N_\alpha} - k^2 C_{N_{\dot q}}$ . . .	14	15	16			
$C_{l_p} + C_{l_{\dot\beta}} \sin\alpha$, $C_{l_\beta}\sin\alpha - k^2 C_{l_{\dot p}}$		17	18	19		

RESULTS AND DISCUSSION

Static Tests

The results from the static force and moment tests of the finned projectile model are contained in figures 4 to 10. The effect of the fins on the static longitudinal characteristics of the model is shown in figure 4. The body with the fins on is seen to be statically stable over the low angle-of-attack range, but the stability decreases and becomes neutral or somewhat unstable as the angle of attack is increased. The body without the fins is slightly unstable for the reference center-of-gravity position.

Figure 5 shows the result of varying the model roll angle on the static longitudinal characteristics. Although the model layout is similar in the plan and side views for a roll angle of 0°, the fin pair in the horizontal plane (pitch fins) is 1.78 cm farther rearward than the fin pair in the vertical plane (yaw fins, see fig. 2). At a roll angle of 0° the rearmost pair of fins lies in the horizontal plane. The fin orientation for a roll angle of 45° is seen to be the most effective aerodynamically of the various roll angles tested because it results in the highest lift coefficients and provides static stability over the largest angle-of-attack range.

The effect of deflection of the pitch fins on the static longitudinal characteristics is shown in figure 6 for a roll angle of 0°. A pitch fin deflection of -10° (trailing edge up) is seen to trim the model in the range between 8° and 10° over the free-stream Mach number range of 0.7 to 1.2. For the Mach numbers of 0.7 and 0.9, deflection of the pitch fins becomes ineffective at angles of attack between 12° and 16° for a maximum deflection of -10°. For a Mach number of 1.1, the pitch fins begin to lose their effectiveness at an angle of attack of about 19° but at M_∞ = 1.2 the pitch fins are still effective at about 22°, the highest angle of attack tested.

The only effect on the static longitudinal characteristics of a deflection of the yaw fins for a model roll angle of 0° is a small increase in the drag coefficient as shown in figure 7.

As figure 8 shows, for a model roll angle of 90°, the deflection of the yaw fins for pitch control resulted in static longitudinal characteristics almost identical to those achieved by the deflection of the pitch fins for 0° model roll angle (see fig. 6). The small longitudinal separation of the two pairs of fins did not seem to cause any dissimilar aerodynamic interference between the fin pairs as a result of different roll angles.

Combined pitch and yaw fin deflection for a 45° model roll angle shown in figure 9 indicates that in this position the fins are more effective as pitch control devices than pitch fins alone at a 0° roll angle. The combined pitch and yaw fin deflection is also effective to higher angles of attack. Thus for the same amount of fin deflection, a higher trim angle of attack can be achieved at a roll angle of 45° when compared to a roll angle of 0°. (Compare figs. 6 and 9.)

The only static lateral characteristics presented for the finned projectile model are shown in figure 10. The effect of a 5° deflection of the yaw fins with the model at a roll angle of 0° indicates that there is a large amount of yawing moment available with very little resultant rolling moment.

Dynamic Tests

The test results for damping-in-pitch parameter $C_{m_q} + C_{m_{\dot{\alpha}}}$ and the oscillatory longitudinal-stability parameter $C_{m_\alpha} - k^2 C_{m_{\dot{q}}}$ are shown in figures 11 to 13 for the various configurations. A comparison for the fins on and off is contained in figure 11. This figure shows that the fins-on configuration has positive damping in pitch $\left(\text{negative values of } C_{m_q} + C_{m_{\dot{\alpha}}}\right)$ for the subsonic free-stream Mach numbers. There are regions of negative damping for the Mach numbers of 1.1 and 1.2 above a 10° angle of attack for the fins-on configuration. The fins-off configuration had positive damping in pitch over the entire ranges of both angle of attack and Mach number. The oscillatory longitudinal stability is seen to decrease above an angle of attack of 4° for the fins-on configuration; and, except for M_∞ = 1.2, there were some regions of negative oscillatory longitudinal stability $\left(\text{positive values of } C_{m_\alpha} - k^2 C_{m_{\dot{q}}}\right)$. With the fins removed,

7

the body has negative oscillatory stability in pitch at all test conditions
except at the highest angle of attack for Mach numbers of 1.1 and 1.2.

The effect of the roll angle of the model on the damping in pitch is shown
in figure 12 for roll angles of 0°, 45°, and 90°. The results for the roll
angles of 0° and 90° generally appear to be similar except for some differences
at the higher angles of attack, and the trends for the 45° roll angle results
with the fins oriented in an "X" configuration tend to be different from the
other two roll angles. For example, for a free-stream Mach number of 0.9 the
45° roll angle configuration had negative damping in pitch above a 16° angle of
attack, whereas the 0° and 90° configurations had positive damping in pitch
over the entire range of angle of attack. The increased effectiveness of the
fins for the roll angle of 45° is evident for angles of attack between 6° and
12° in the oscillatory longitudinal stability results shown in figure 12.

The effect of deflecting the pitch fins -5° (trailing edge up) is contained
in figure 13. For the Mach numbers of 0.7, 0.9, and to a lesser extent 1.1, the
data appear as though they had been shifted 4° to 5° in angle of attack as a
result of the pitch fin deflection of -5°. The effect is noticeable in both the
pitch damping and the oscillatory longitudinal-stability results.

Presented in figures 14 to 16 are the results for the normal force due to
pitch rate parameter $C_{N_q} + C_{N_{\dot\alpha}}$ and the normal force due to pitch displacement

parameter $C_{N_\alpha} - k^2 C_{N_q}$ for the same configurations shown in figures 11 and 13.

The basic finned body has positive values of the normal force due to pitch rate
over the entire range of angle of attack and free-stream Mach number. The body
with the fins removed had small positive and negative values for $C_{N_q} + C_{N_{\dot\alpha}}$.

The results for the different roll angles shown in figure 15 generally have the
same trends with angle of attack.

The results for the damping in roll parameter $C_{l_p} + C_{l_{\dot\beta}} \sin \alpha$ and for the

rolling moment due to roll displacement parameter $C_{l_\beta} \sin \alpha - k^2 C_{l_{\dot p}}$ are shown

in figures 17 to 19. Generally the damping in roll is larger for $\phi = 45^\circ$ than
for $\phi = 0^\circ$ up to an angle of attack between 8° and 10°; above this angle
range the 0° roll angle configuration had more roll damping. Negative damping
in roll $\left(\text{positive } C_{l_p} + C_{l_{\dot\beta}} \sin \alpha\right)$ occurred for the 45° roll angle at $M_\infty = 0.9$

at angles of attack near 12° to 15°. Figure 18 shows that the damping in roll
did not fall off as much for $\delta_p = -5^\circ$ as it did for $\delta_p = 0^\circ$ in the 6° to 12°
angle-of-attack range for Mach numbers of 0.7 and 0.9. This difference in roll
damping is a result of the lower effective angle of attack of the pitch fins.
In figure 19, a 5° deflection of the yaw fins resulted in slightly more roll
damping over most of the angle-of-attack range.

Theoretical Estimates Compared With Static and

Dynamic Experimental Results

A vortex-lattice computer program based on the work in reference 3 was used to make theoretical estimates of the subsonic aerodynamic stability derivatives for comparison with the experimentally determined derivatives. The computer program had been modified to include a provision for modeling a cylindrical fuselage with up to three lifting surfaces. The projectile body was modeled as an open-ended circular cylinder of the same length as the original projectile body. The results of the vortex-lattice program are based on the assumption of an attached flow condition and are therefore only valid in the linear range of the lift-curve slope.

Figure 20 contains a comparison of the vortex-lattice theoretical estimates with the static and dynamic experimental results for the fins-on configuration for roll angles of both 0° and 45°. The stability derivatives shown in figure 20 for the static data were determined from the slope at $\alpha = 0^\circ$ of a spline fit to the experimental data, and the stability parameters from the dynamic test are an average of the individual data points at $\alpha = 0^\circ$. Figure 20(a) is a comparison between the experimentally determined pitching-moment parameters and the theoretical estimates. In the top half of figure 20(a), the vortex-lattice C_{m_q} estimates are seen to overpredict the damping in pitch

parameter $C_{m_q} + C_{m_{\dot\alpha}}$ measured at subsonic speeds for both the 0° and 45° roll

angle configurations. In the bottom half of figure 20(a), the static and dynamic results for the longitudinal stability are seen to be in good agreement. However, the vortex-lattice results for C_{m_α} have a negative slope with free-

stream Mach number while the experimental results have essentially a zero slope with free-stream Mach number.

The comparison for the normal-force parameters is shown in figure 20(b) where the vortex-lattice estimates were larger than the experimental results for both the normal force due to pitch rate and the normal force due to pitch displacement. There was good agreement between the static test values of C_{N_α} and the dynamic test values of $C_{N_\alpha} - k^2 C_{n_{\dot q}}$.

The comparison of the theoretical estimates with the experimental results for the damping in roll is shown in figure 20(c), and good agreement is seen between the theoretical and experimental values. Since all of figure 20 is for $\alpha = 0^\circ$, the second term of the experimental damping-in-roll parameter $C_{l_p} + C_{l_{\dot\beta}} \sin \alpha$ should be zero.

The reason for the lack of agreement between the vortex-lattice estimates and the experimental results for the pitching-moment and normal-force derivatives is thought to be a result of the simplified modeling of the body for the computer program. The assumption of an open-ended cylindrical body could have affected the pitching-moment and normal-force estimates while still giving good agreement for the roll damping.

SUMMARY OF RESULTS

An investigation has been made to determine the static and dynamic stability characteristics of a full-scale model of a finned projectile configuration. These tests were made at angles of attack from -4° to 22° and at free-stream Mach numbers of 0.7, 0.9, 1.1, and 1.2. The results may be summarized as follows:

1. The finned projectile was statically stable at low angles of attack, but the stability decreased and became neutral or slightly unstable as the angle of attack was increased.

2. A roll angle of 45°, when compared to 0° or 90°, was the most effective aerodynamically because it resulted in the highest lift coefficients and provided static stability over the largest angle-of-attack range.

3. The finned projectile had positive damping in pitch for a free-stream Mach number of 0.7, but there were regions of negative damping at the other free-stream Mach numbers for the various model roll orientations.

4. The model generally had positive damping in roll except between 12° and 15° angle of attack for a roll angle of 45° and a free-stream Mach number of 0.9.

5. The theoretical estimates showed a lack of agreement with the experimental pitching-moment and normal-force derivatives for the fins-on configuration. However, good agreement was obtained for the roll damping case.

Langley Research Center
National Aeronautics and Space Administration
Hampton, VA 23665
March 6, 1978

REFERENCES

1. Schaefer, William T., Jr.: Characteristics of Major Active Wind Tunnels at the Langley Research Center. NASA TM X-1130, 1965.

2. Freeman, Delma C., Jr.; Boyden, Richmond P.; and Davenport, E. E.: Supersonic Dynamic Stability Characteristics of a Space Shuttle Orbiter. NASA TN D-8043, 1976.

3. Lamar, John E.; and Gloss, Blair B.: Subsonic Aerodynamic Characteristics of Interacting Lifting Surfaces With Separated Flow Around Sharp Edges Predicted by a Vortex-Lattice Method. NASA TN D-7921, 1975.
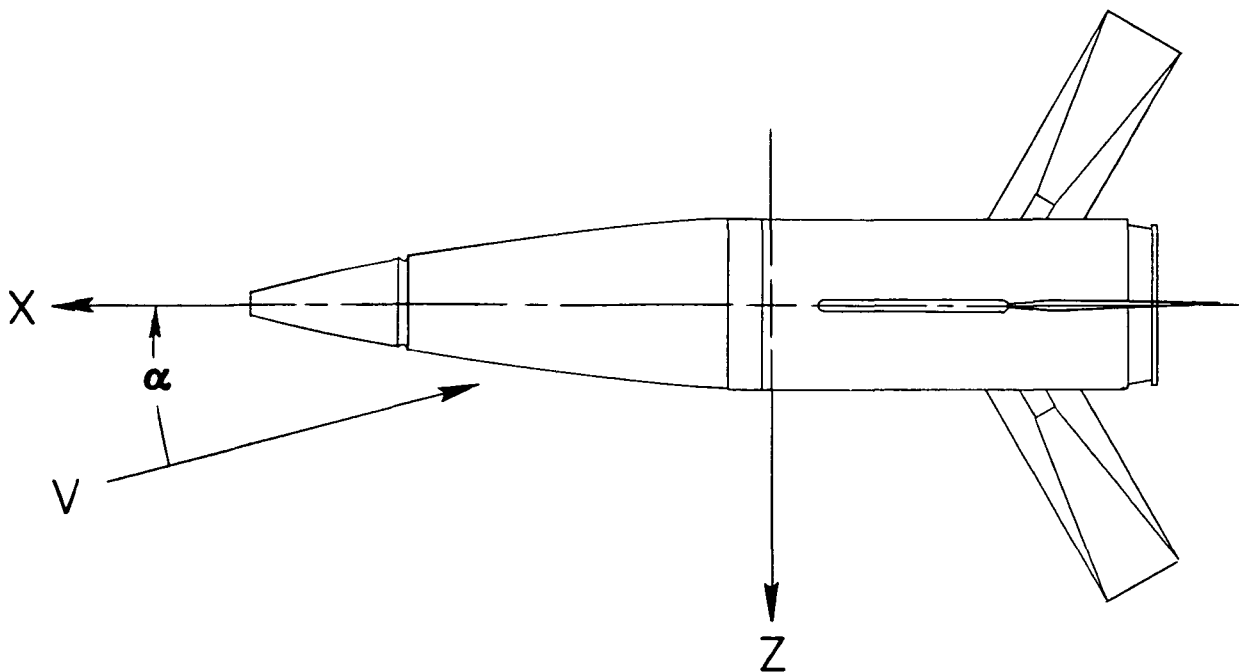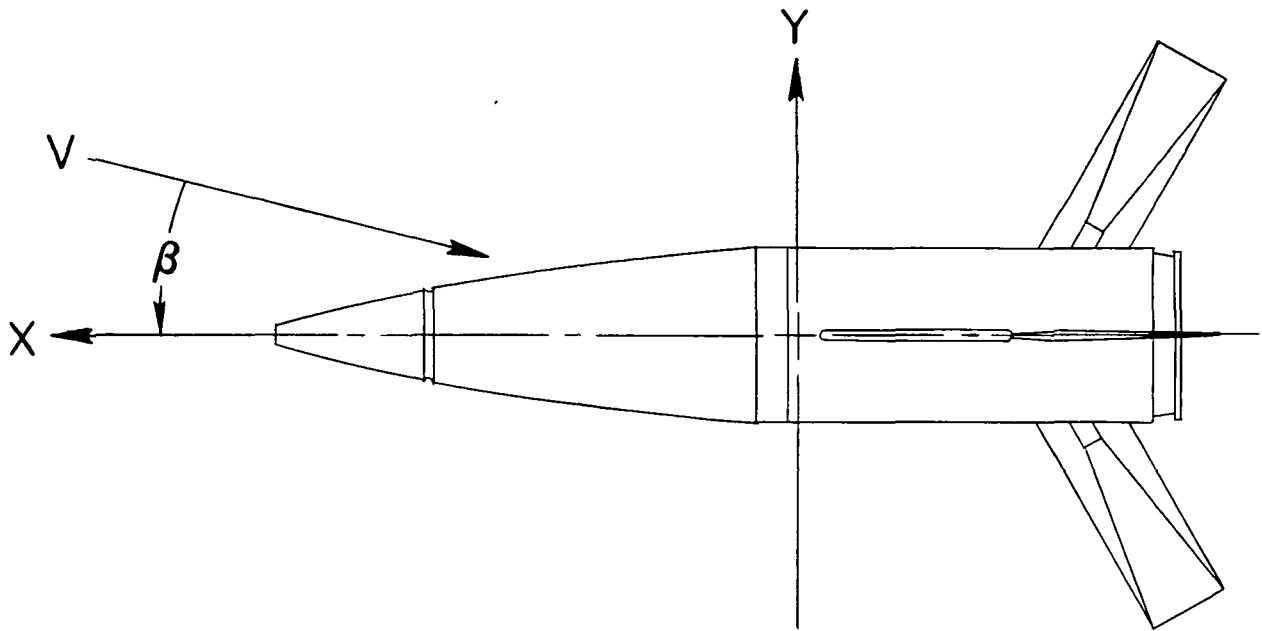
Figure 1.- Body system of axes used in investigation.
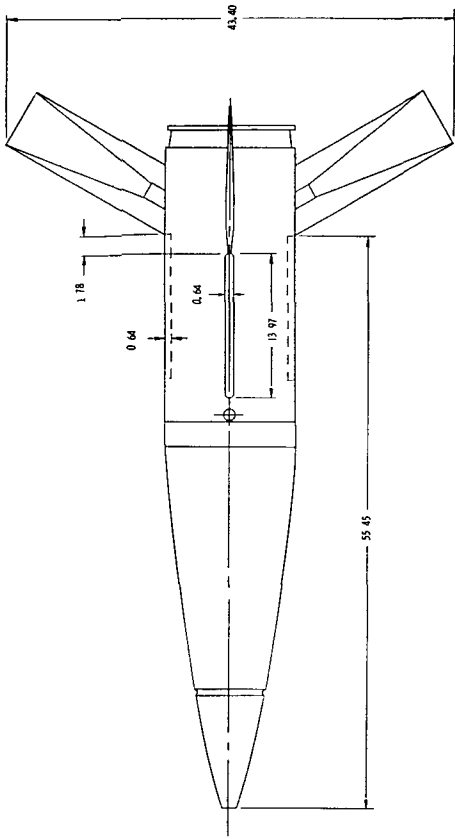
Plan view
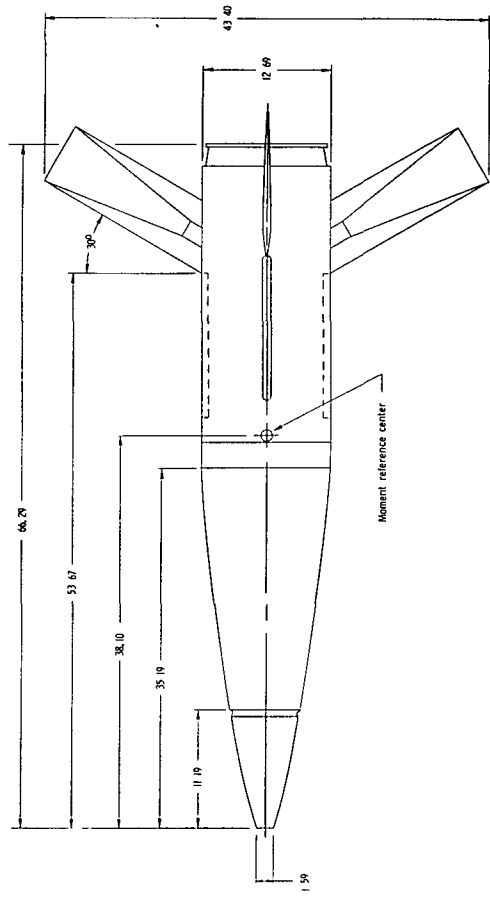
Side view

Front view

Moment reference center
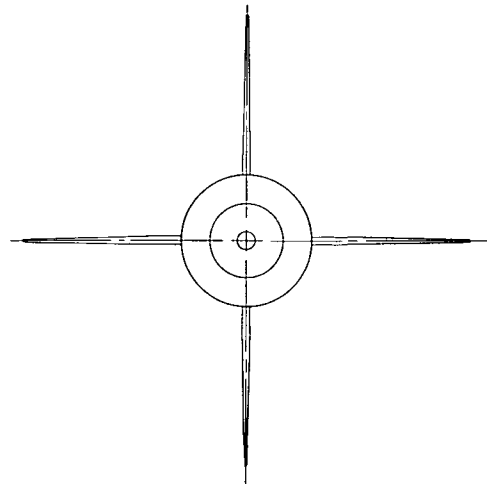
(a) Three-view drawing of complete model configuration.

Figure 2.- Details of model. All linear dimensions are in cm.
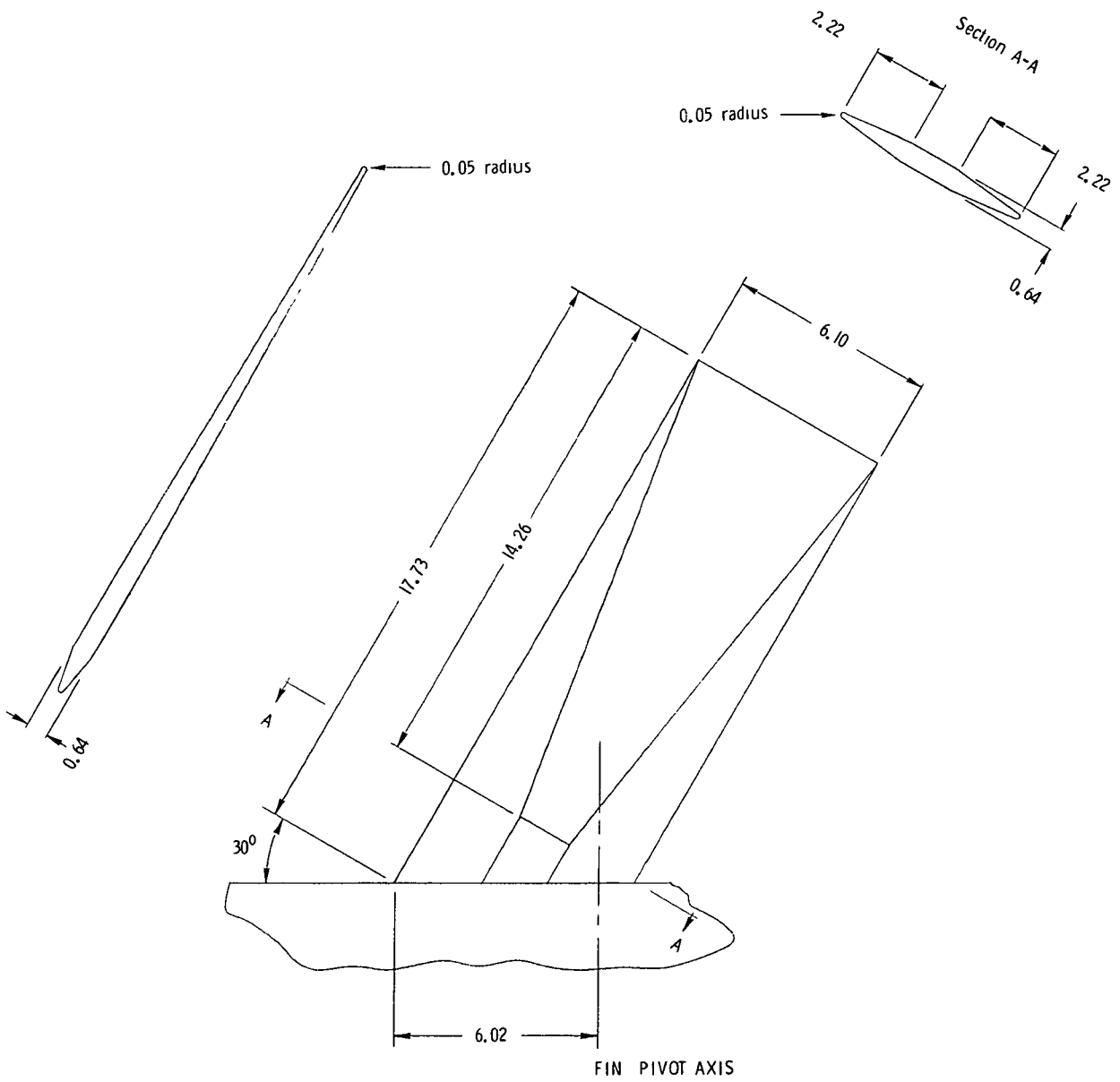
(b) Fin details.

Figure 2.- Concluded.
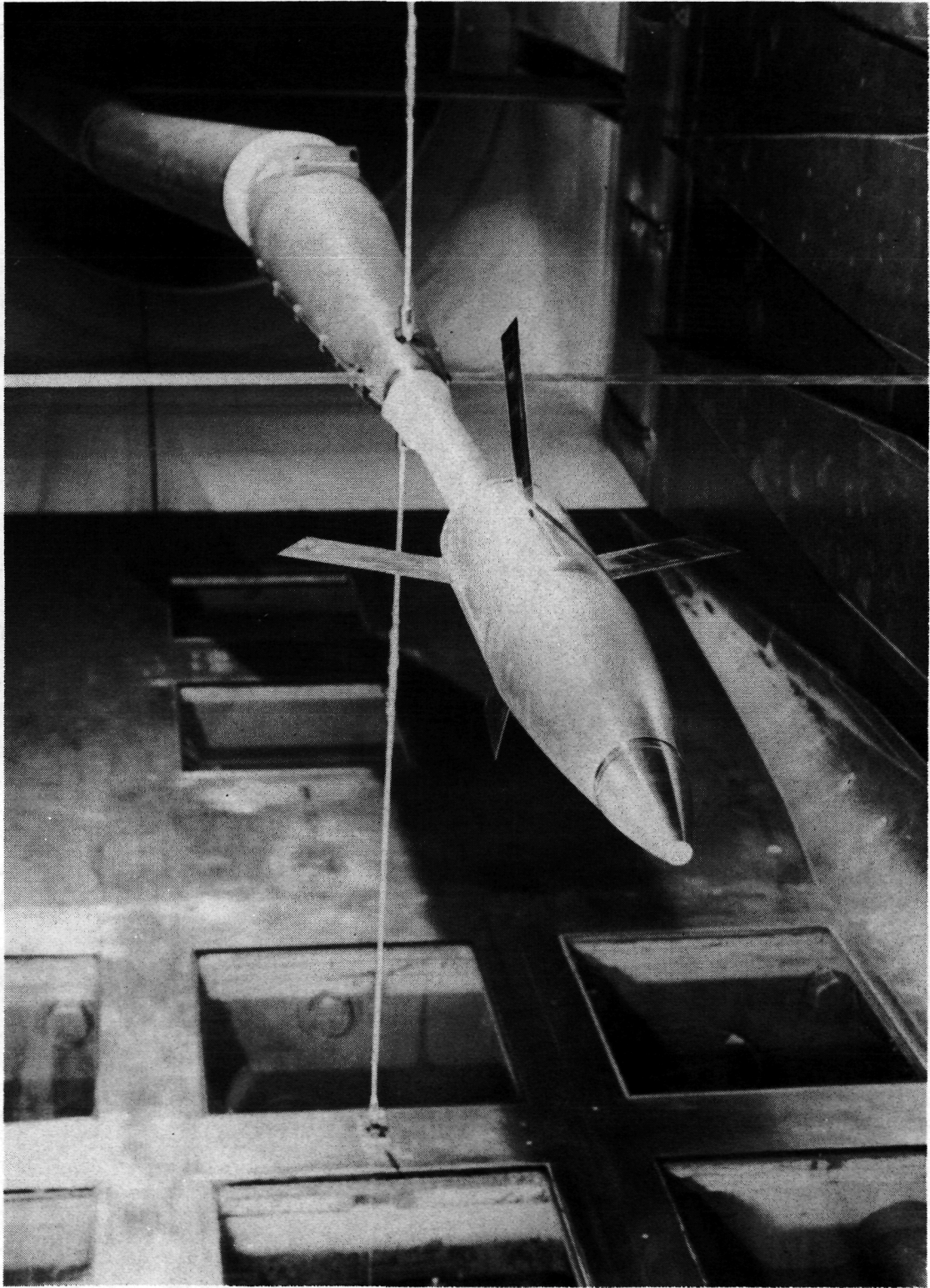
Figure 3.- Photograph of model in Langley 8-foot transonic pressure tunnel.

L-76-2235
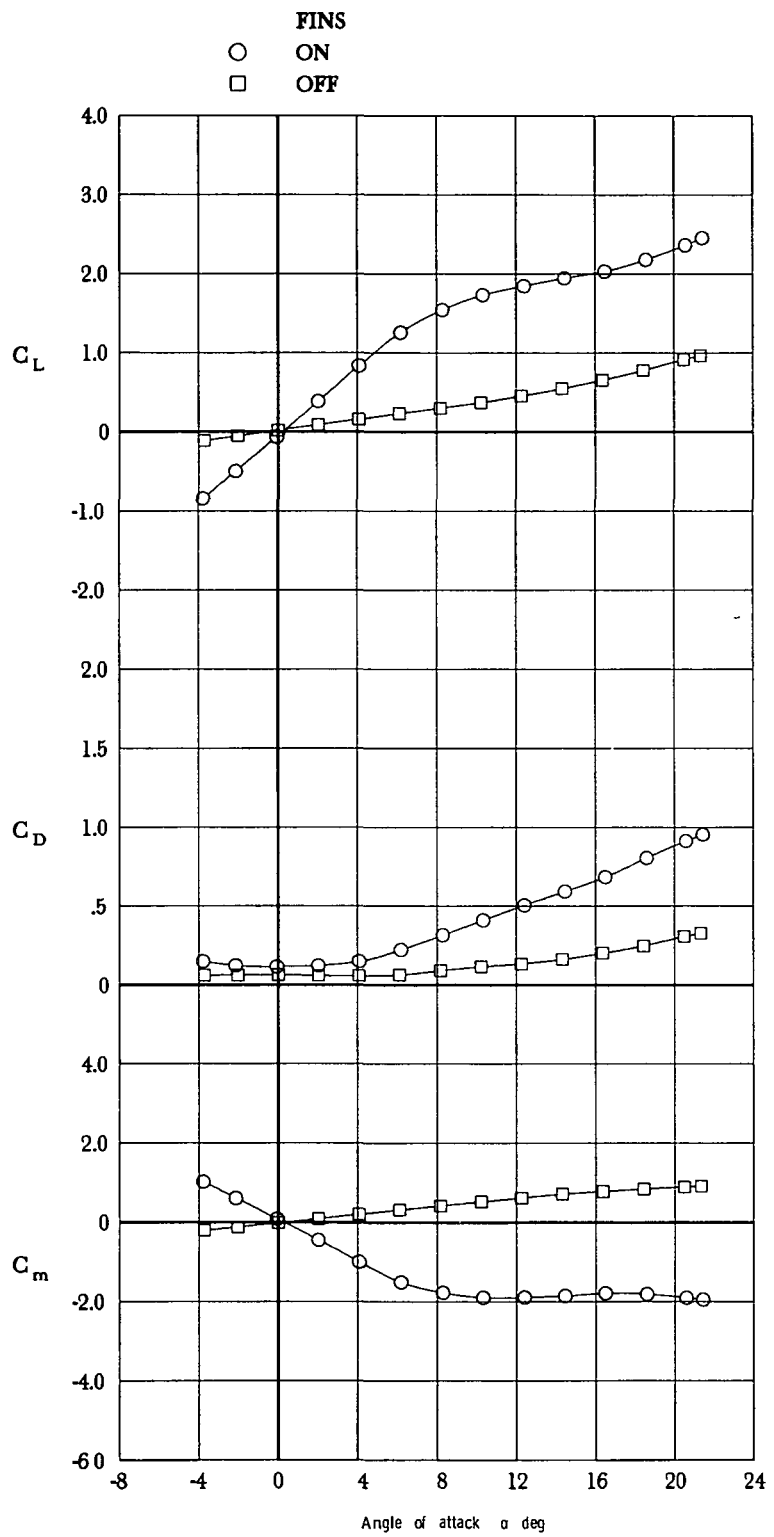
(a) $M_\infty = 0.7$.

Figure 4.- Effect of tail fins on static longitudinal characteristics.
$\phi = 0^\circ$; $\delta_p = 0^\circ$; $\delta_y = 0^\circ$.

FINS
O ON
□ OFF

C_L

C_D

C_m

Angle of attack α deg
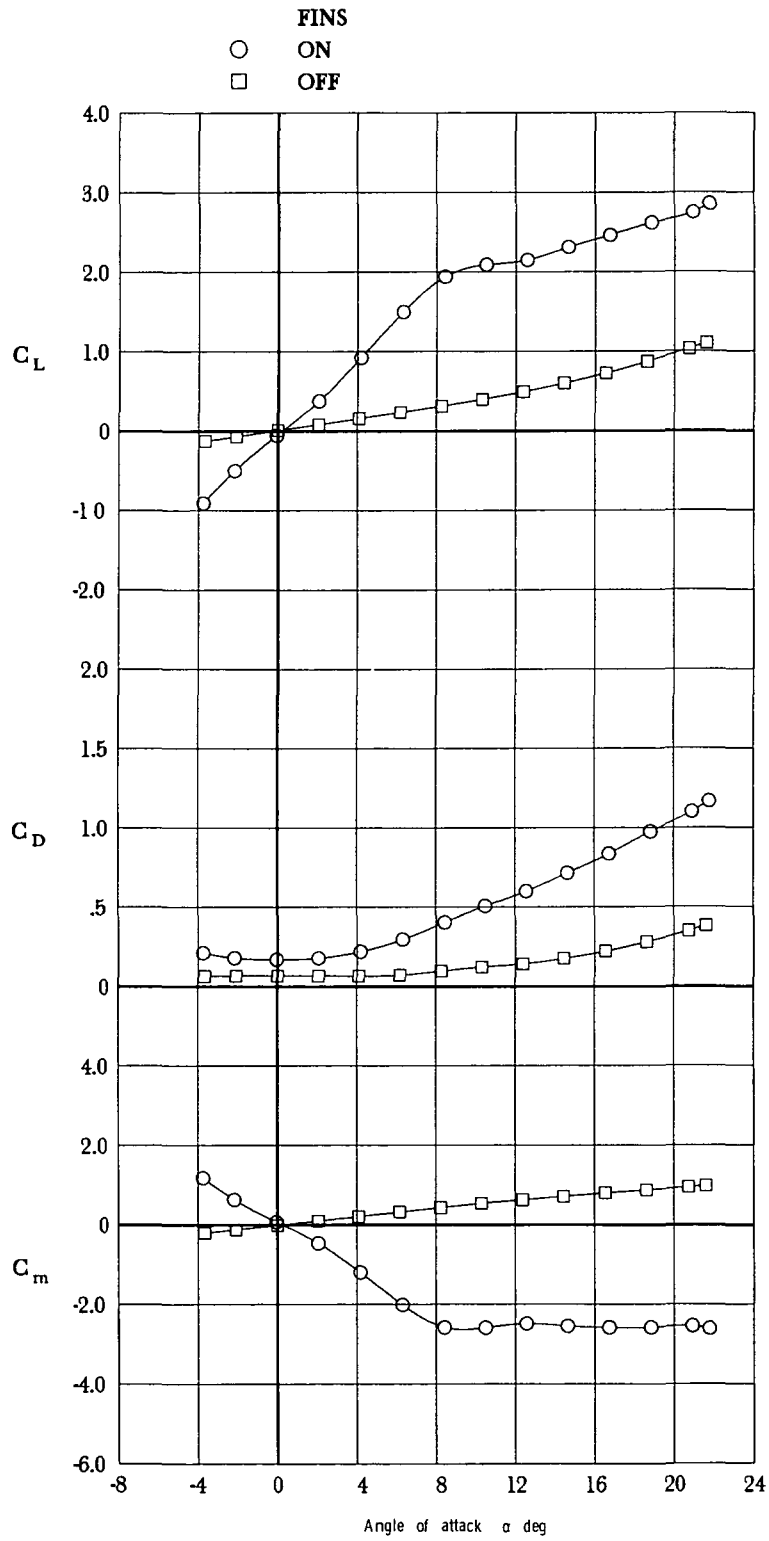
(b) $M_\infty = 0.9$.

Figure 4.- Continued.

16
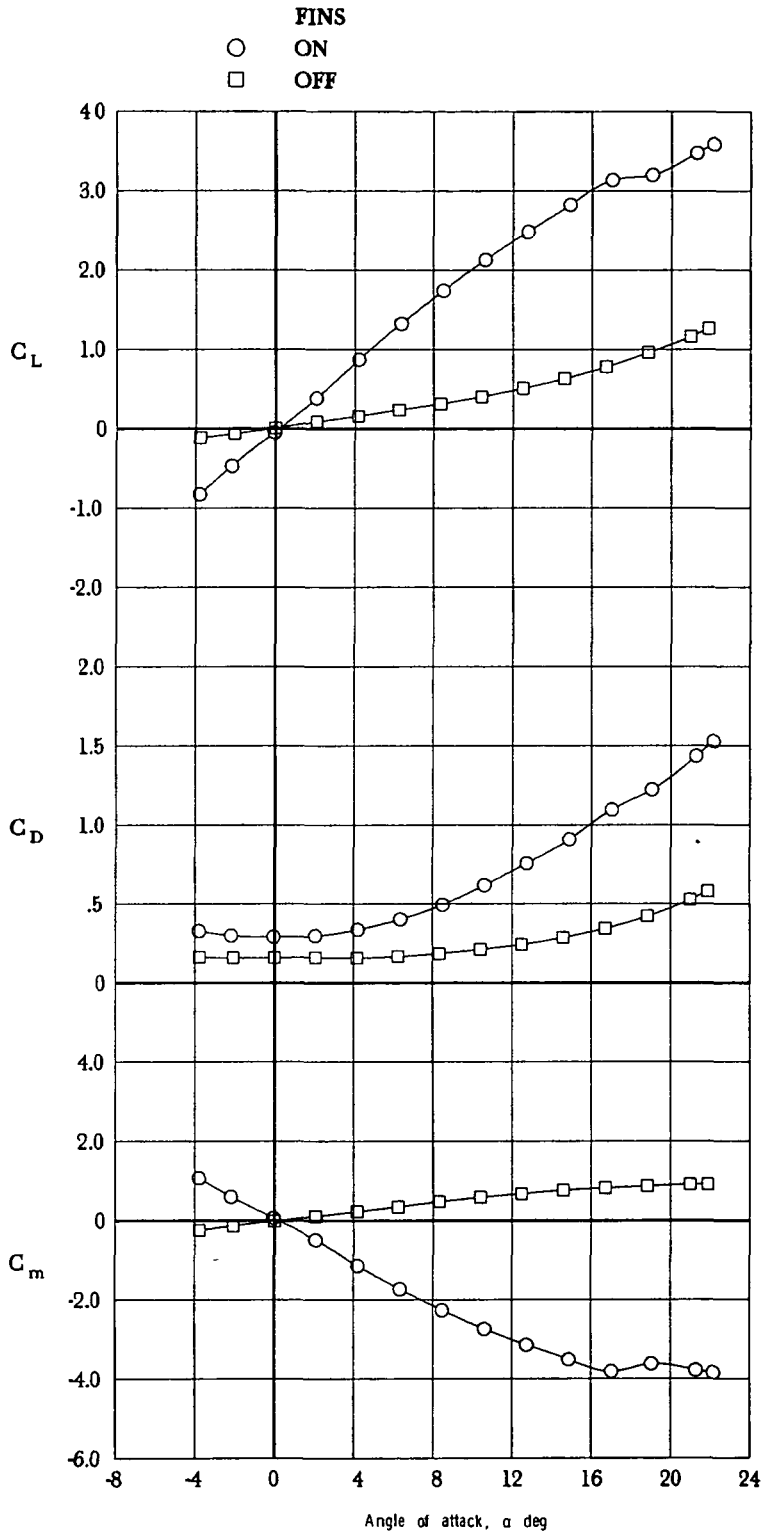
(c) M_∞ = 1.1.

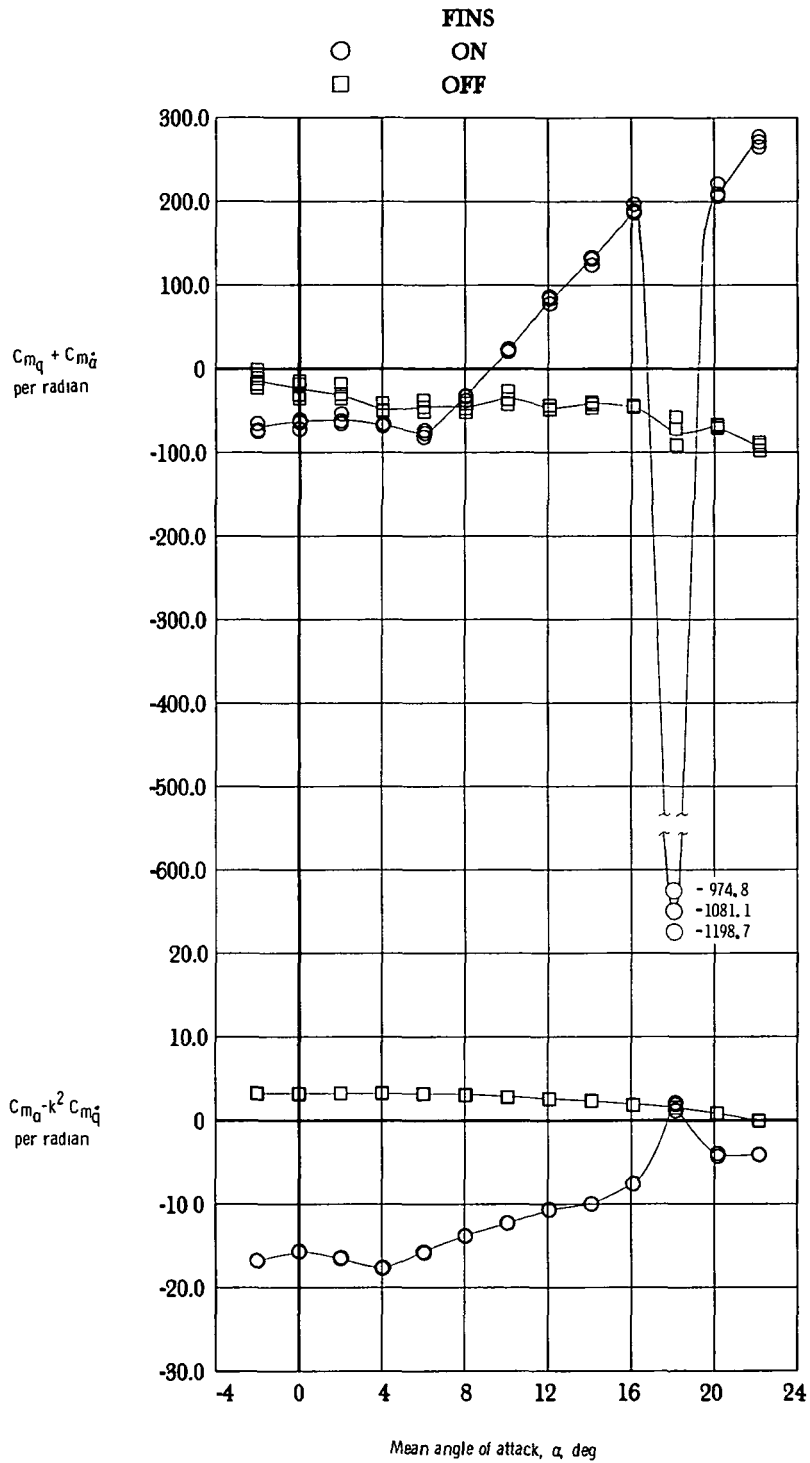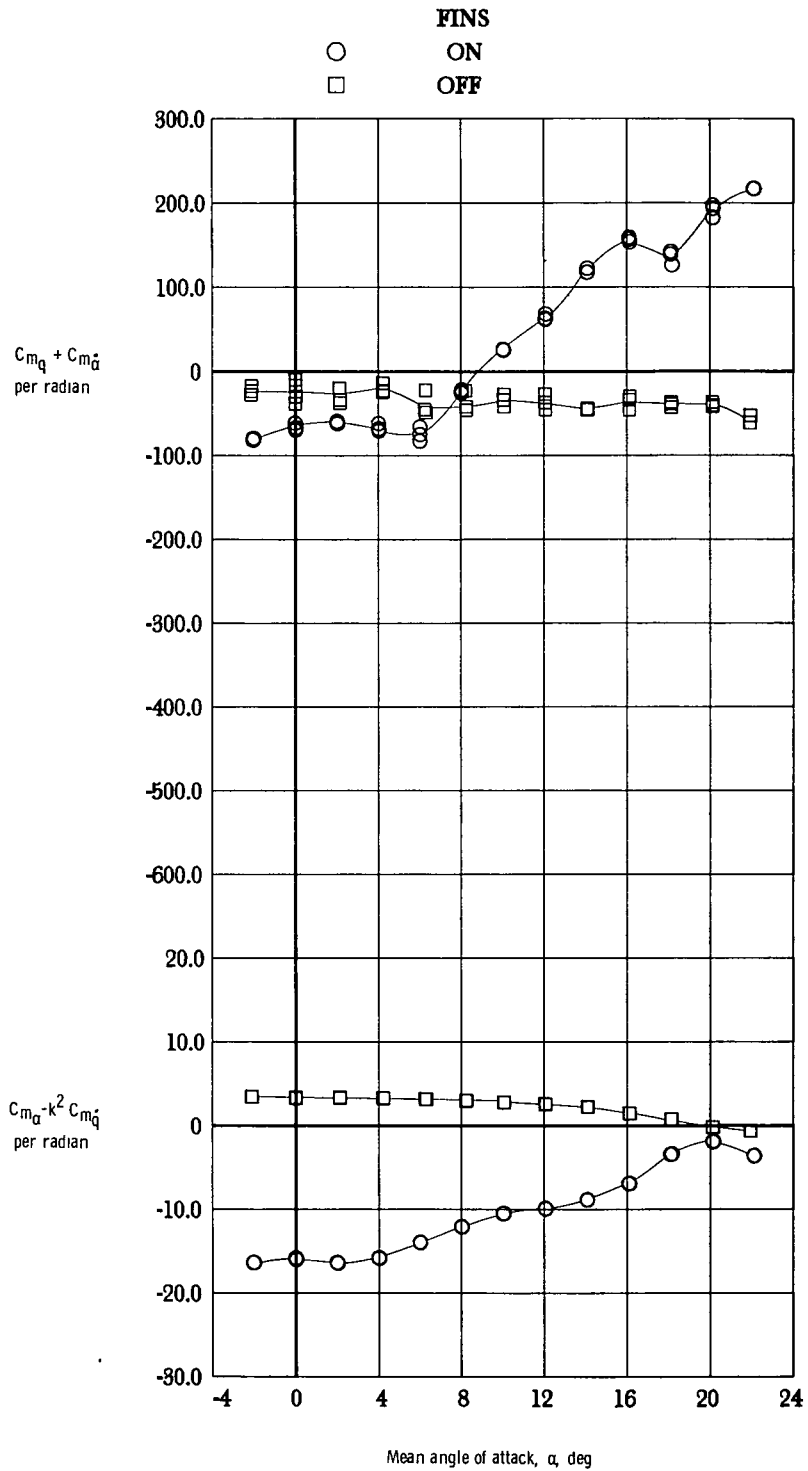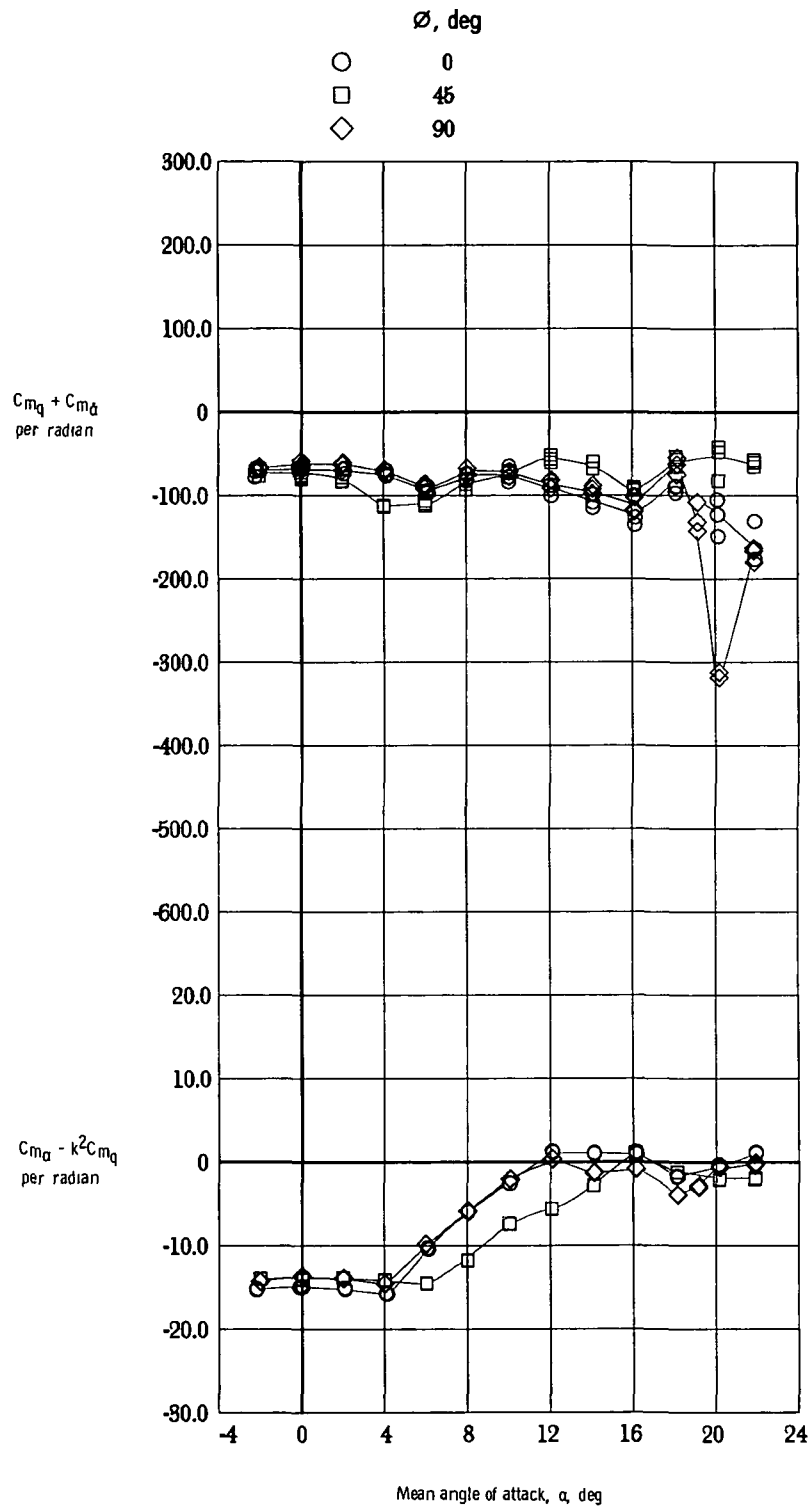Figure 4.- Continued.
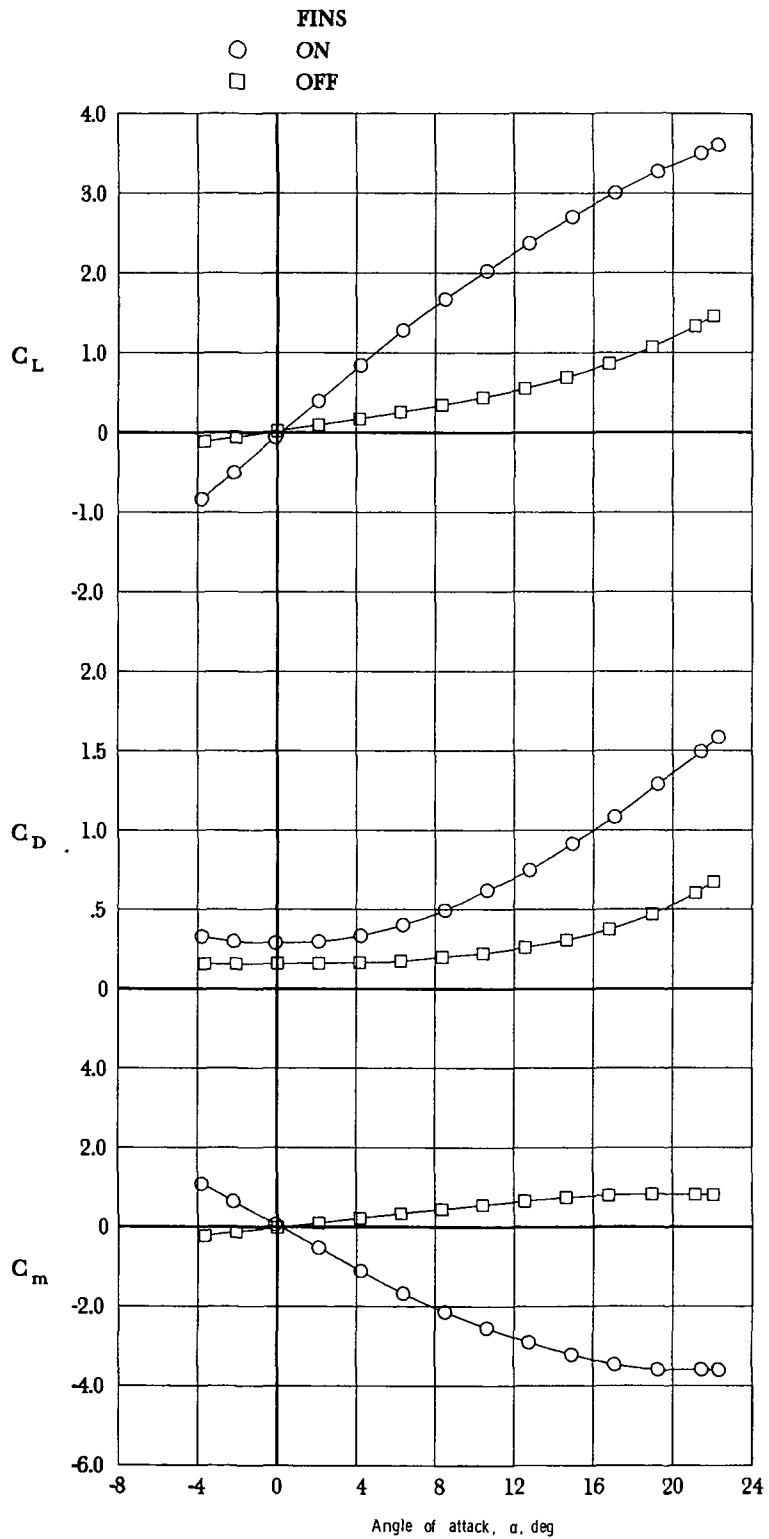
(d) $M_\infty = 1.2$.

Figure 4.- Concluded.
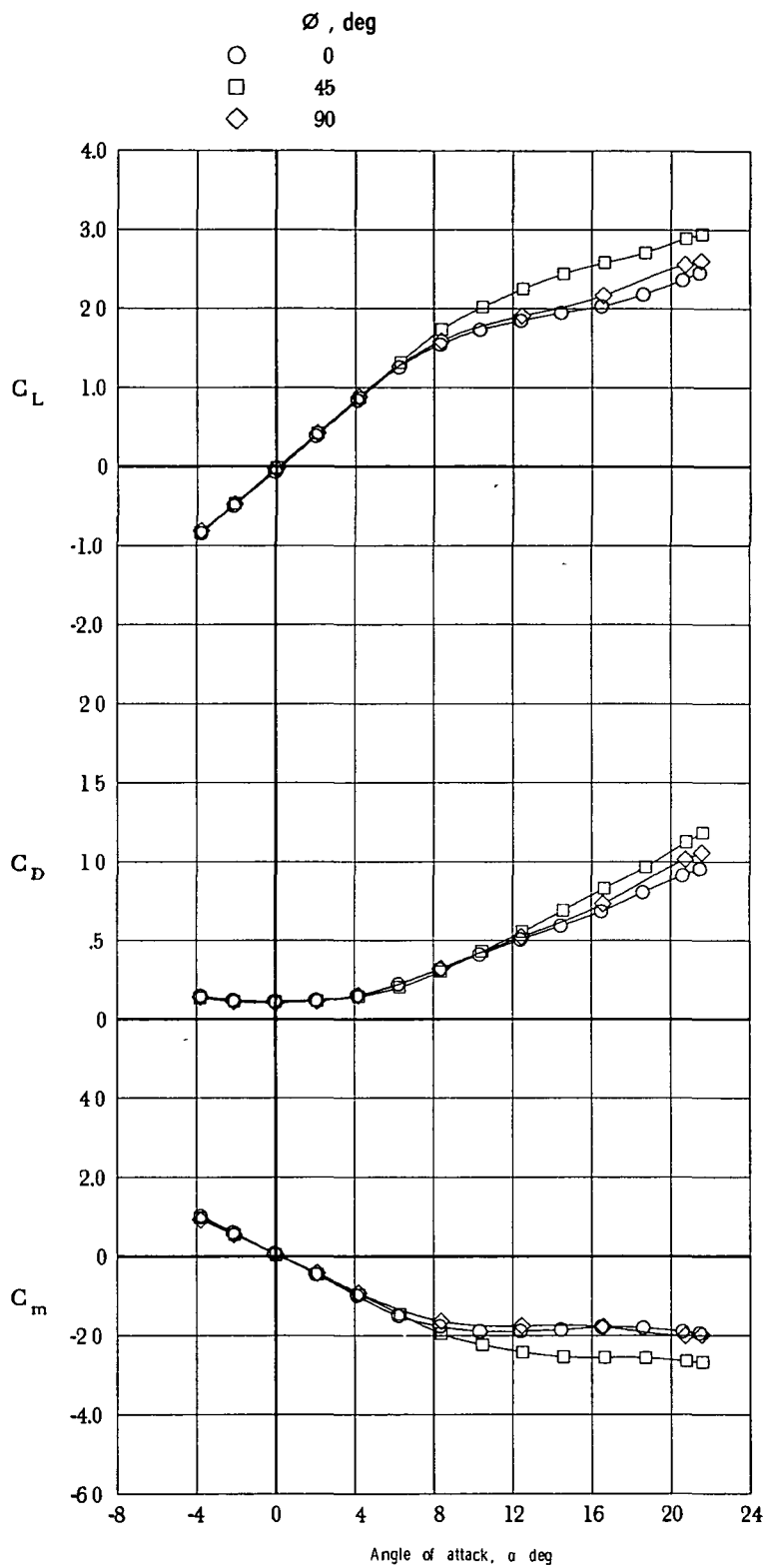
(a) $M_\infty = 0.7$.

Figure 5.- Effect of configuration roll angle on static longitudinal
characteristics. $\delta_p = 0^o$; $\delta_y = 0^o$.

19
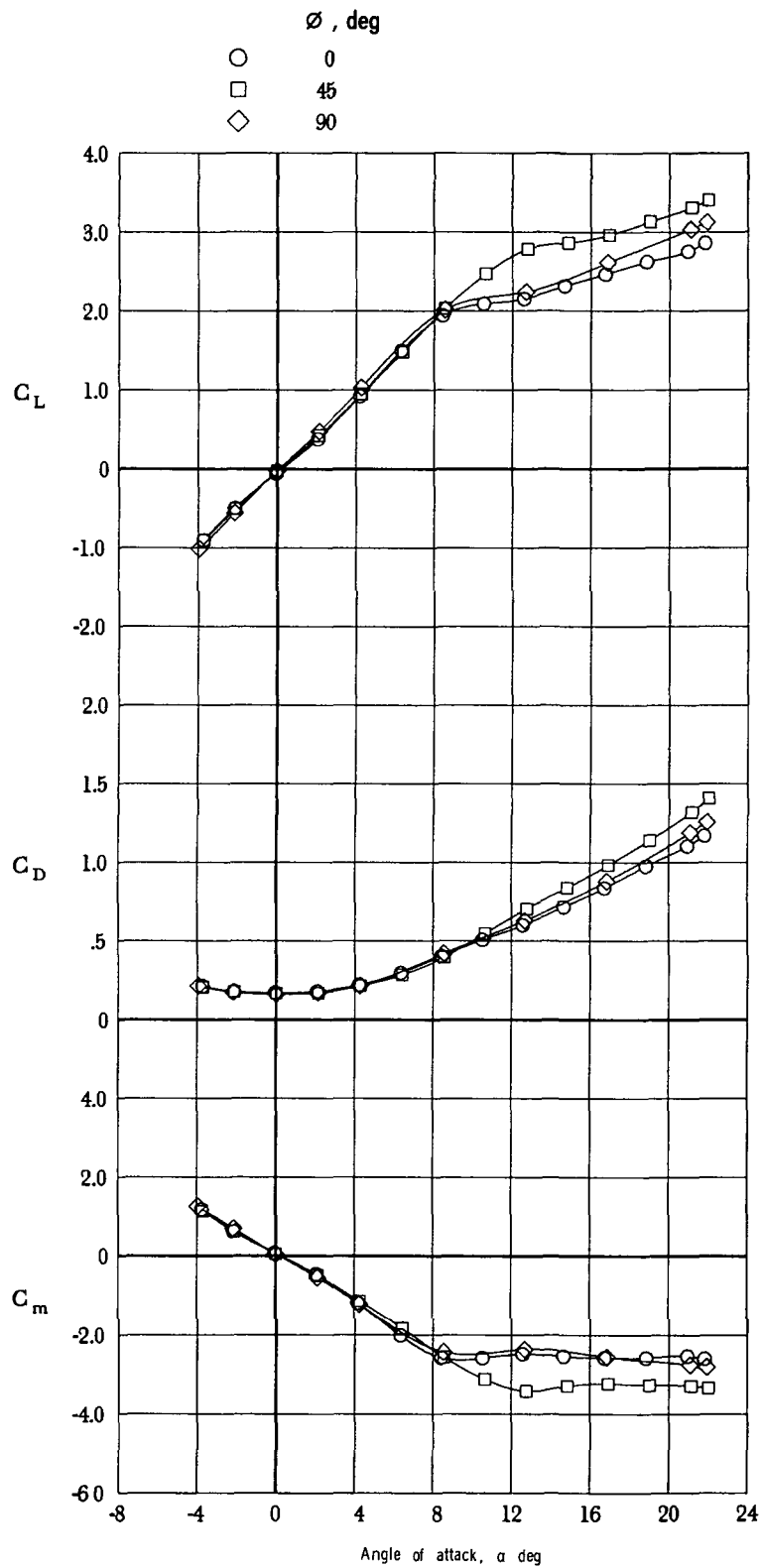
(b) $M_\infty = 0.9$.

Figure 5.- Continued.
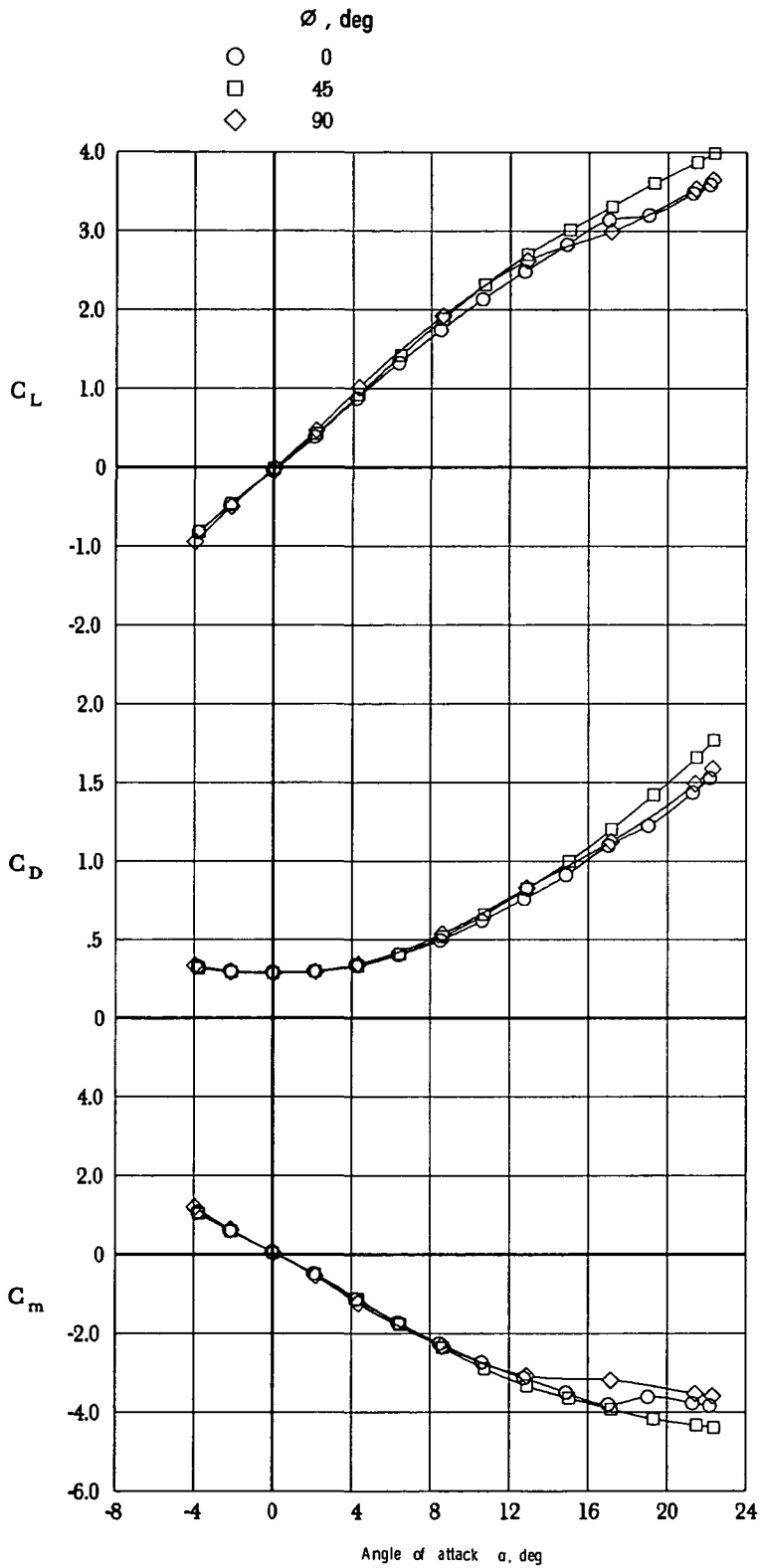
(c) $M_\infty = 1.1$.

Figure 5.- Continued.
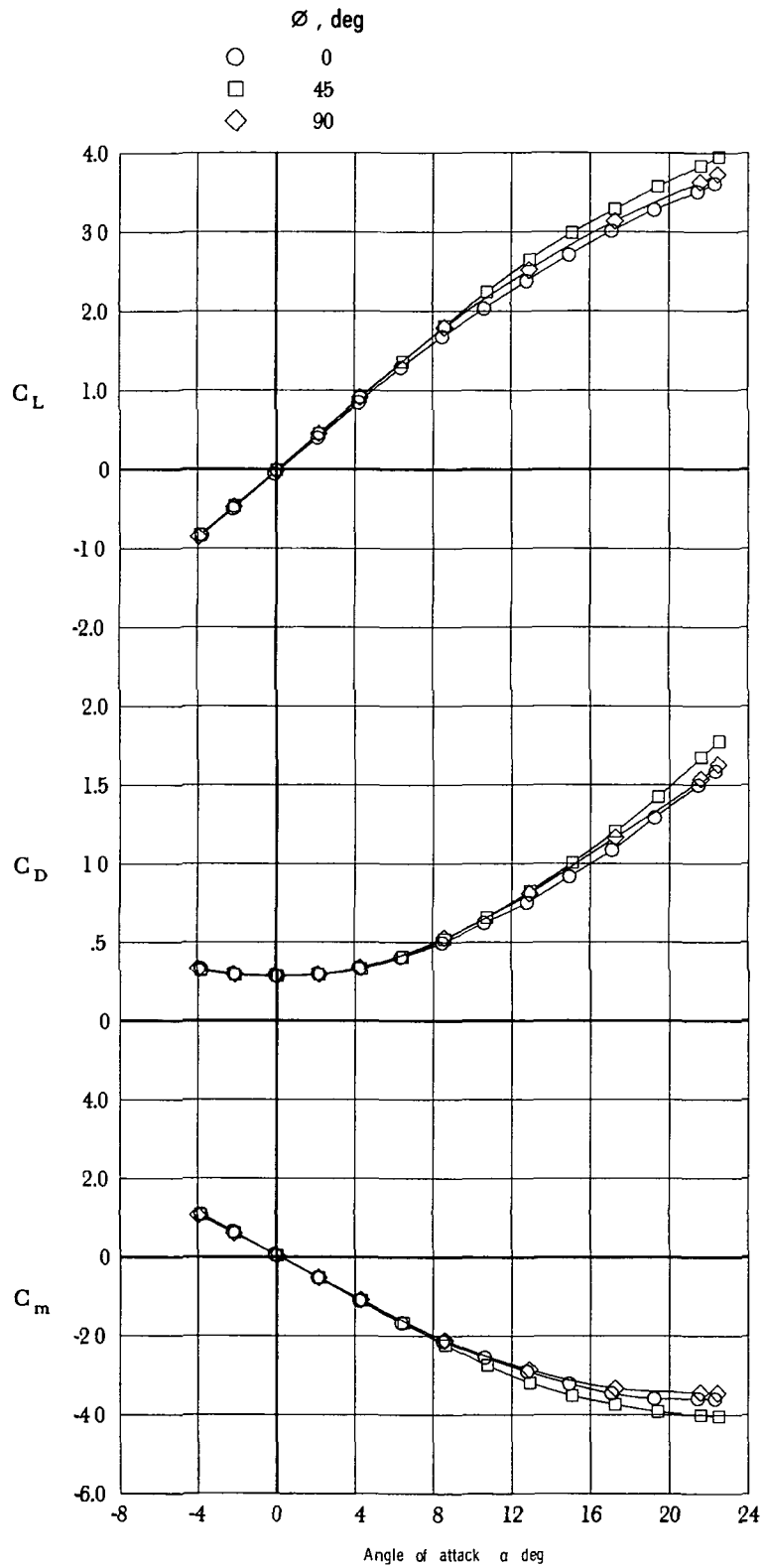
(d) $M_\infty = 1.2$.

Figure 5.- Concluded.
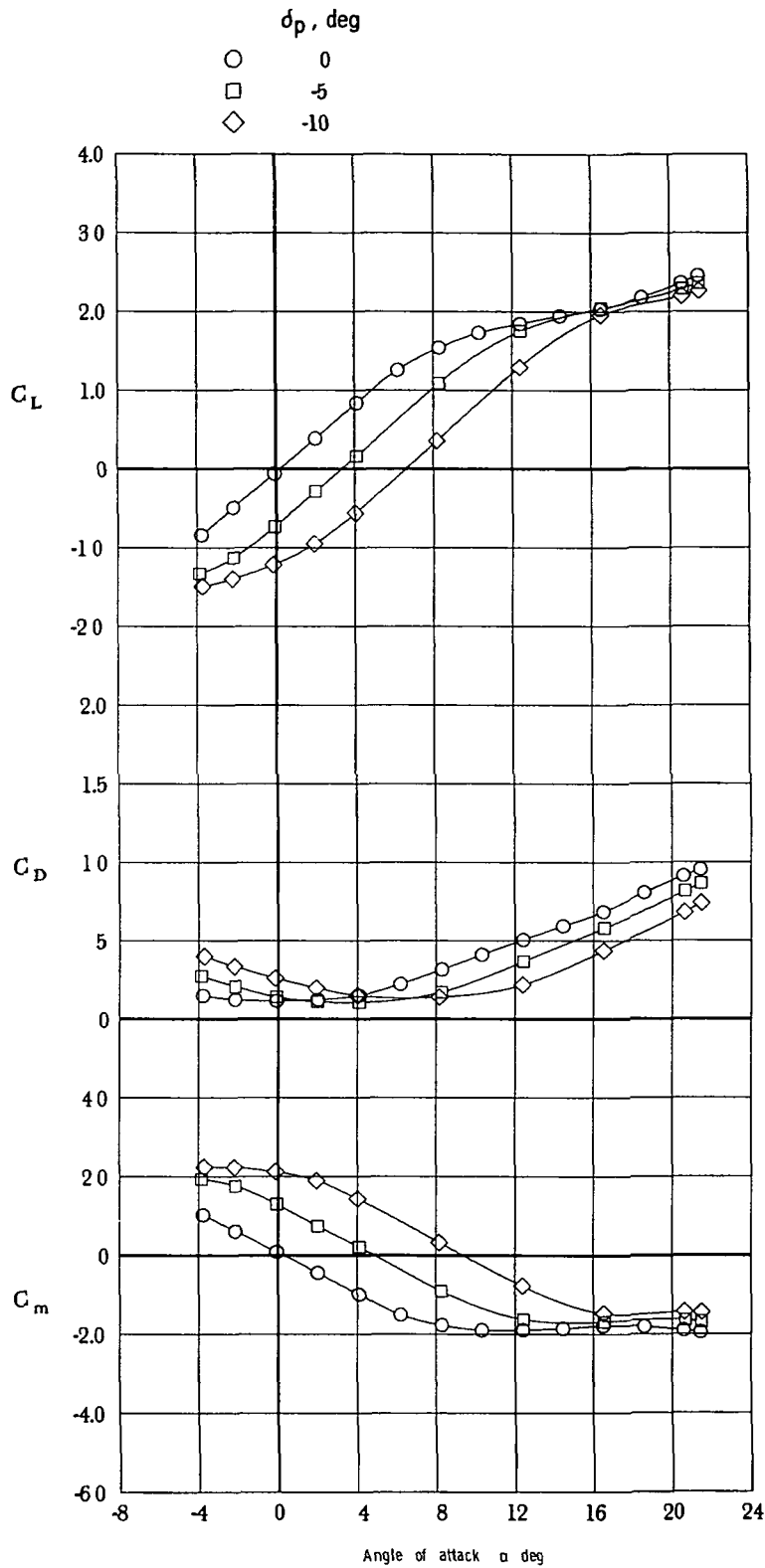
(a) $M_\infty = 0.7$.

Figure 6.- Effect of pitch fin deflection on static longitudinal
characteristics. $\phi = 0°$; $\delta_y = 0°$.
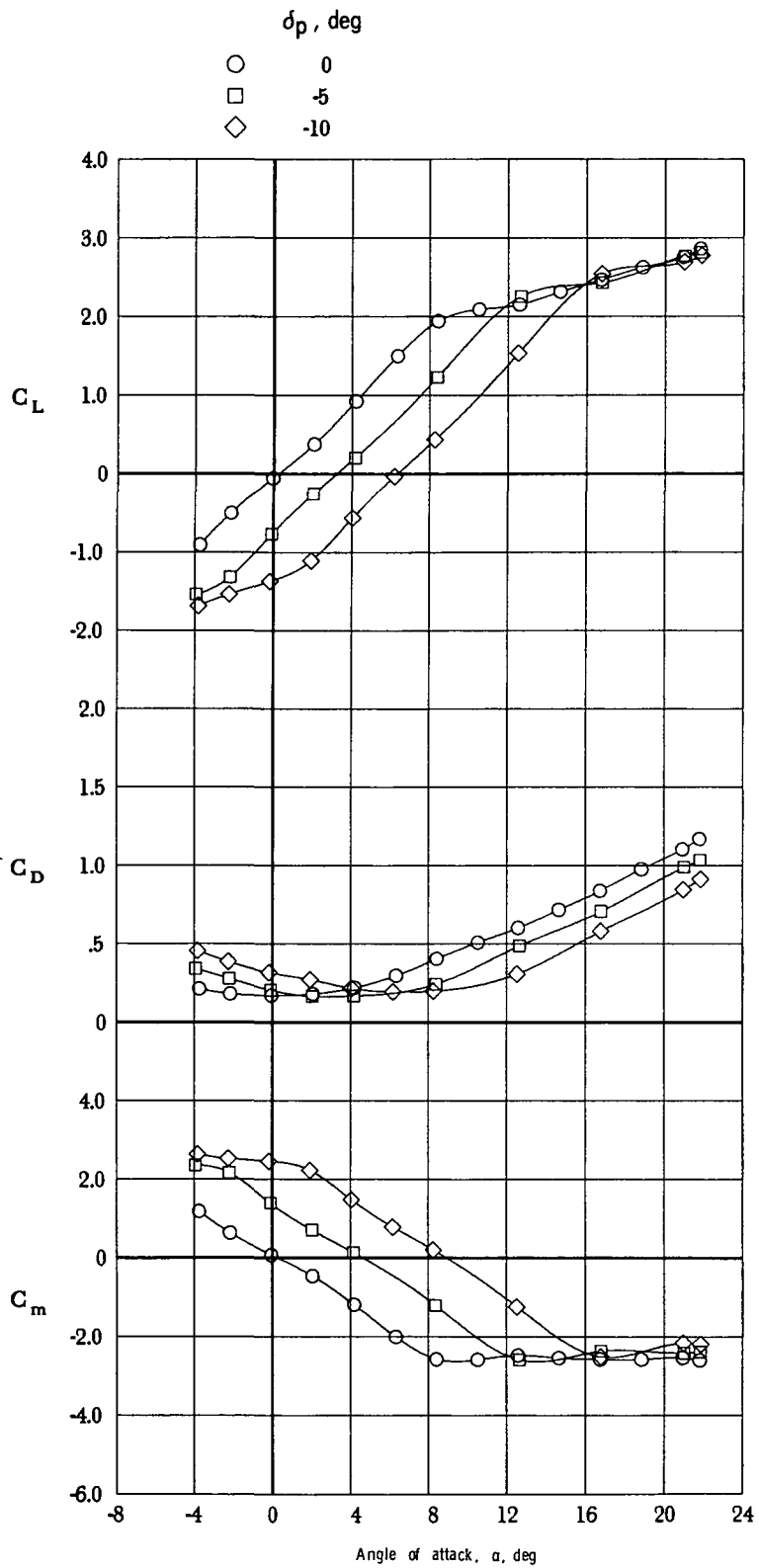
(b) $M_\infty = 0.9$.

Figure 6.- Continued.
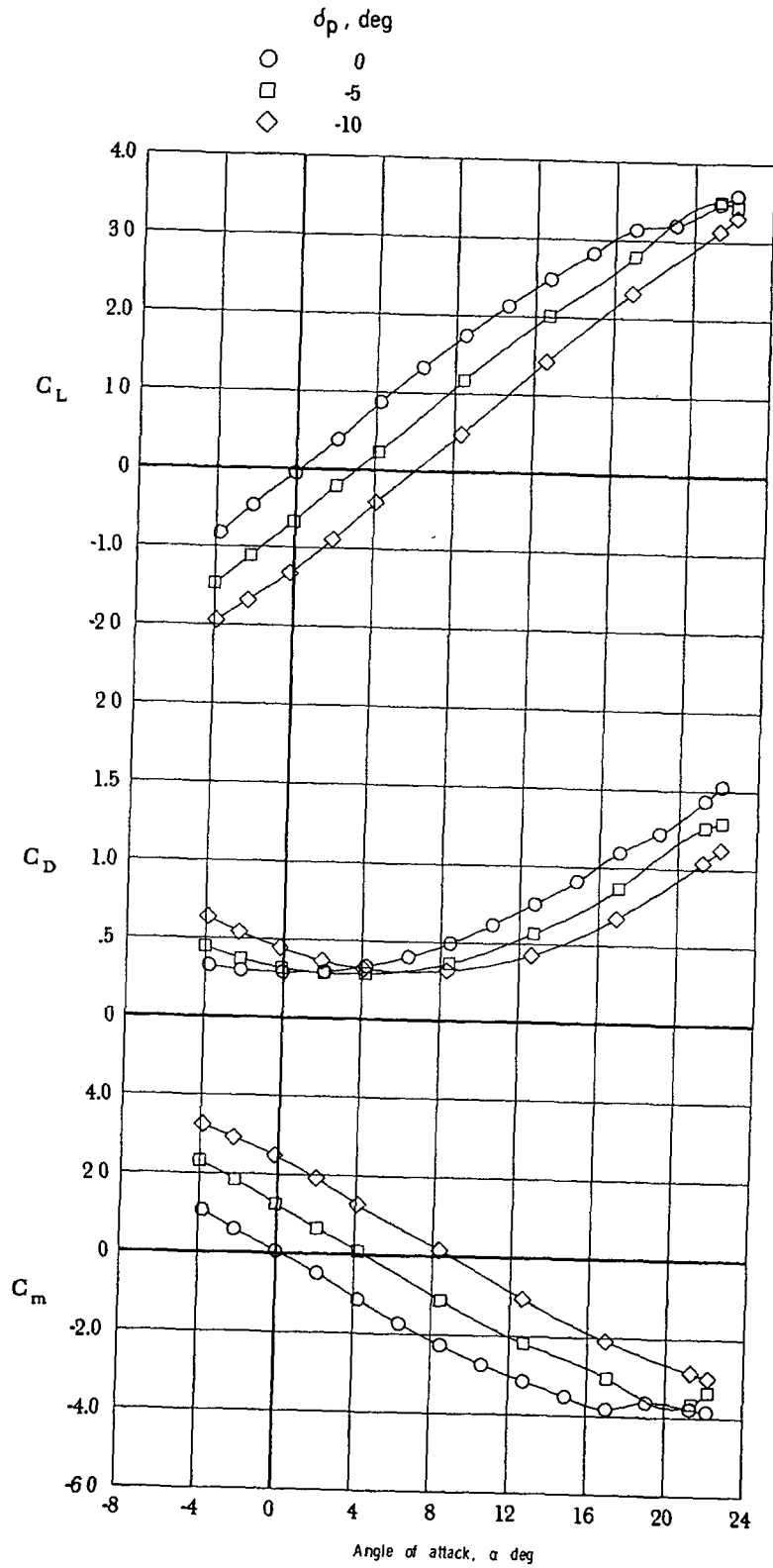
(c) $M_{\infty} = 1.1$.

Figure 6.- Continued.
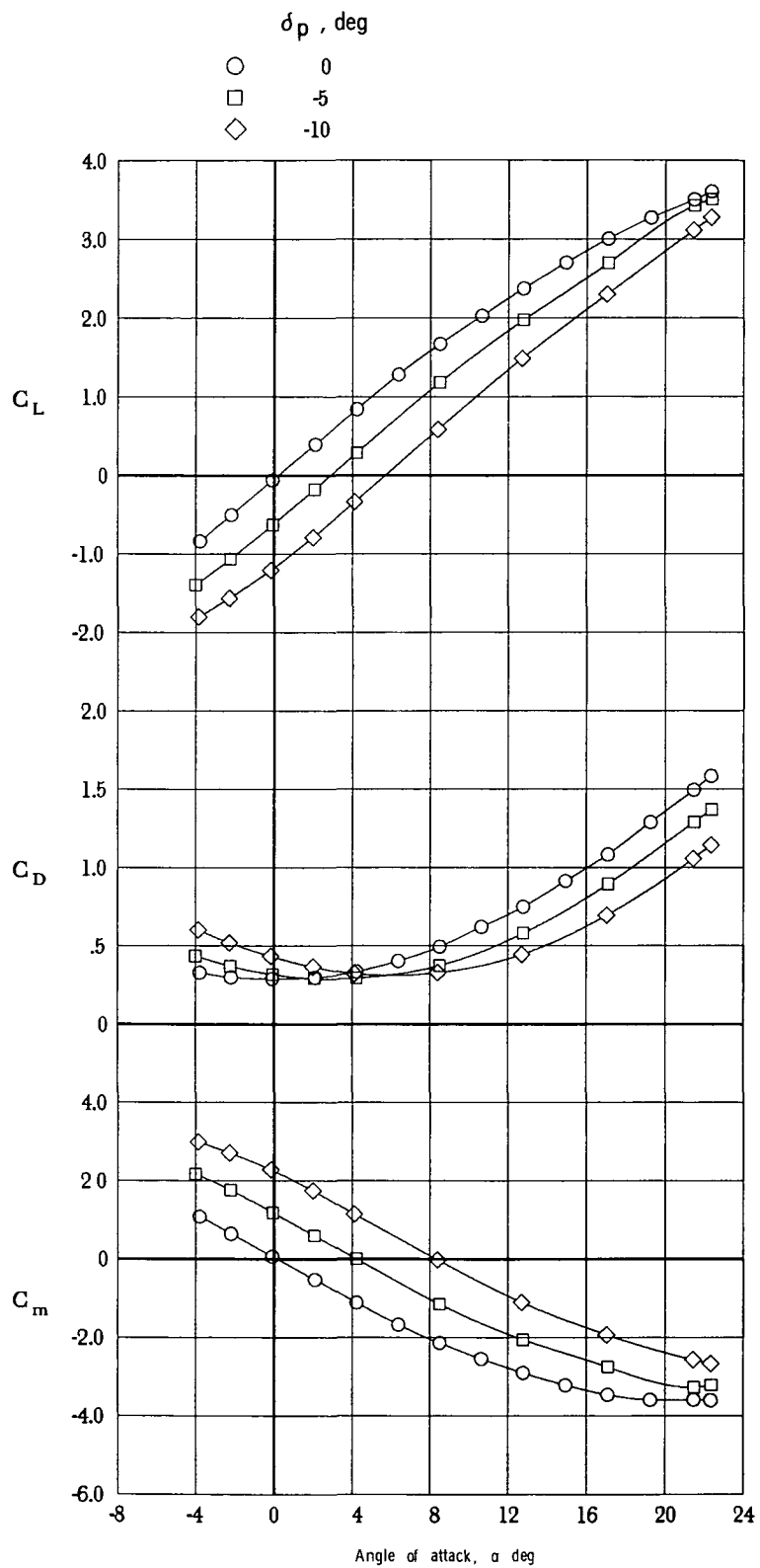
(d) $M_\infty = 1.2.$

Figure 6.- Concluded.
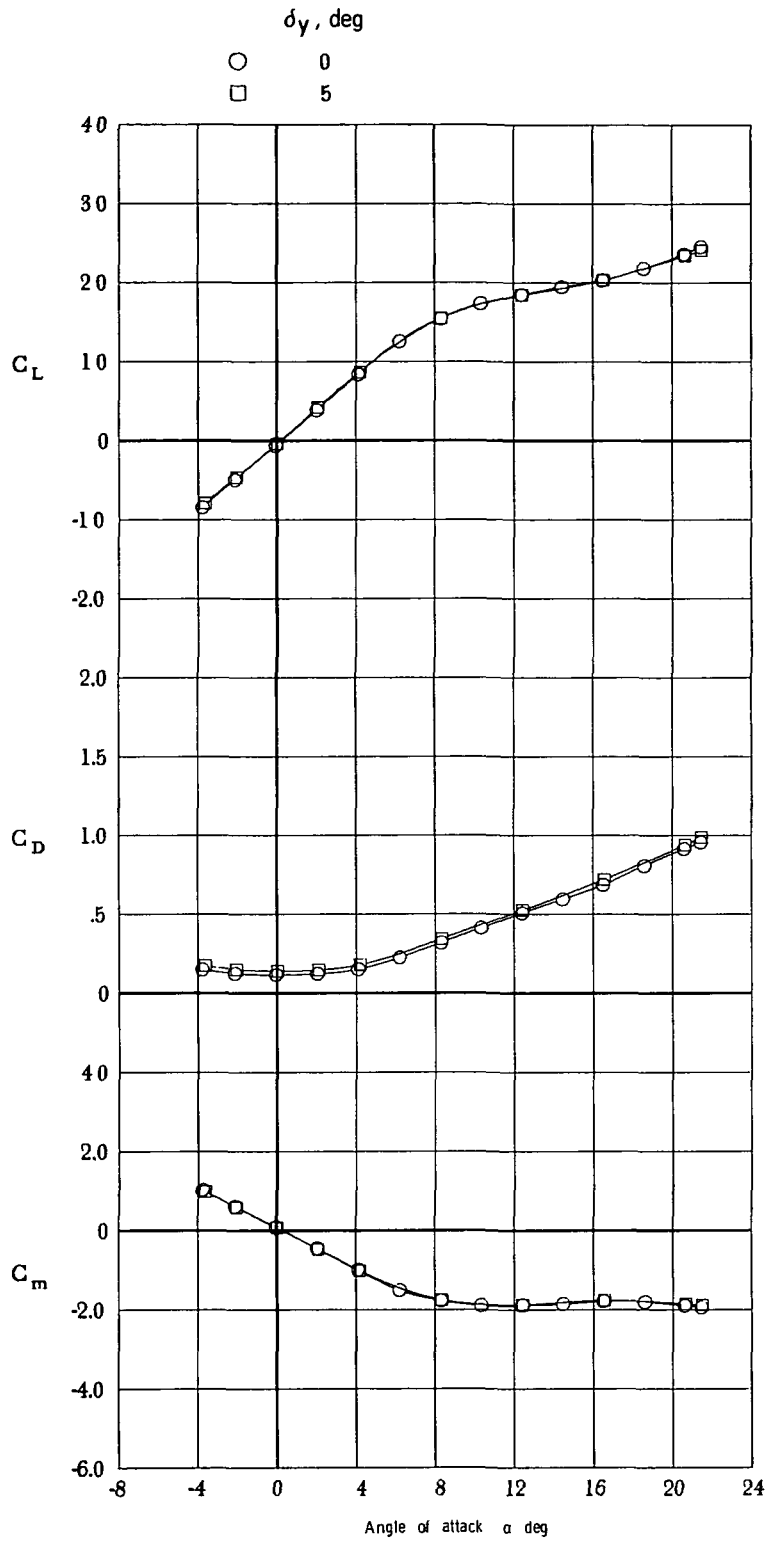
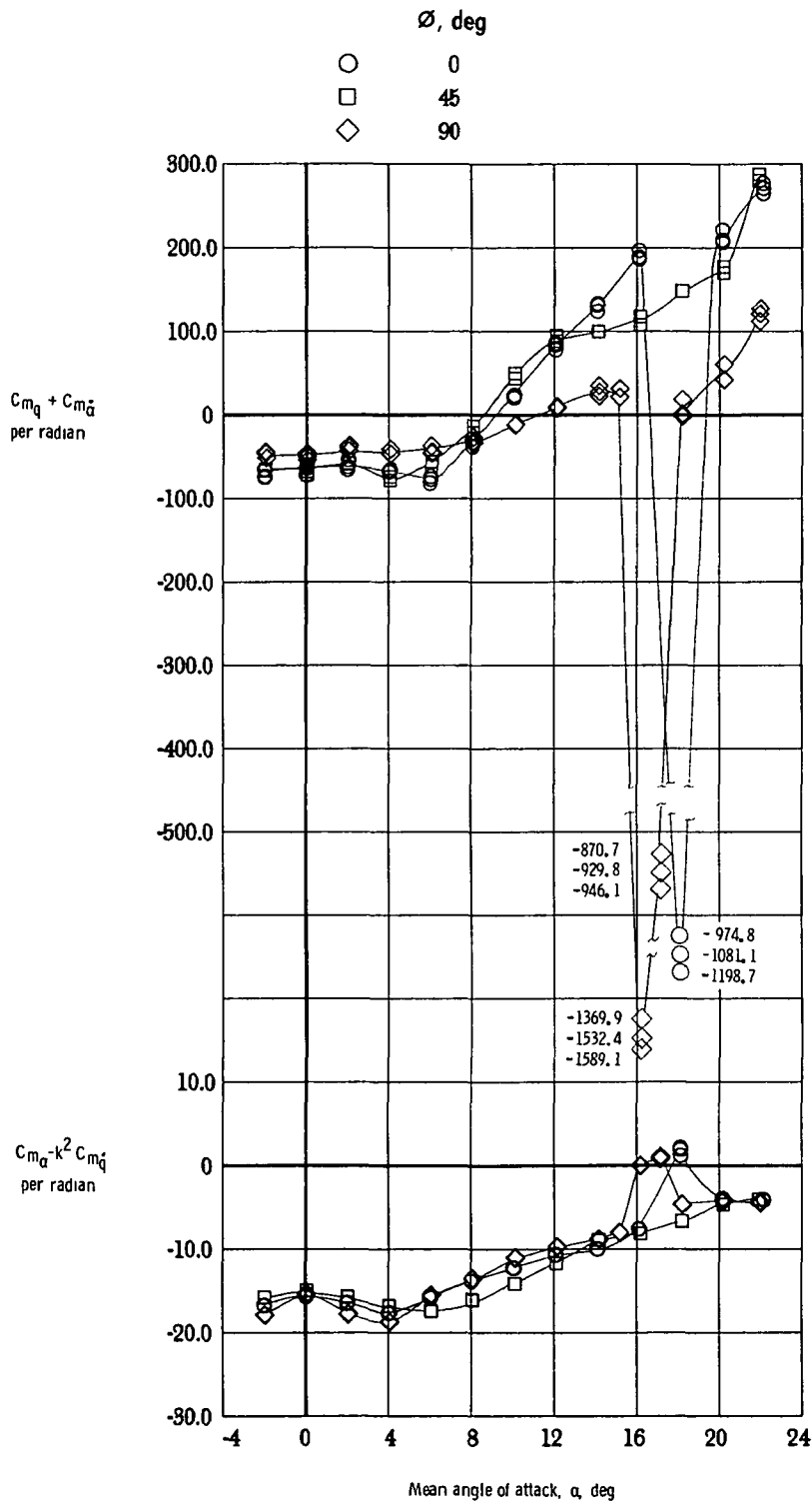(a) $M_{\infty} = 0.7$.

Figure 7.- Effect of yaw fin deflection on static longitudinal
characteristics. $\phi = 0^{\circ}$; $\delta_p = 0^{\circ}$.
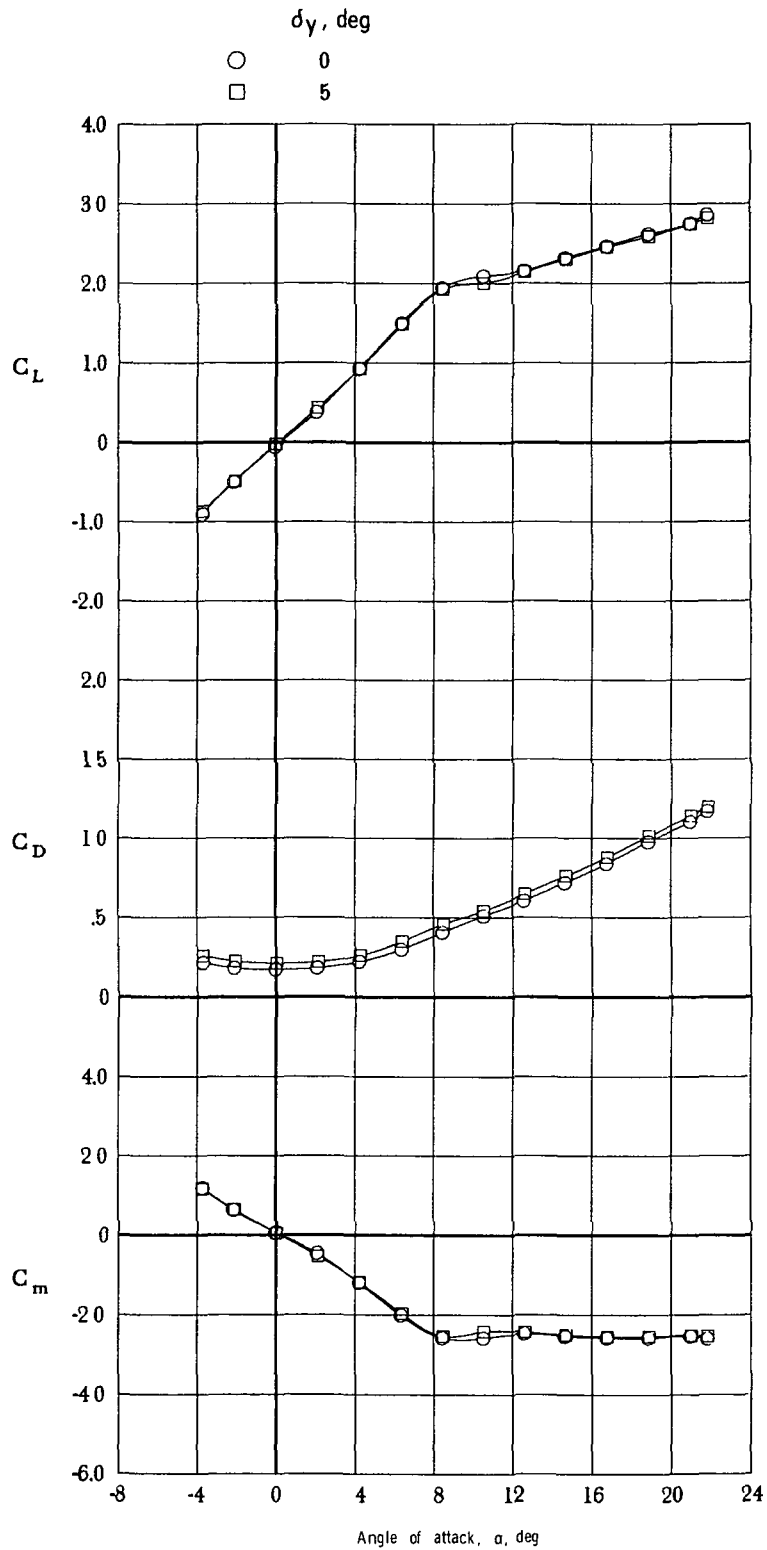
(b) $M_{\infty} = 0.9$.

Figure 7.- Continued.
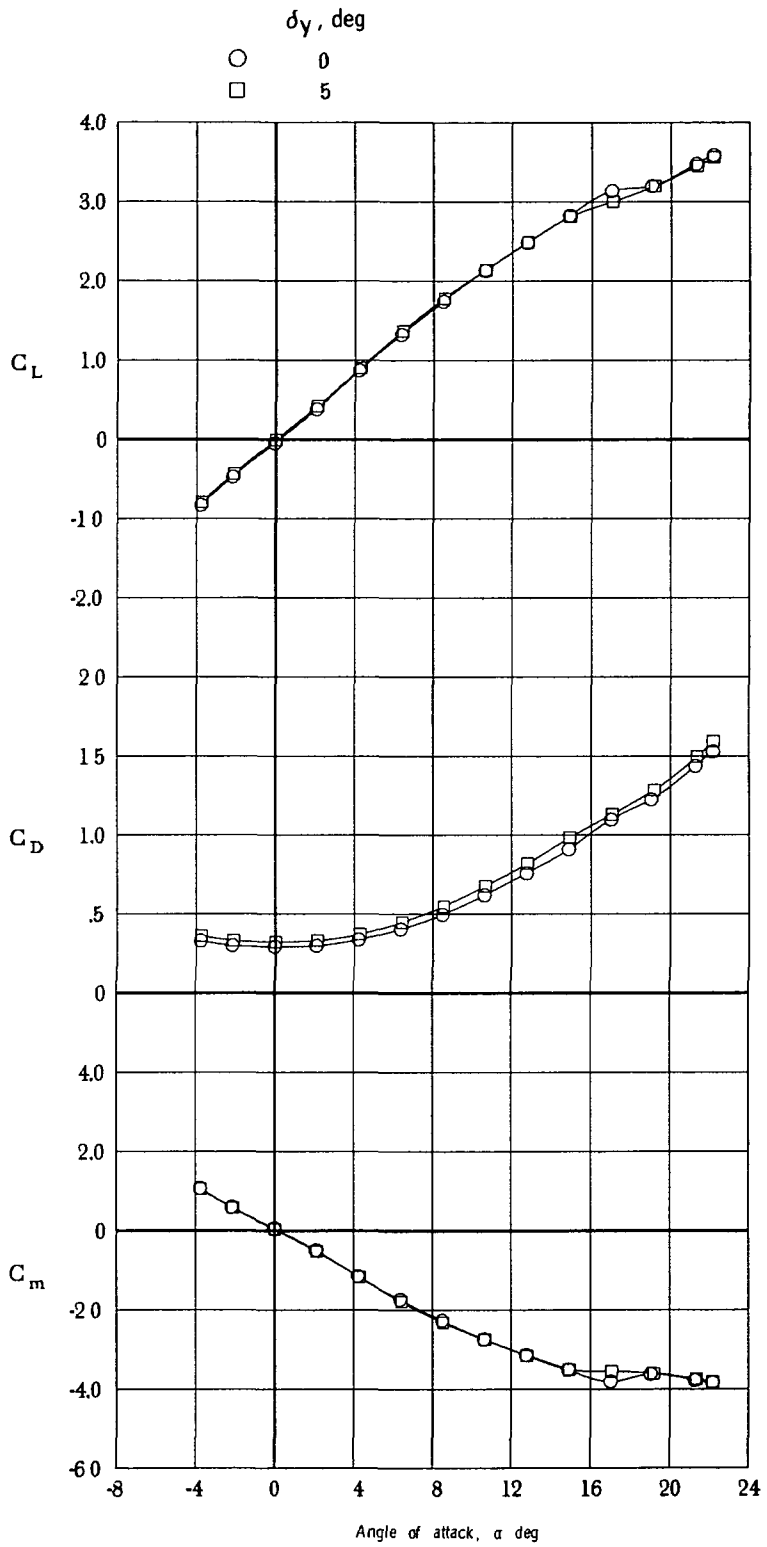
(c) $M_\infty = 1.1$

Figure 7.- Continued.
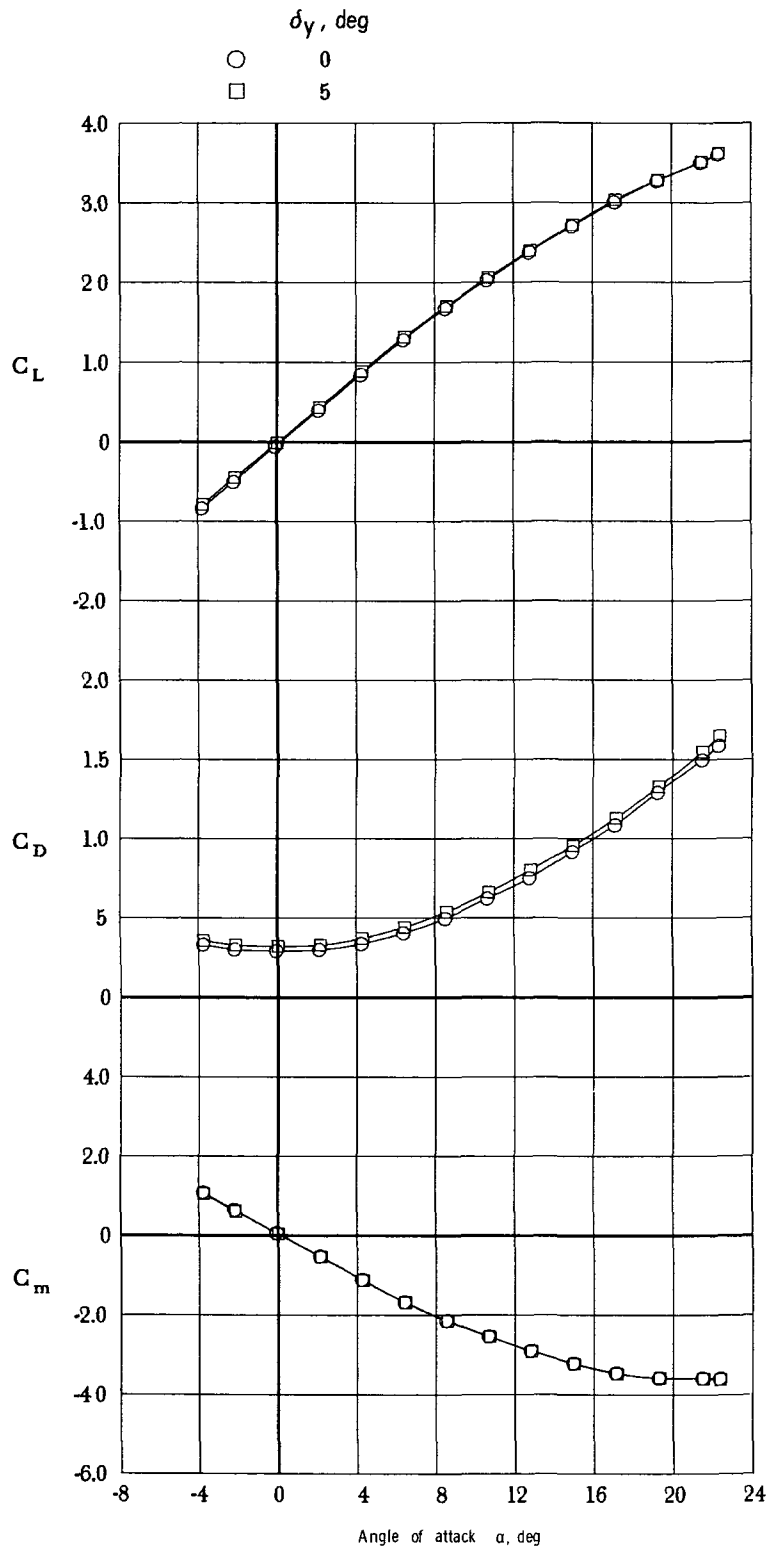
(d) $M_\infty = 1.2$.

Figure 7.- Concluded.
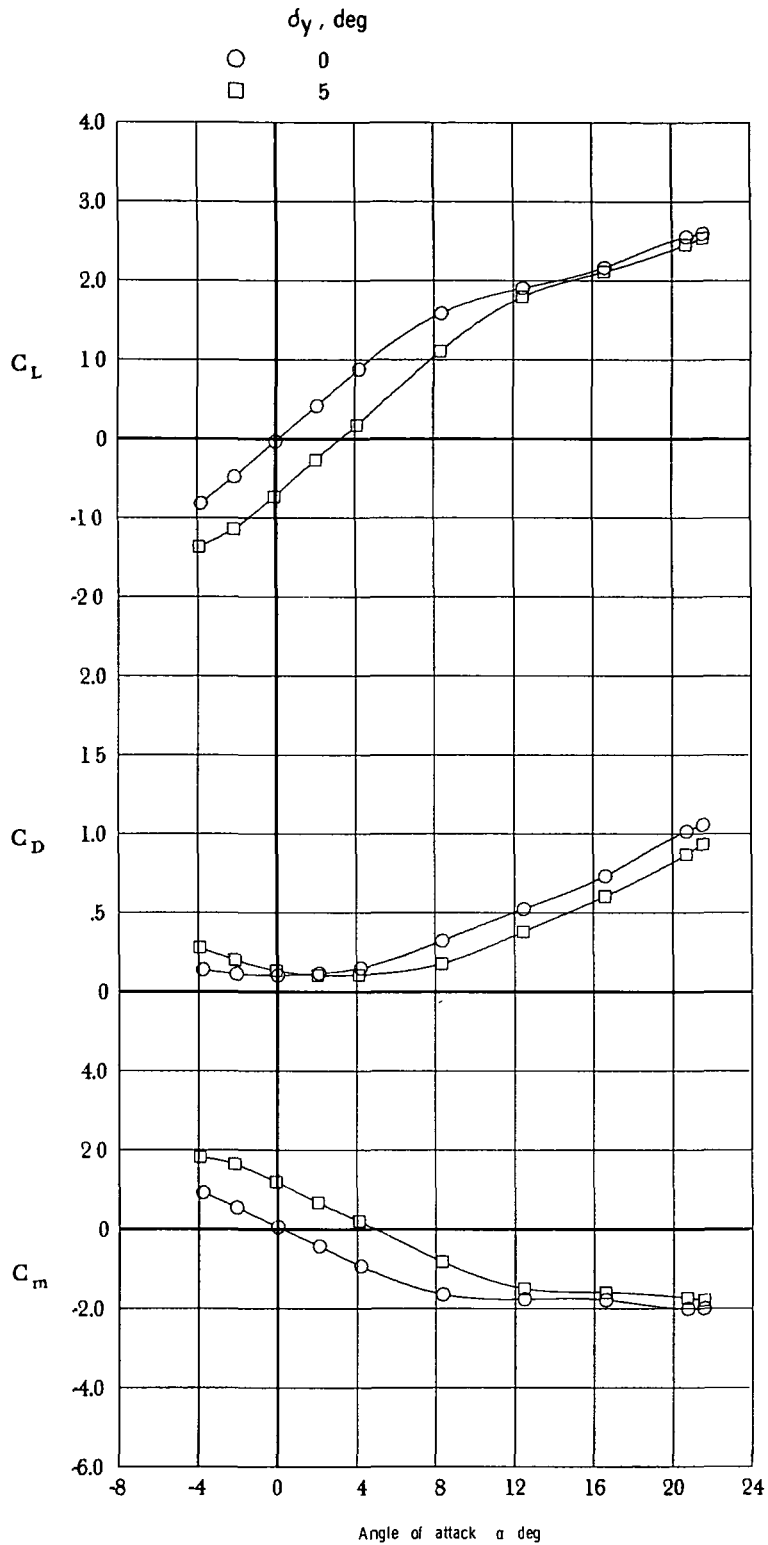
(a) M_∞ = 0.7.

Figure 8.- Effect of yaw fin deflection on static longitudinal
characteristics. ϕ = 90°; δ_p = 0°.
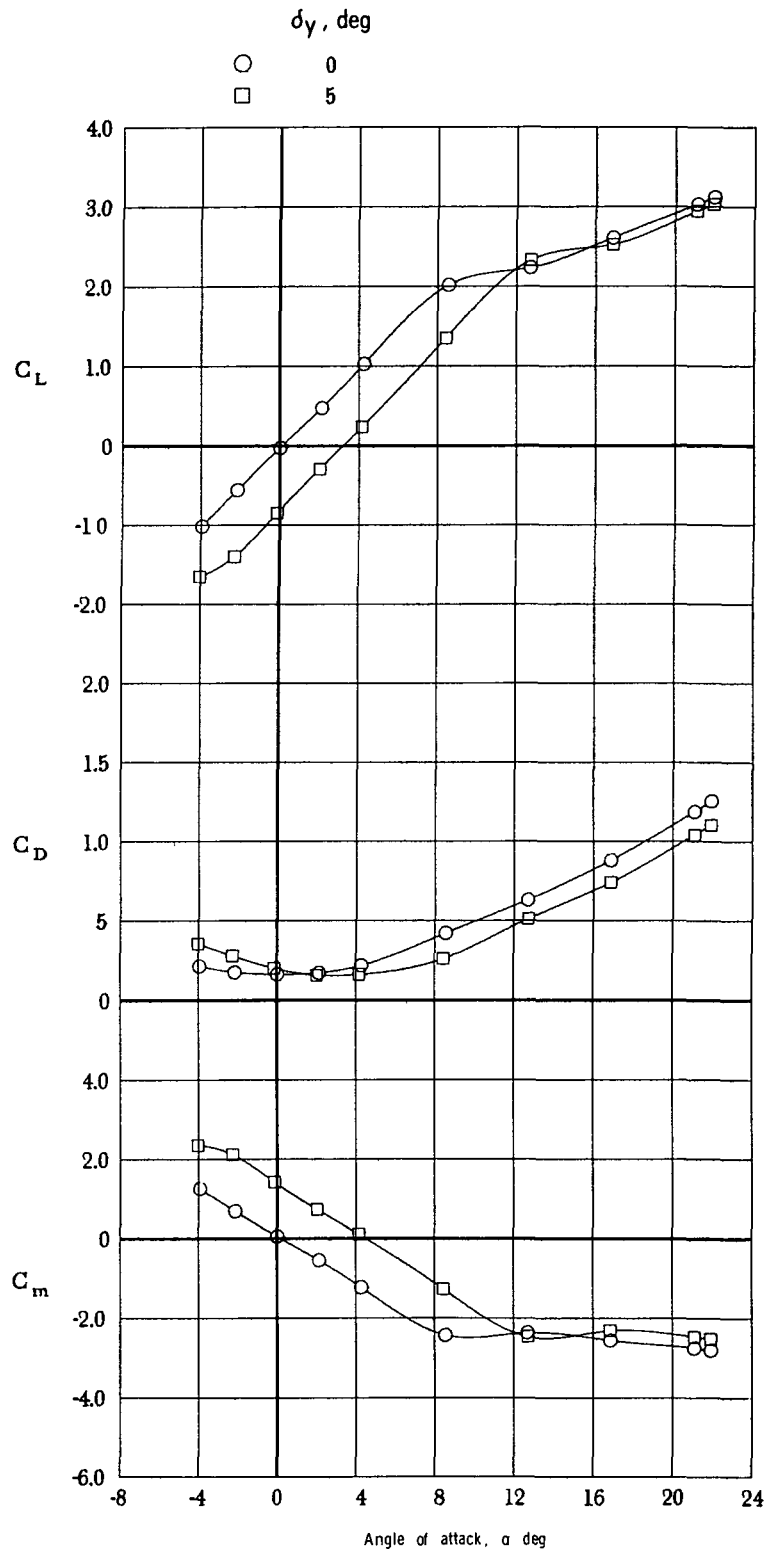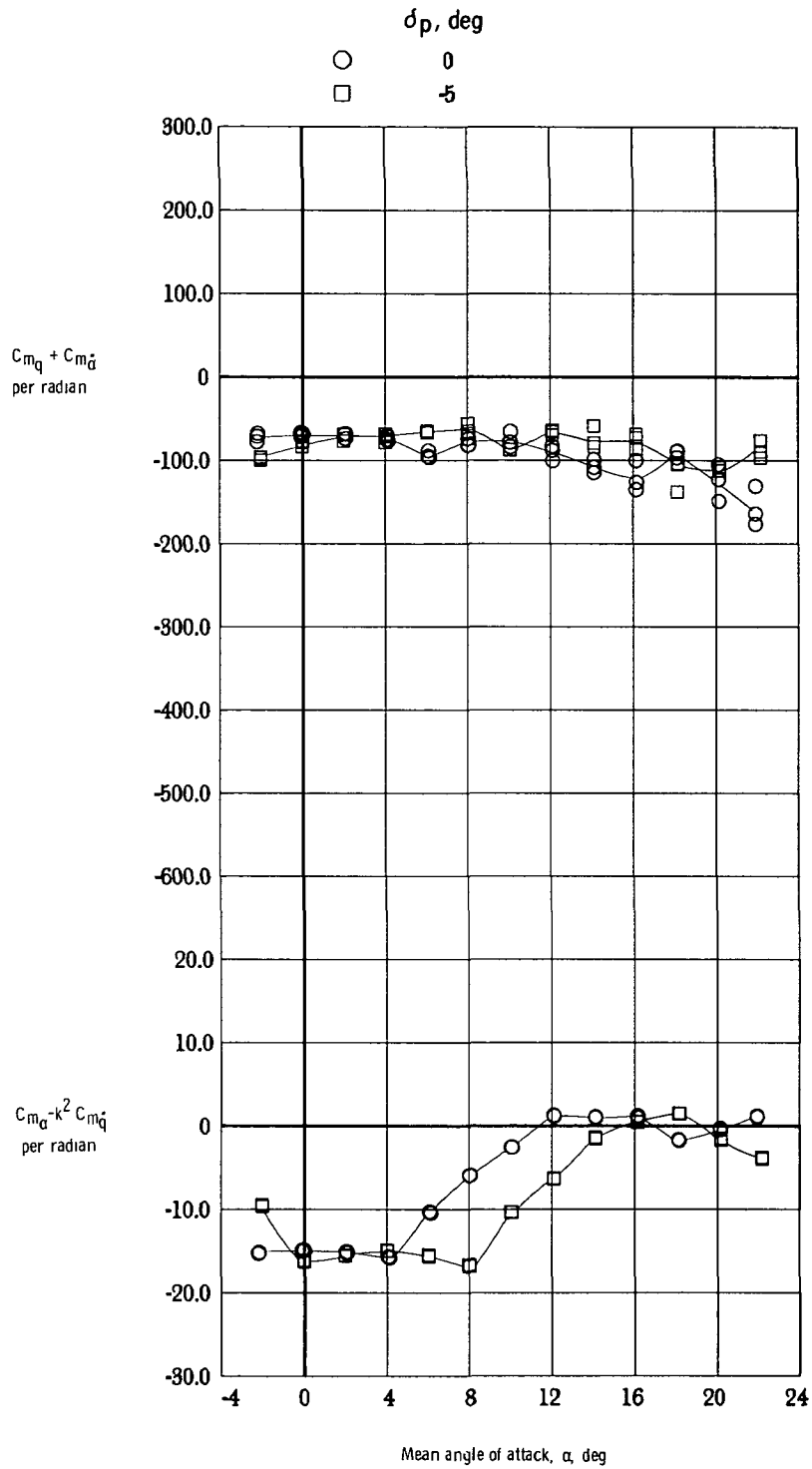
(b) $M_\infty = 0.9$.

Figure 8.- Continued.
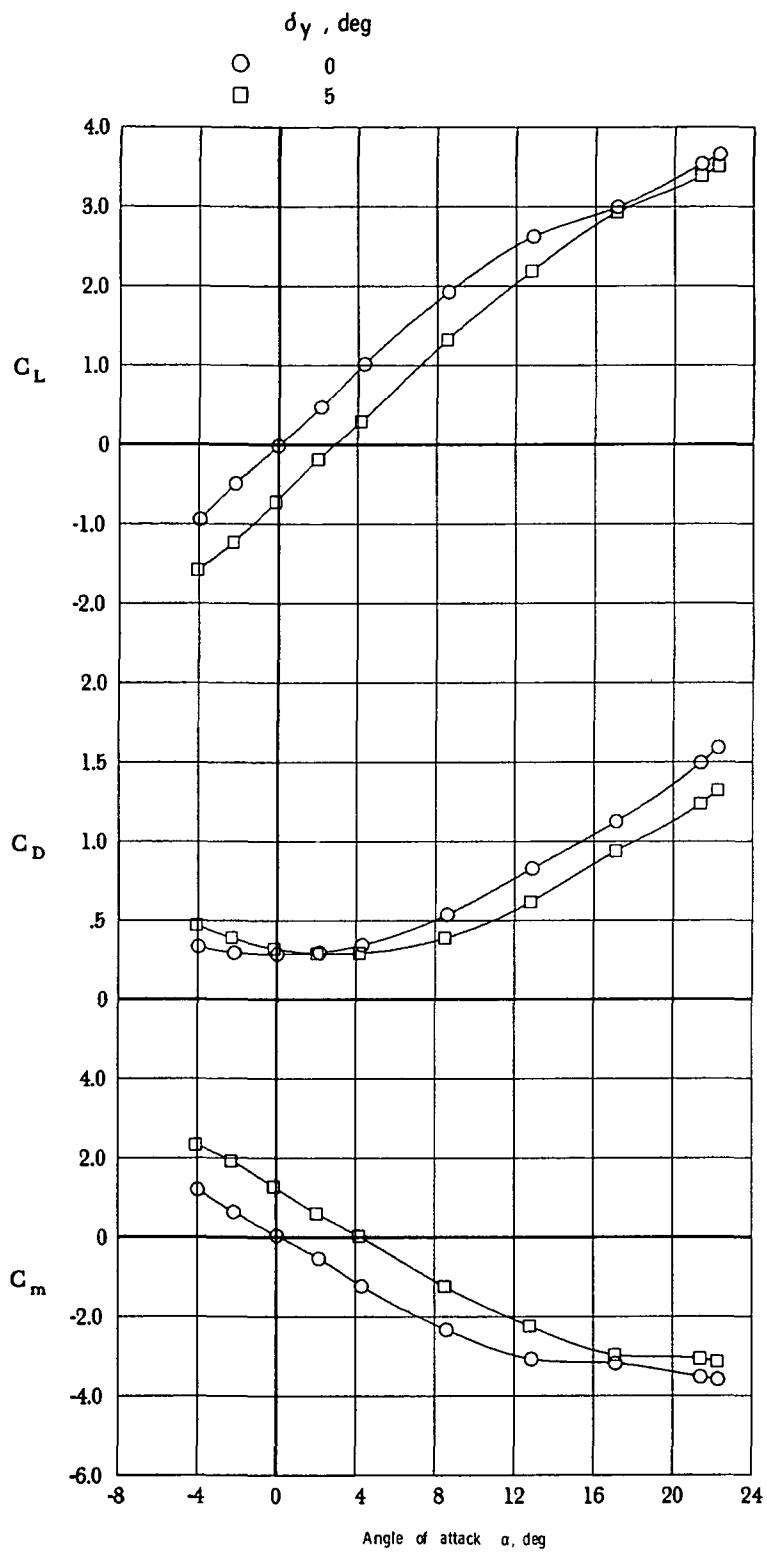
(c) $M_\infty = 1.1$.

Figure 8.- Continued.
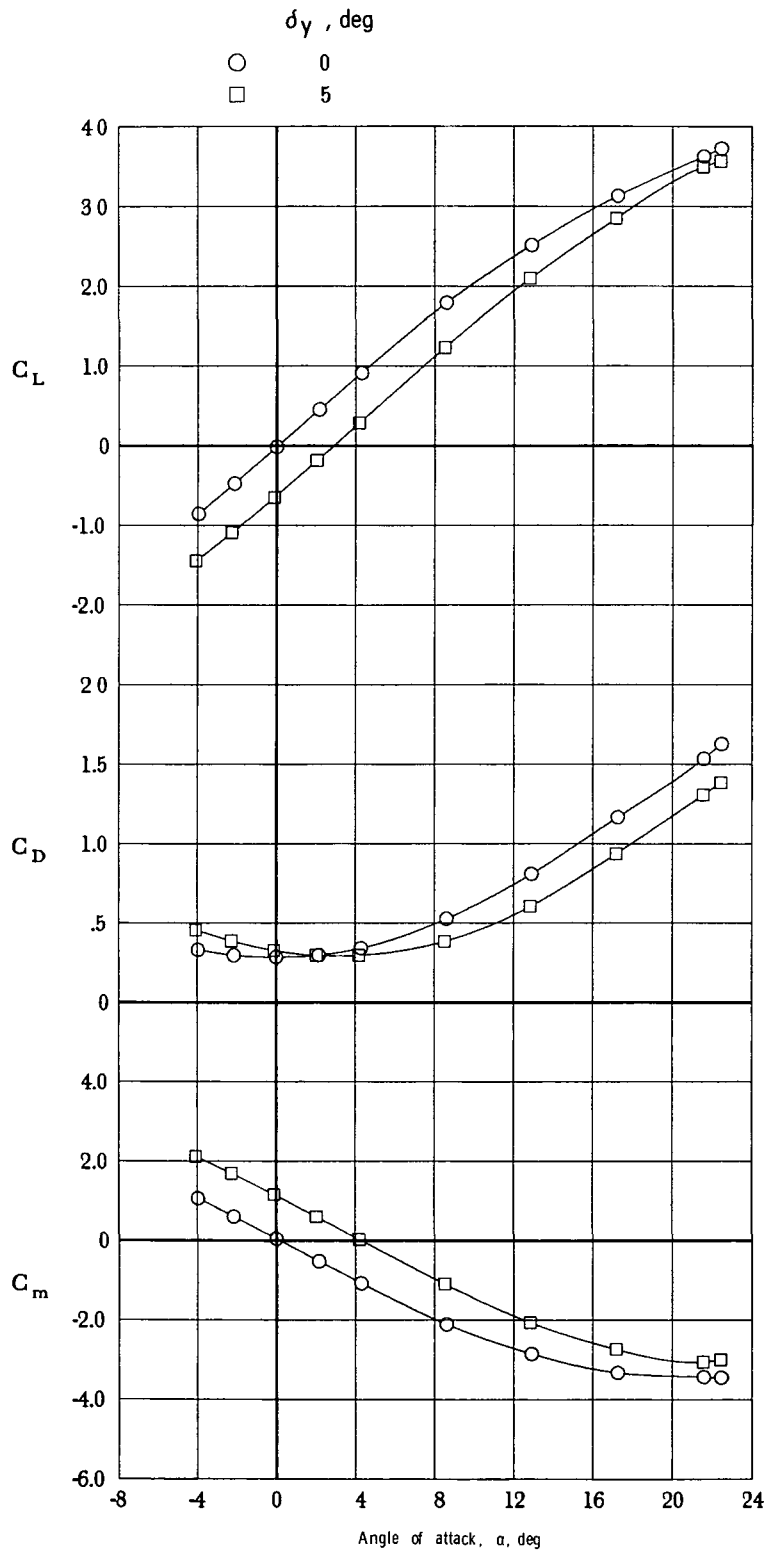
(d) $M_\infty = 1.2.$

Figure 8.- Concluded.
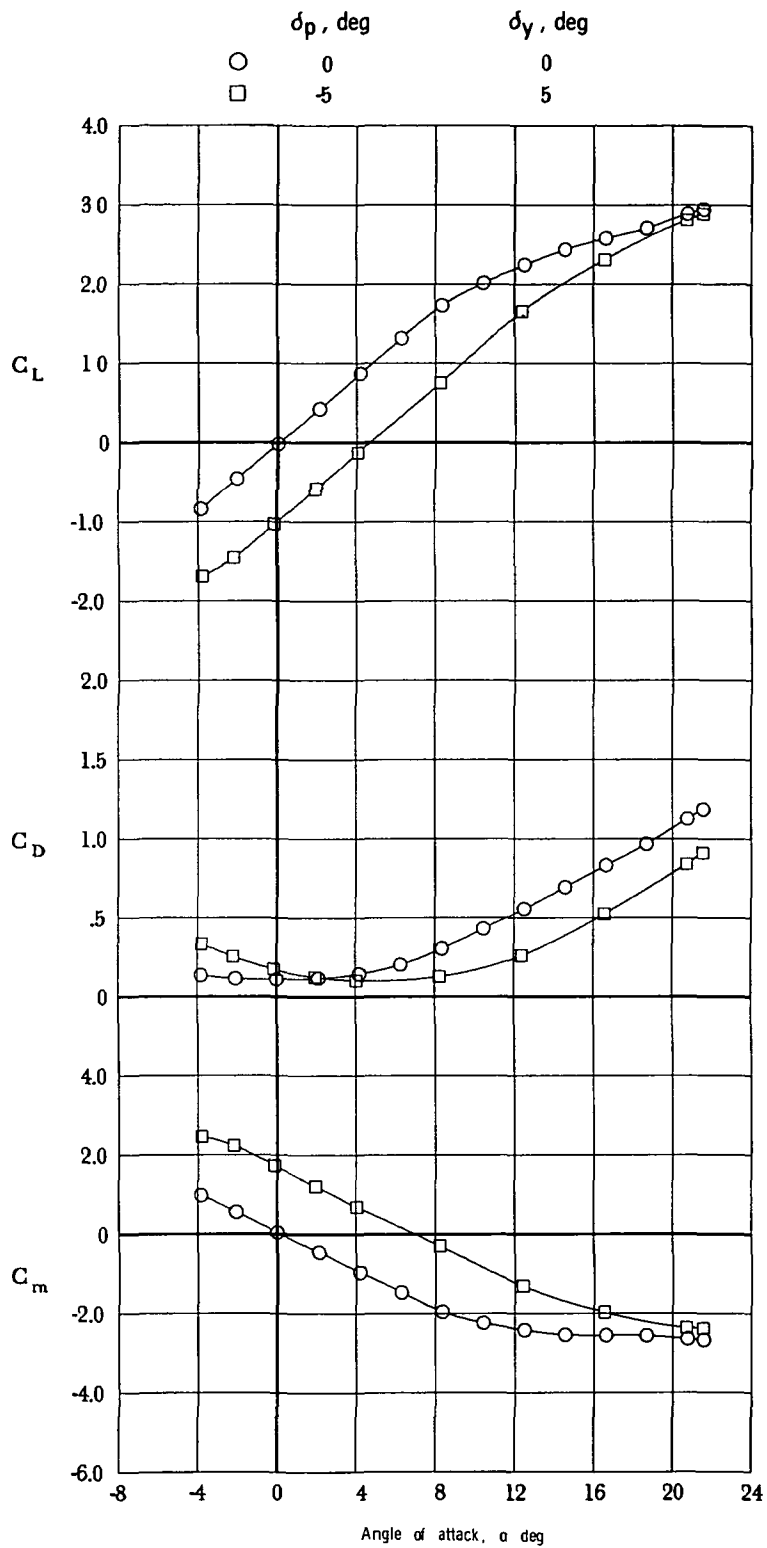
(a) M_{∞} = 0.7.

Figure 9.- Effect of pitch and yaw fin deflection on static longitudinal characteristics. ϕ = 45°.
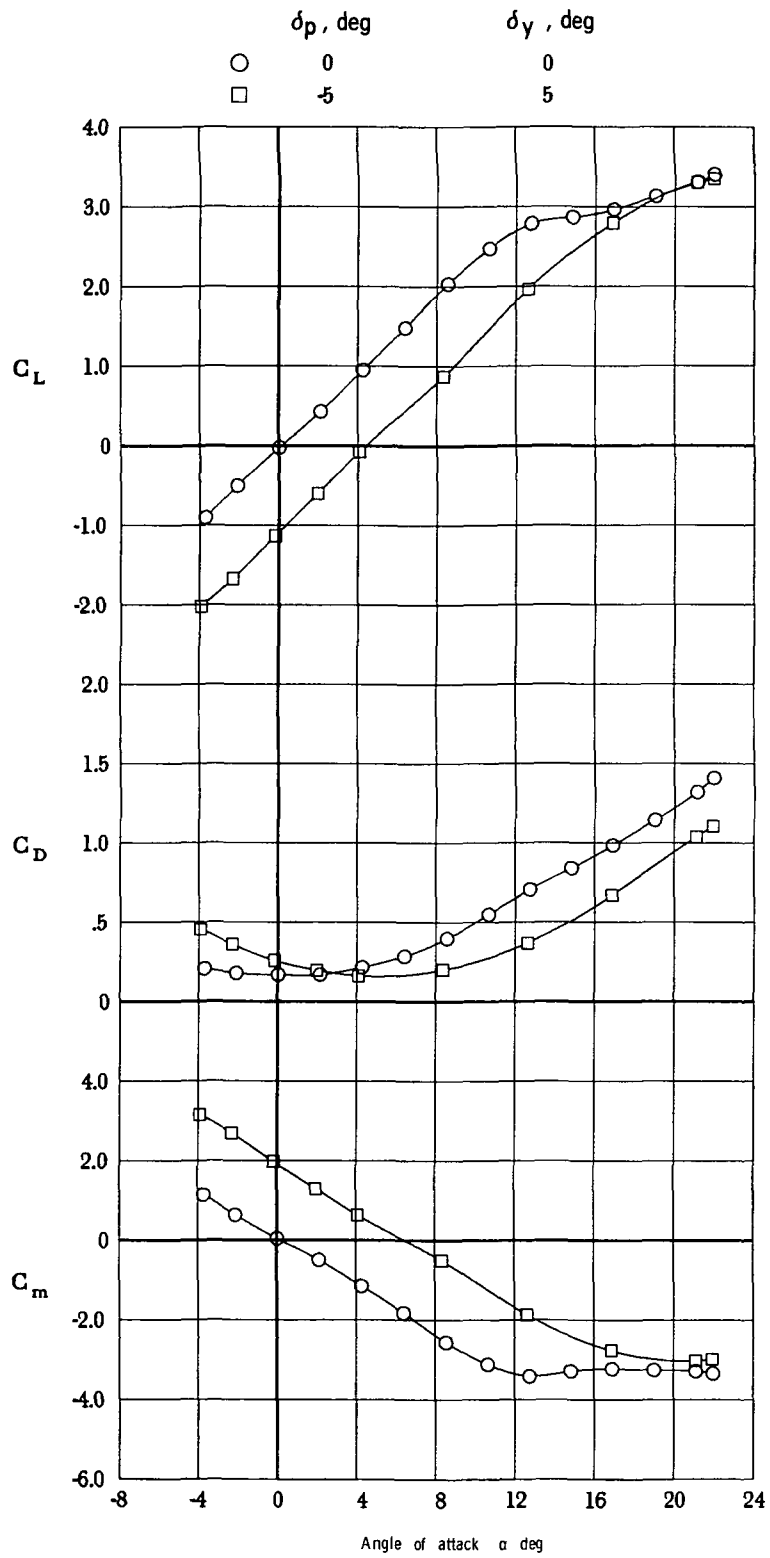
(b) $M_\infty = 0.9$.

Figure 9.- Continued.
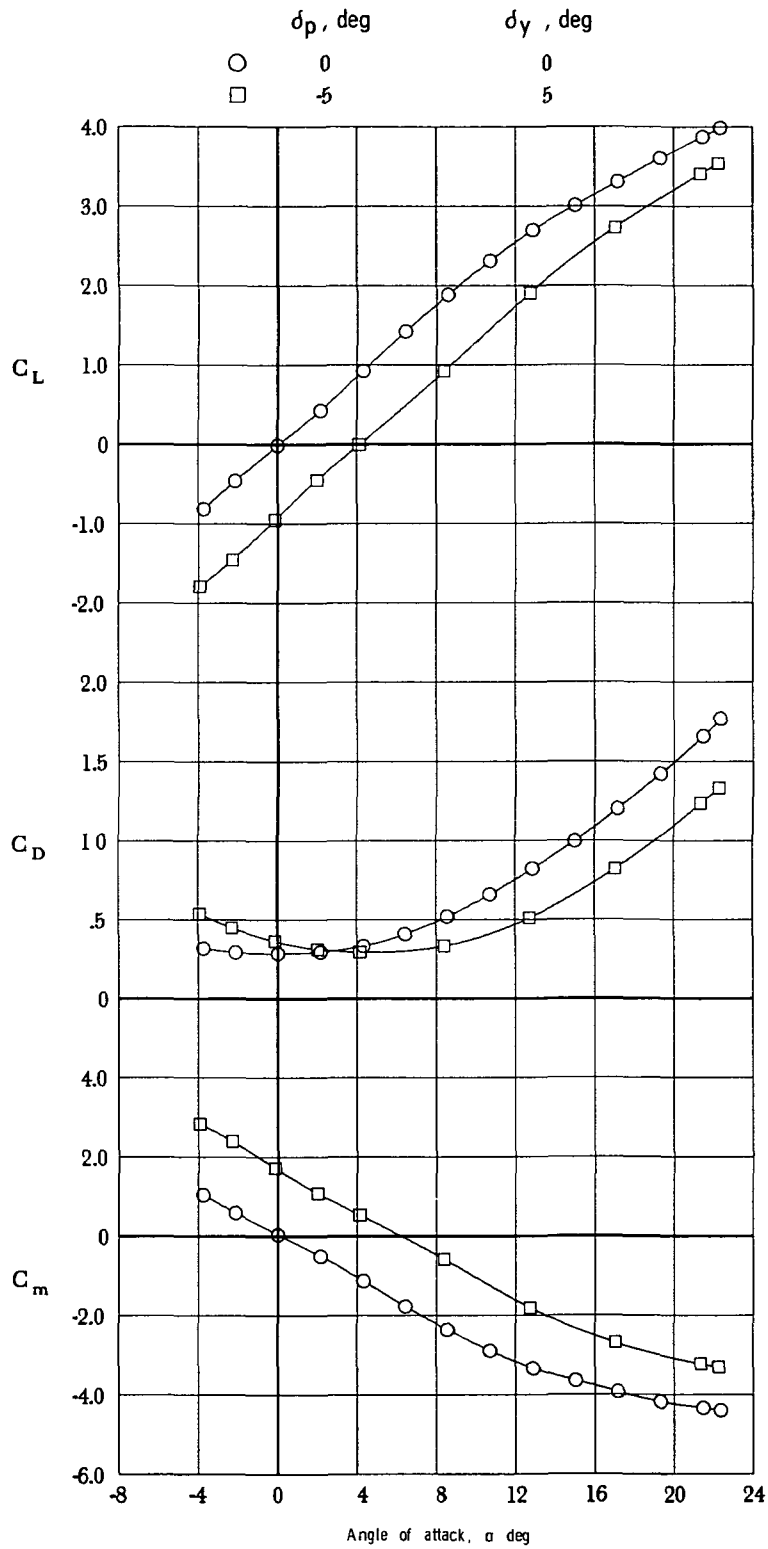
(c) $M_\infty = 1.1.$

Figure 9.- Continued.
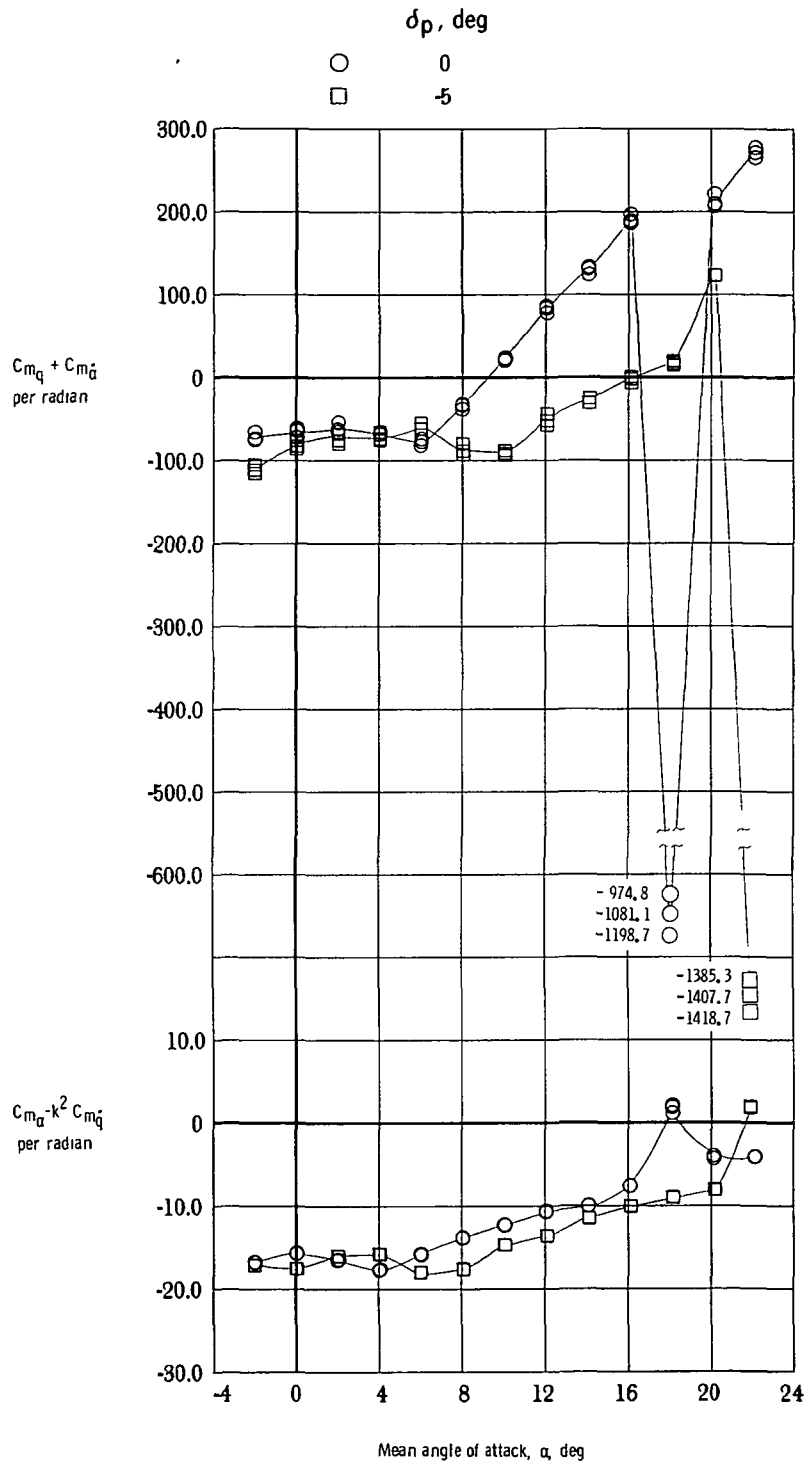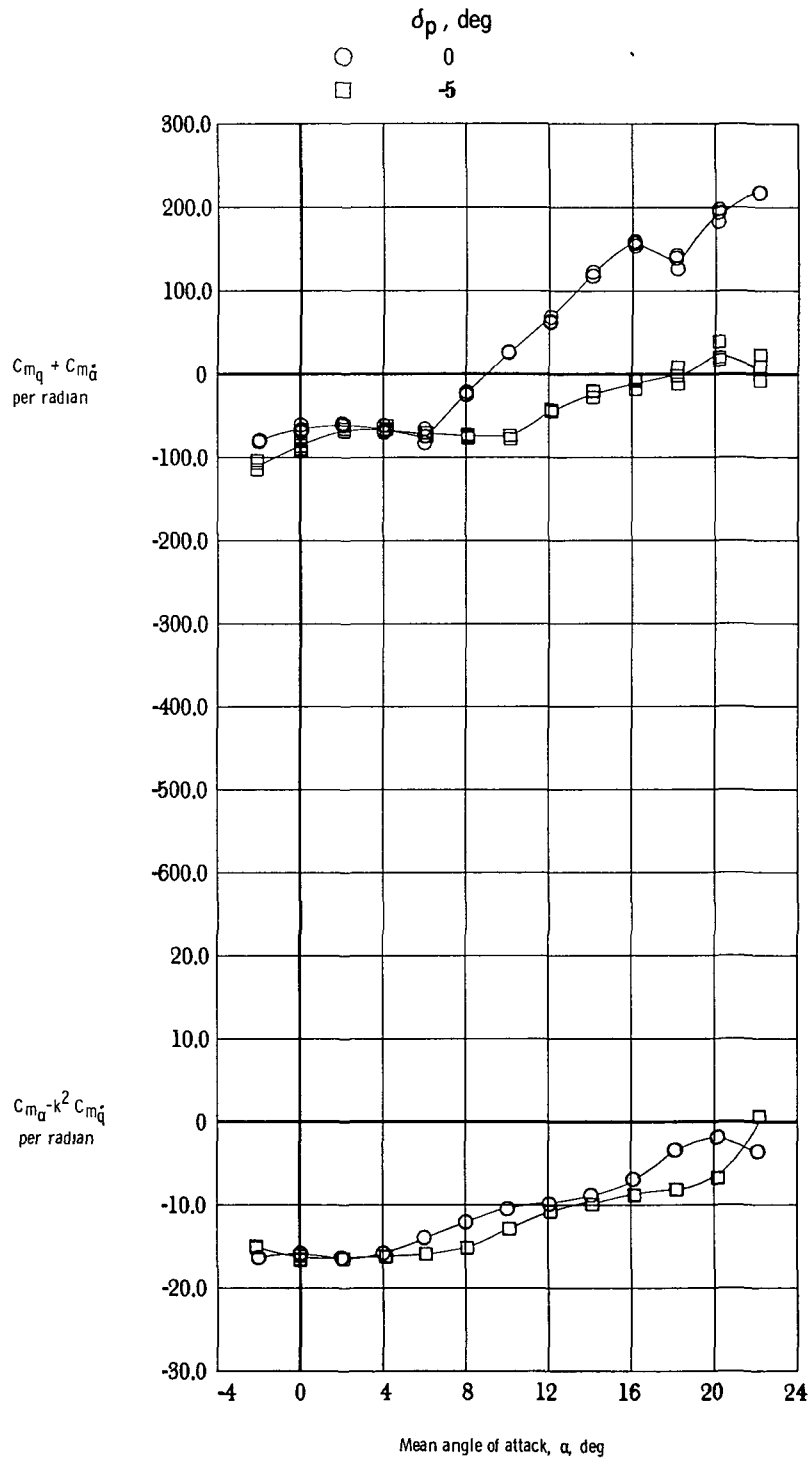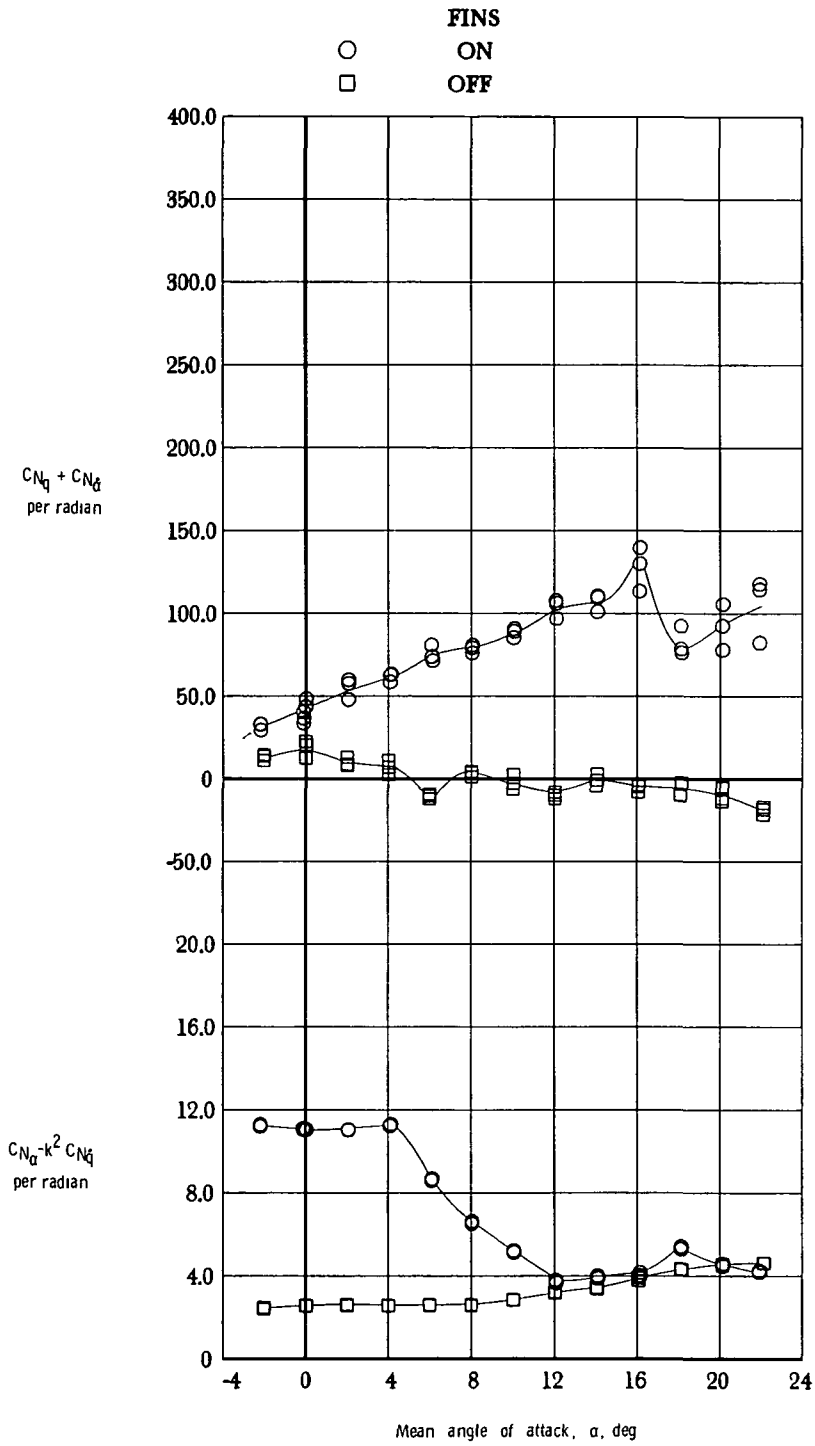
37
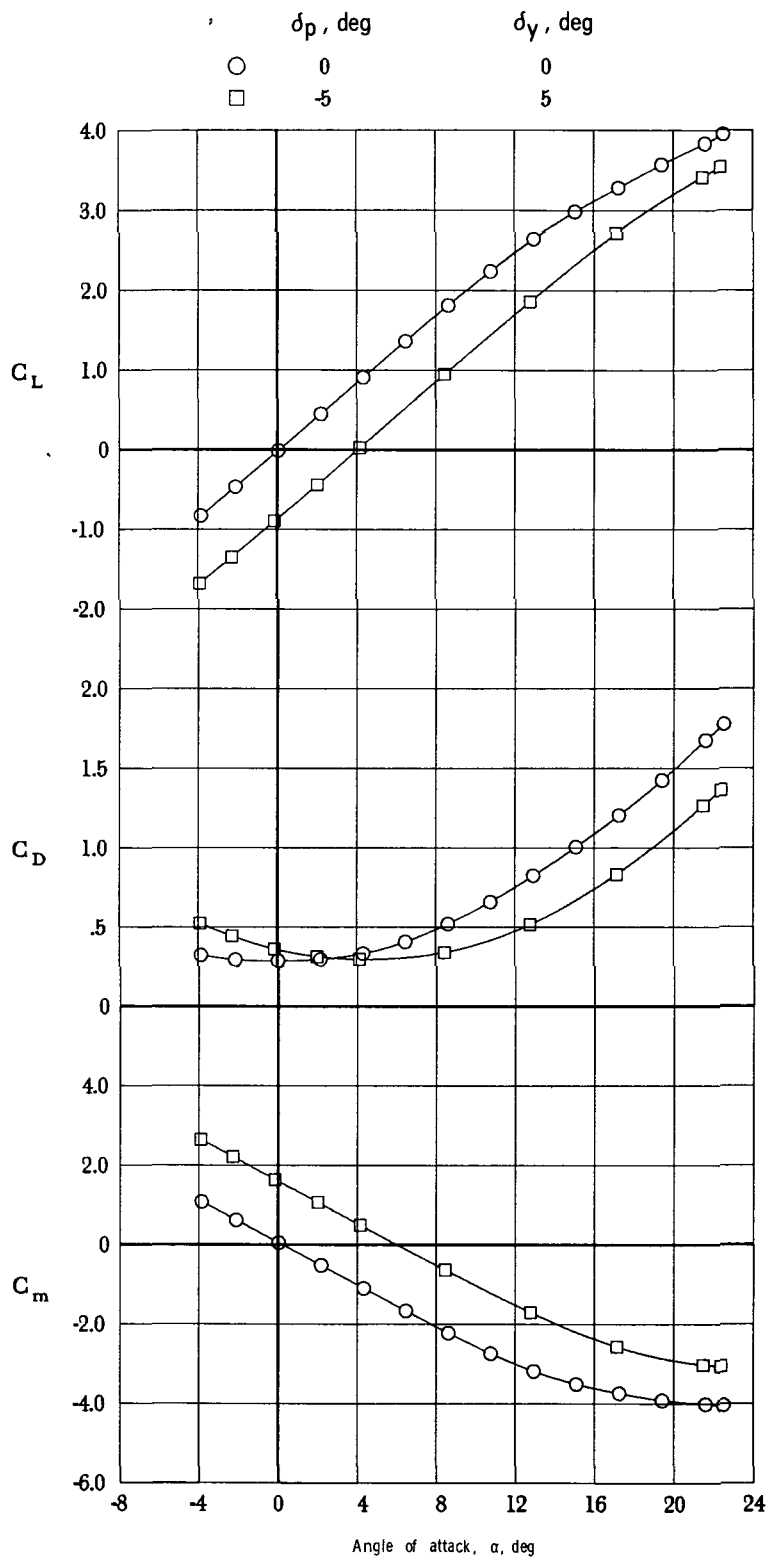
(d) $M_\infty = 1.2$.

Figure 9.- Concluded.
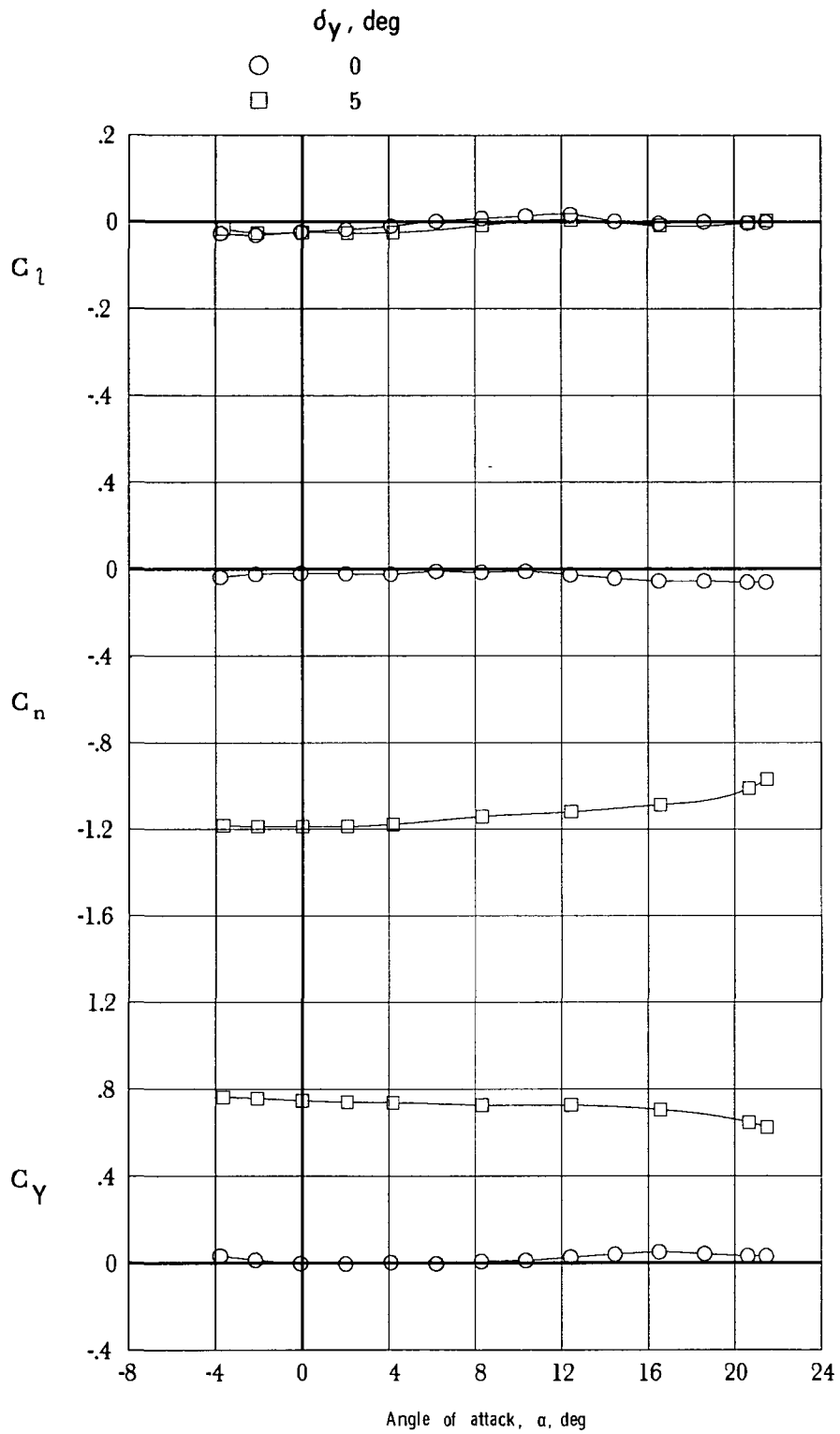
(a) $M_\infty = 0.7$.

Figure 10.- Effect of yaw fin deflection on static lateral characteristics. $\phi = 0^\circ$; $\delta_p = 0^\circ$.
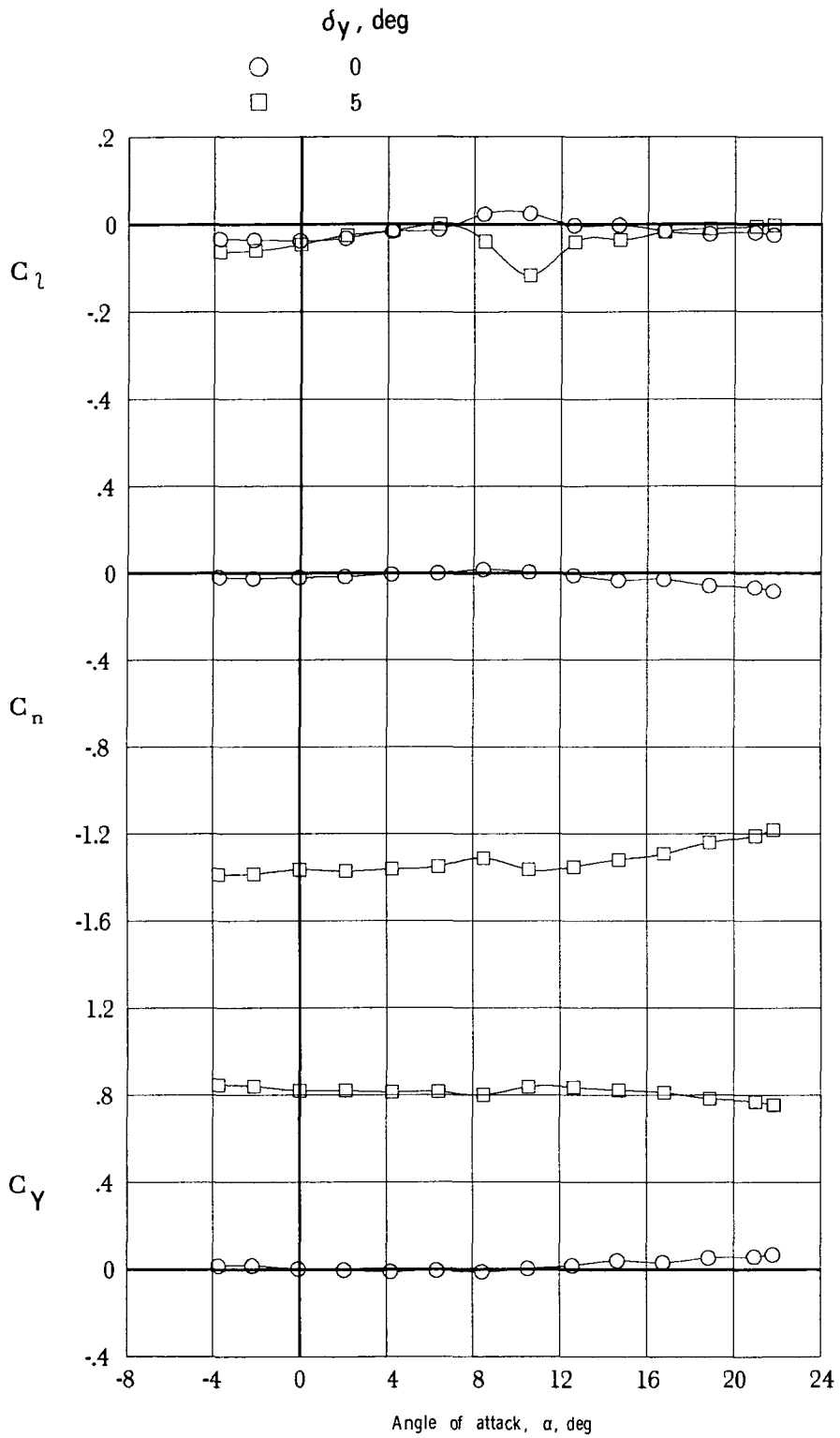
(b) $M_\infty = 0.9$.

Figure 10.- Continued.

δ_Y , deg

○   0
□   5
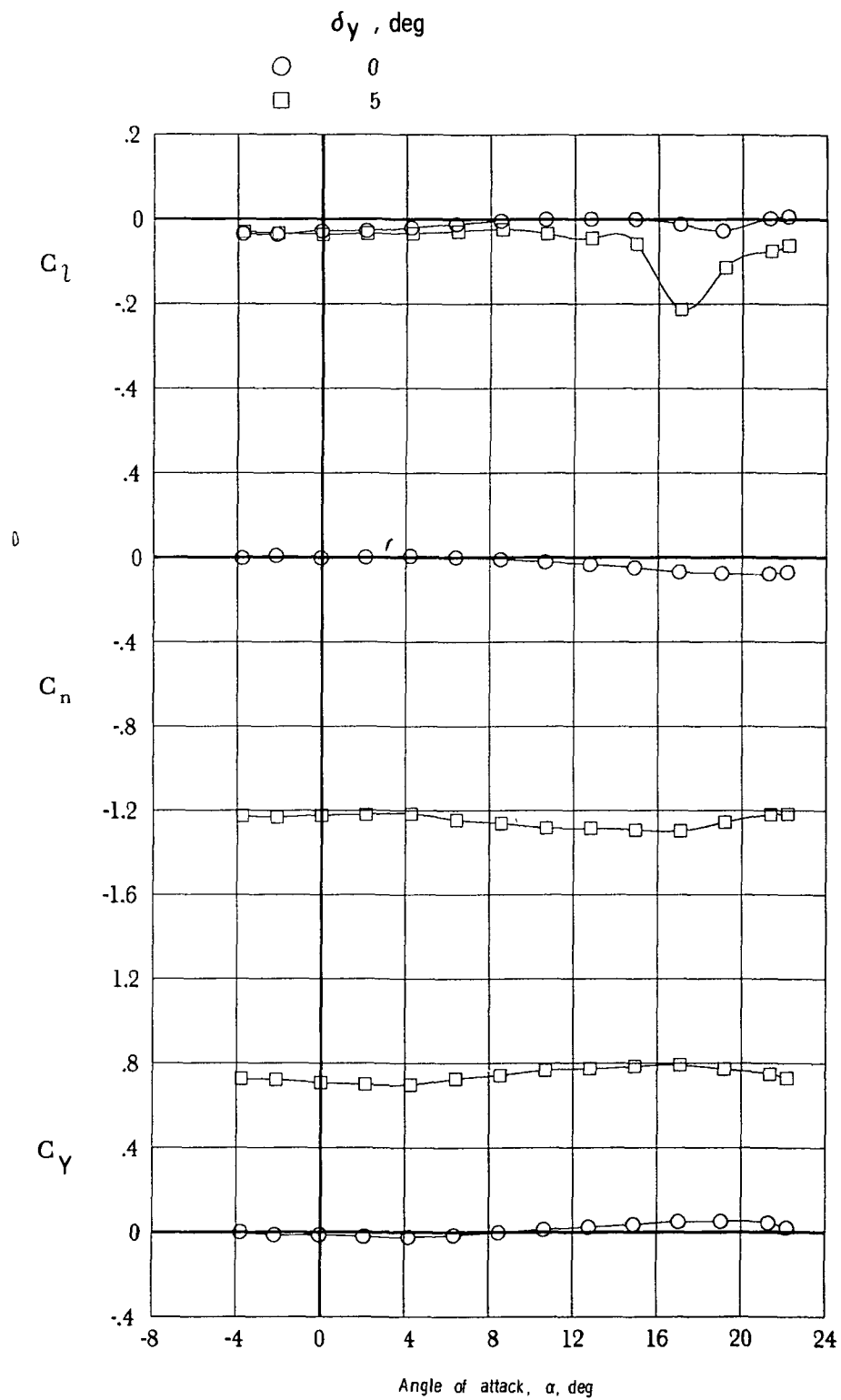
(c) $M_\infty = 1.1$.

Figure 10.- Continued.

δ_y, deg
○   0
□   5
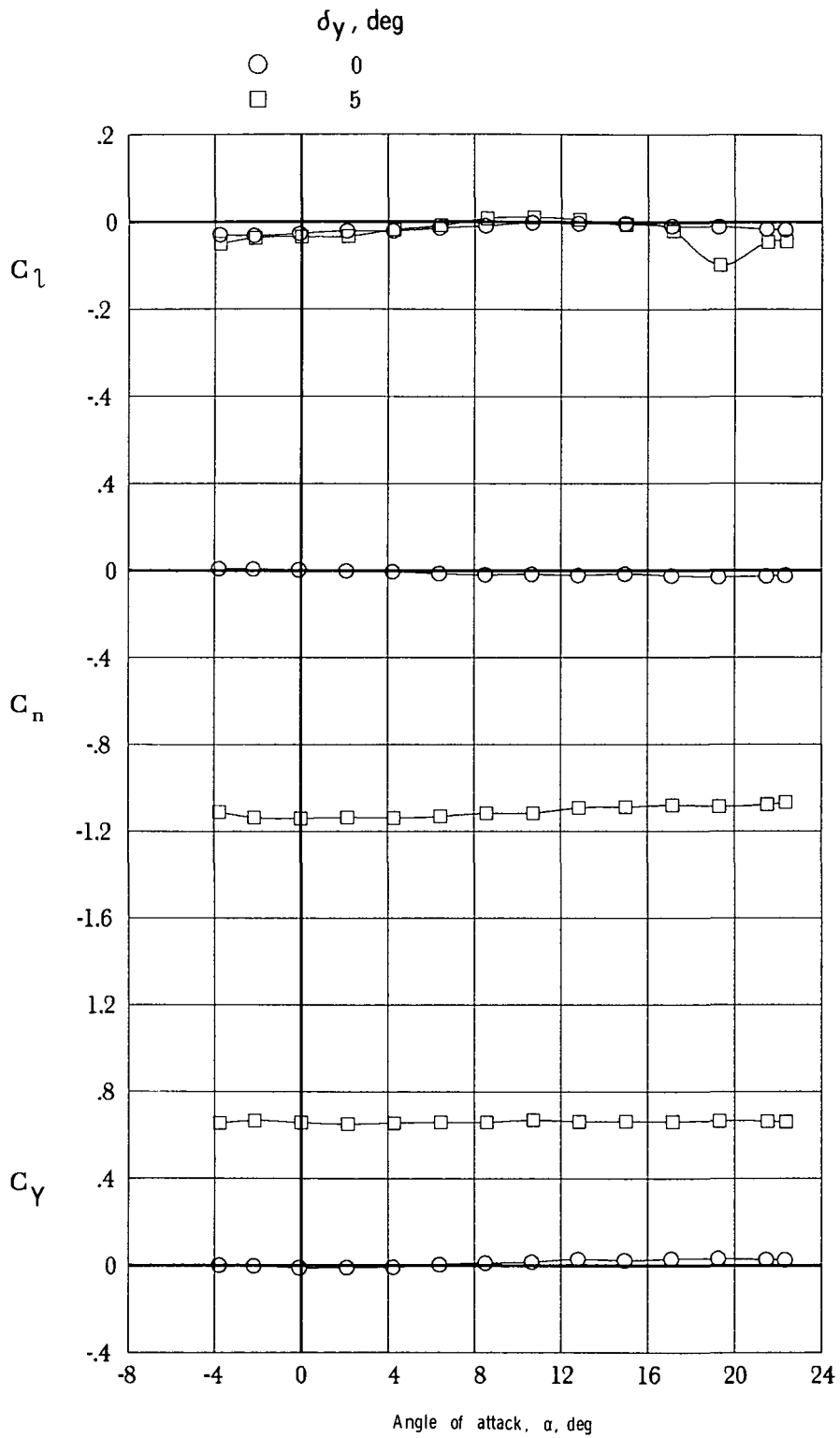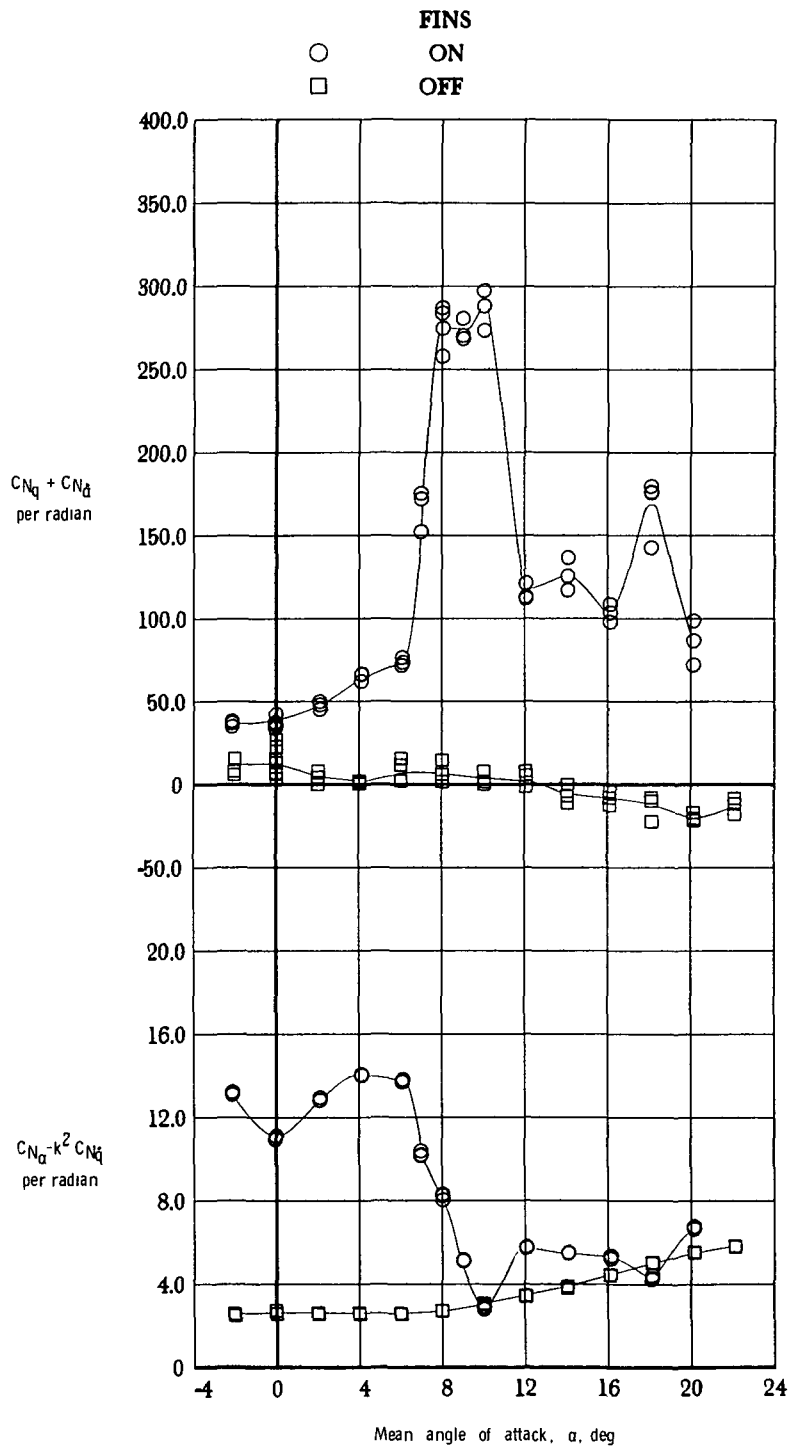
(d) $M_\infty = 1.2$.

Figure 10.- Concluded.
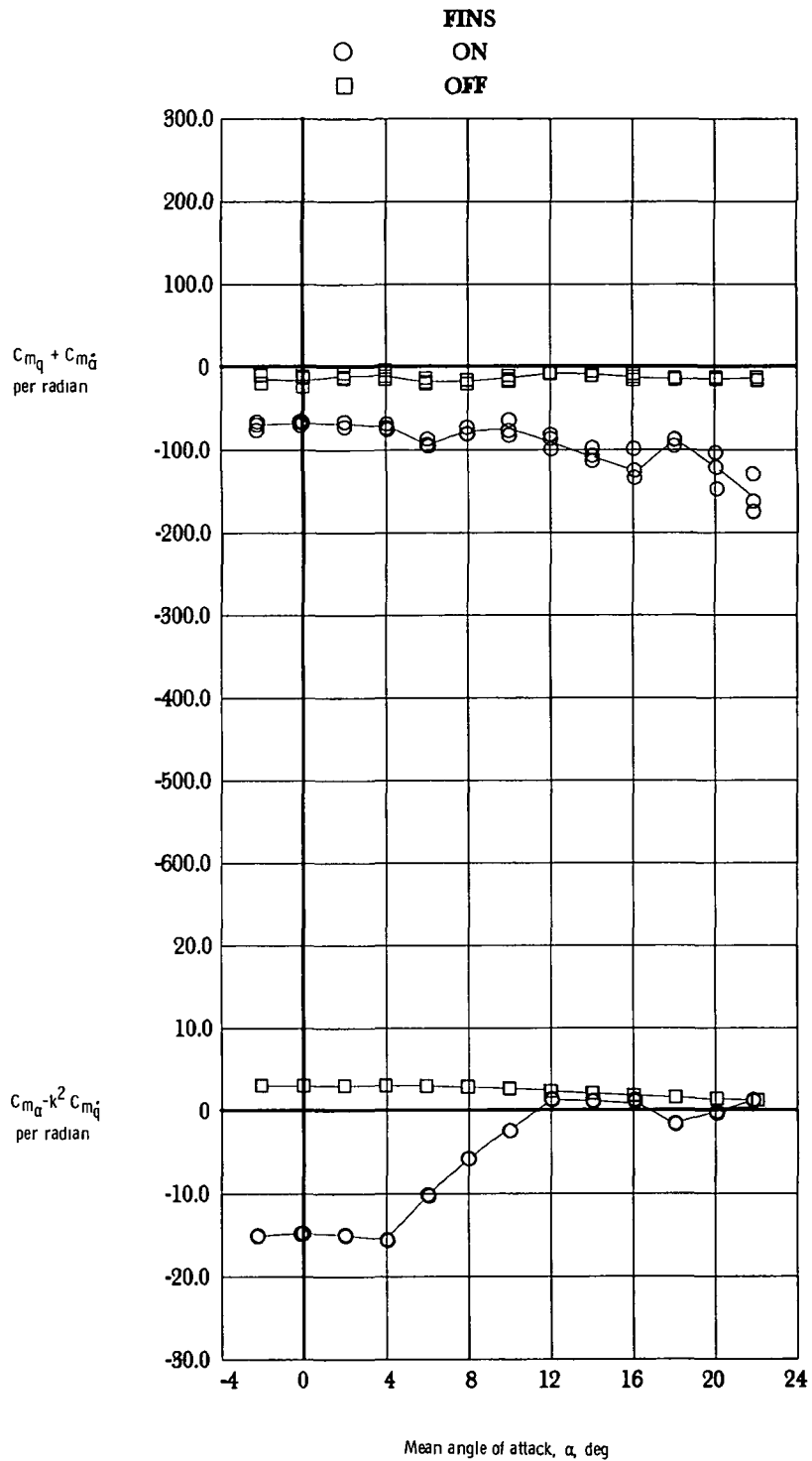
(a) $M_\infty = 0.7$.

Figure 11.- Effect of tail fins on damping-in-pitch parameter and on oscillatory longitudinal-stability parameter. $\phi = 0°$; $\delta_p = 0°$; $\delta_y = 0°$.
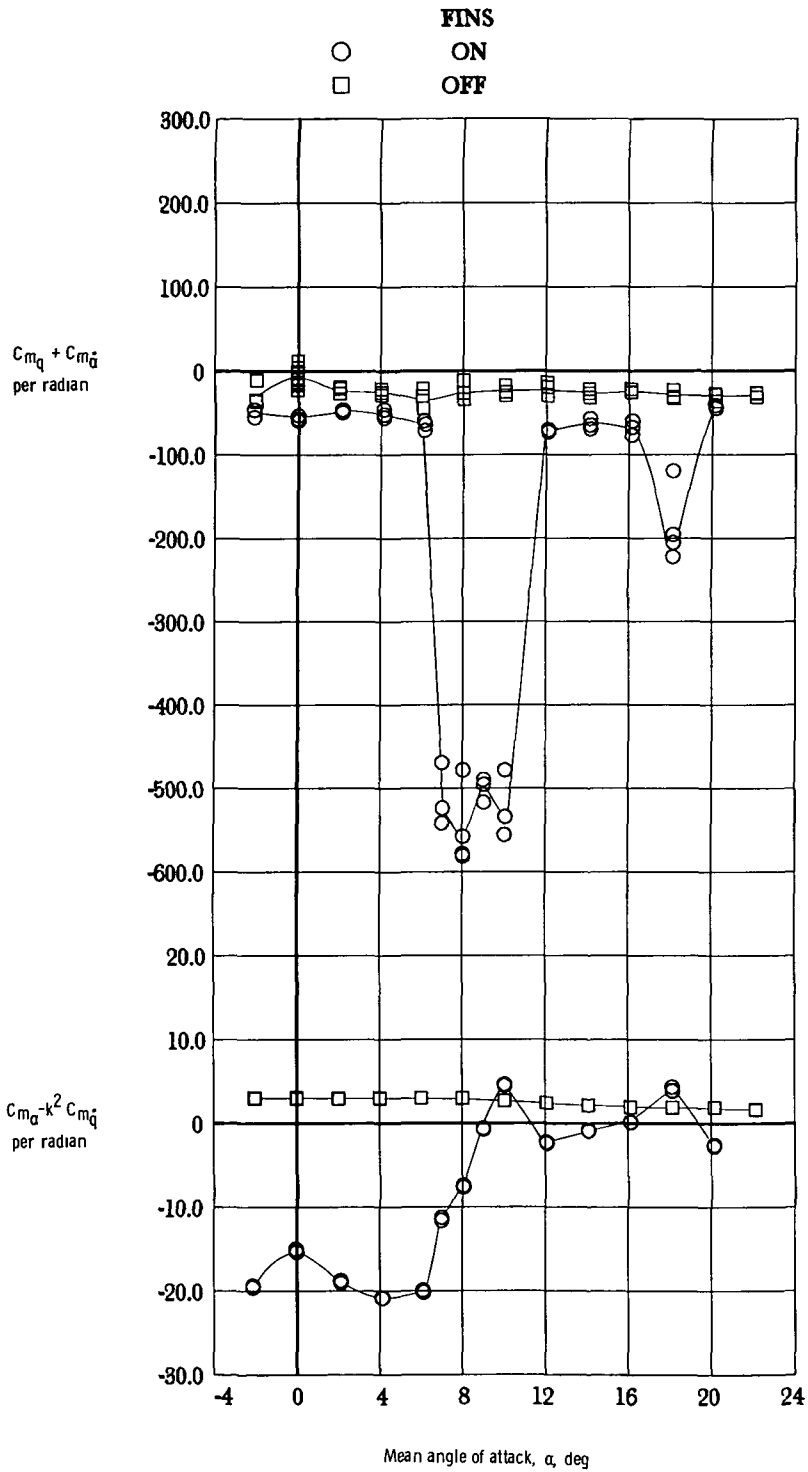
(b) $M_{\infty} = 0.9$.

Figure 11.- Continued.

(c) $M_\infty = 1.1.$

Figure 11.- Continued.

FINS
○   ON
□   OFF

$c_{m_q} + c_{m_{\dot{\alpha}}}$
per radian

$c_{m_\alpha} - k^2 c_{m_{\dot{q}}}$
per radian

Mean angle of attack, α, deg

(d) $M_\infty = 1.2$.

Figure 11.- Concluded.

(a) $M_\infty = 0.7$.

Figure 12.- Effect of configuration roll orientation on damping-in-pitch
parameter and on oscillatory longitudinal-stability parameter. $\delta_p = 0^o$;
$\delta_y = 0^o$.
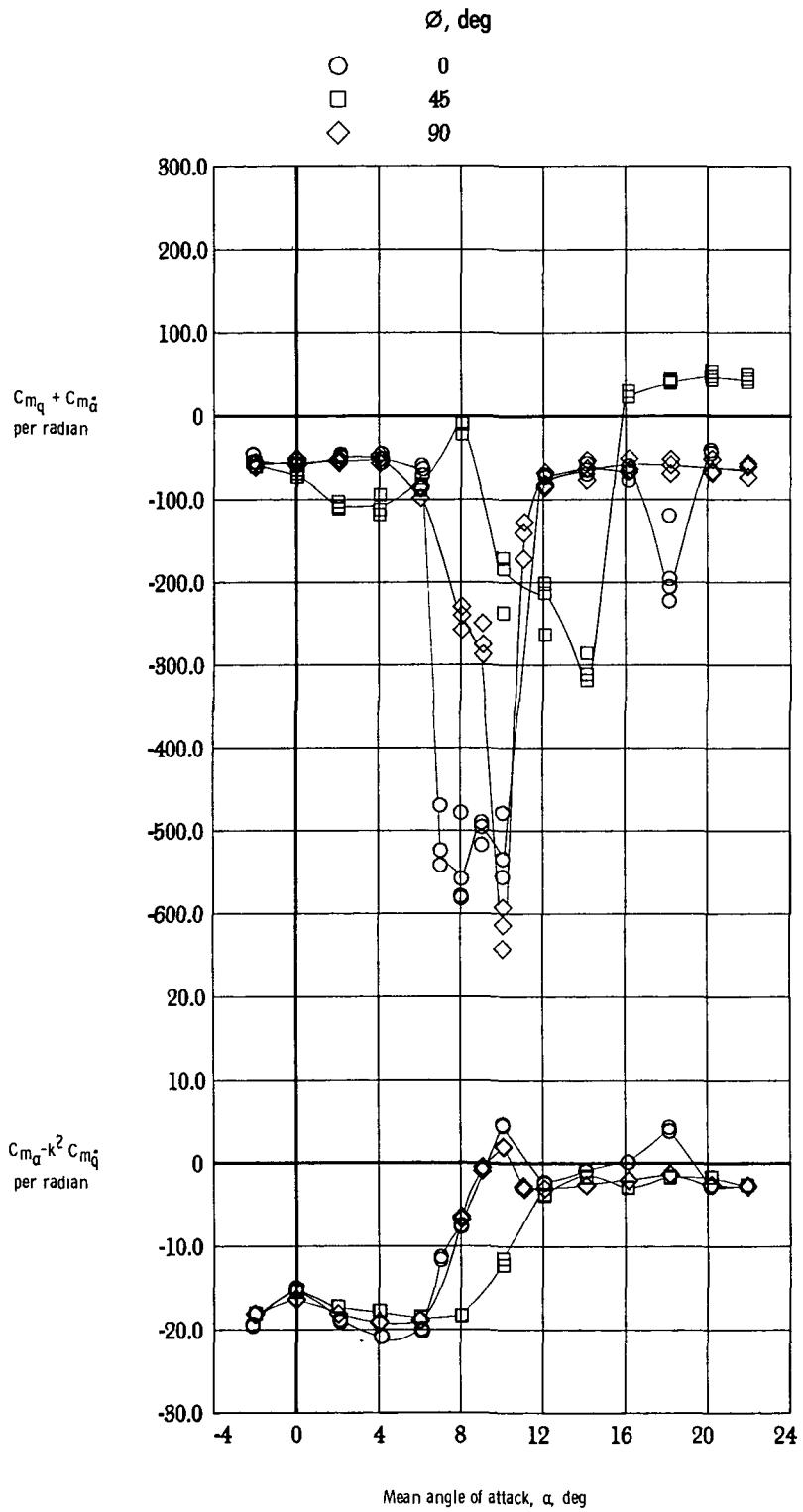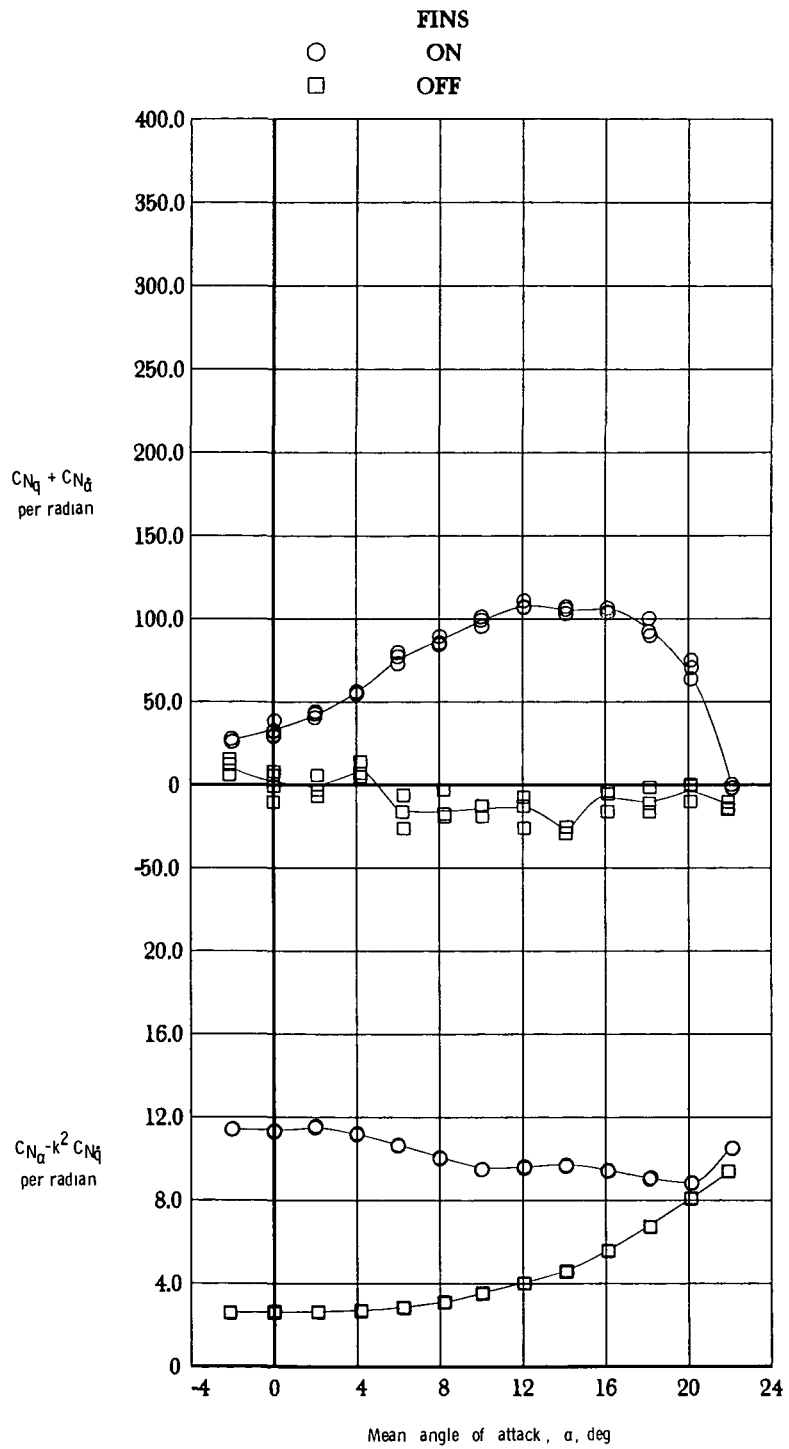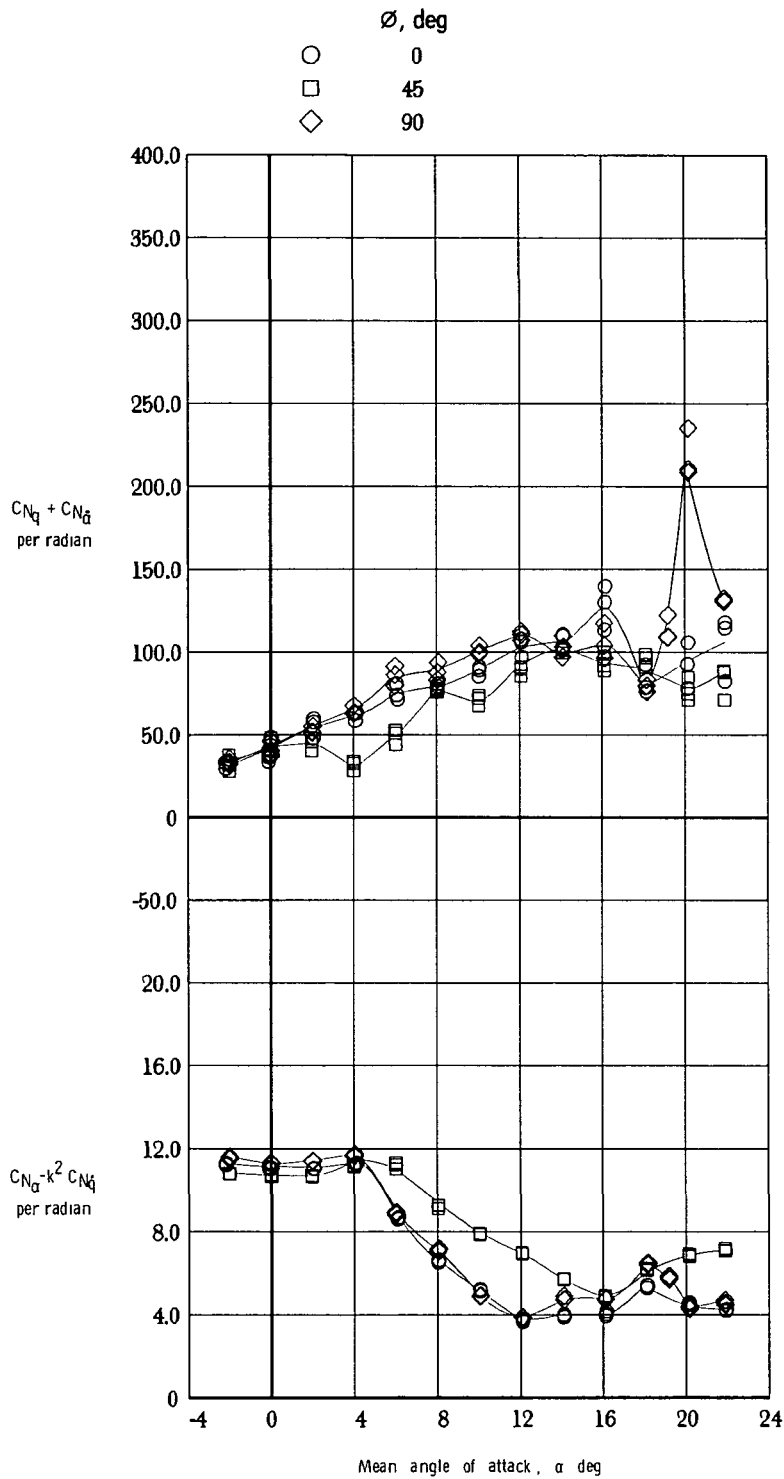
(b) $M_\infty = 0.9$.

Figure 12.- Continued.
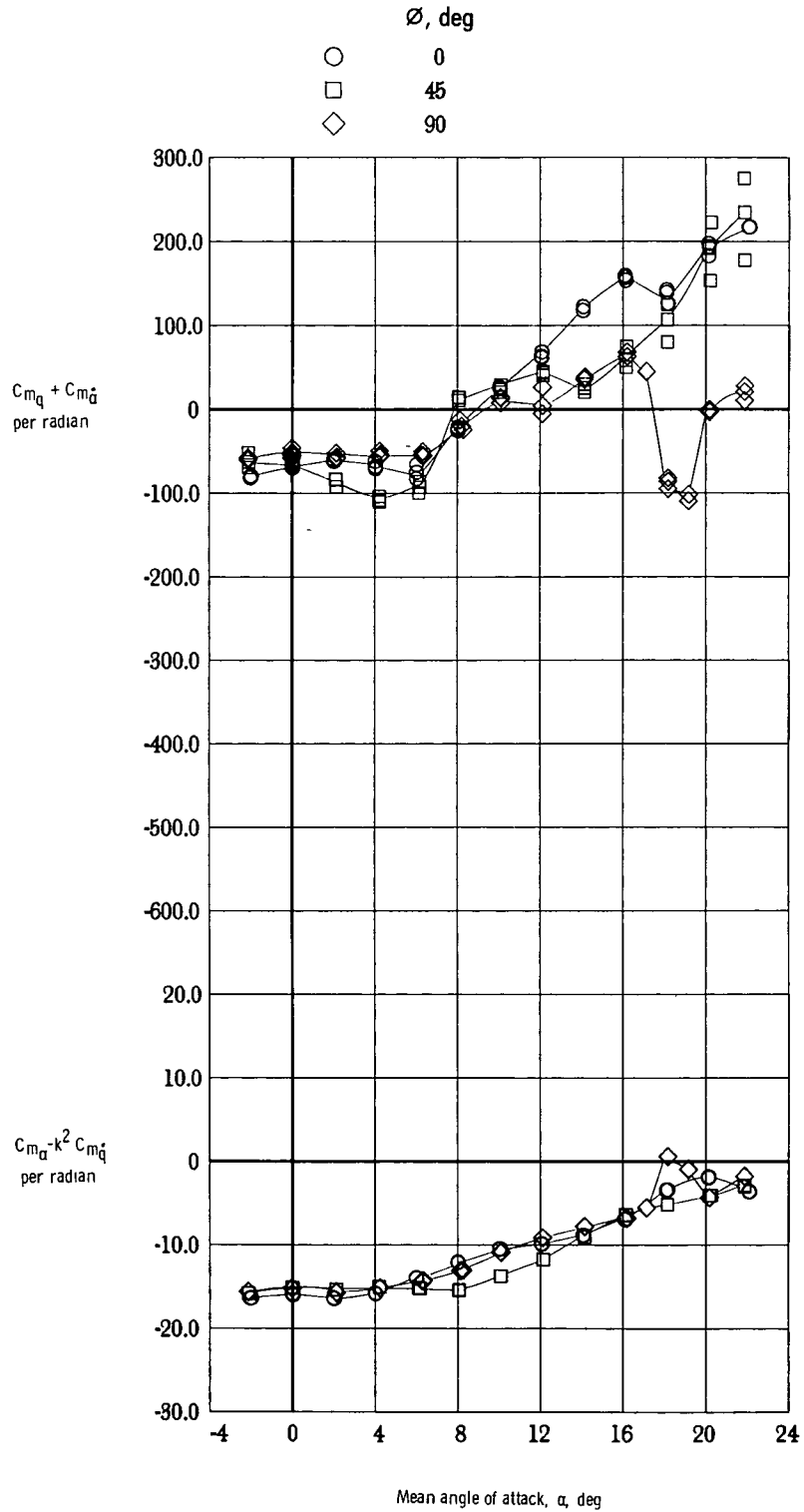
(d) $M_\infty = 1.2$.

Figure 12.- Concluded.

(a) $M_\infty = 0.7$.

Figure 13.- Effect of pitch fin deflection on damping-in-pitch parameter and on oscillatory longitudinal-stability parameter. $\phi = 0^o$; $\delta_y = 0^o$.
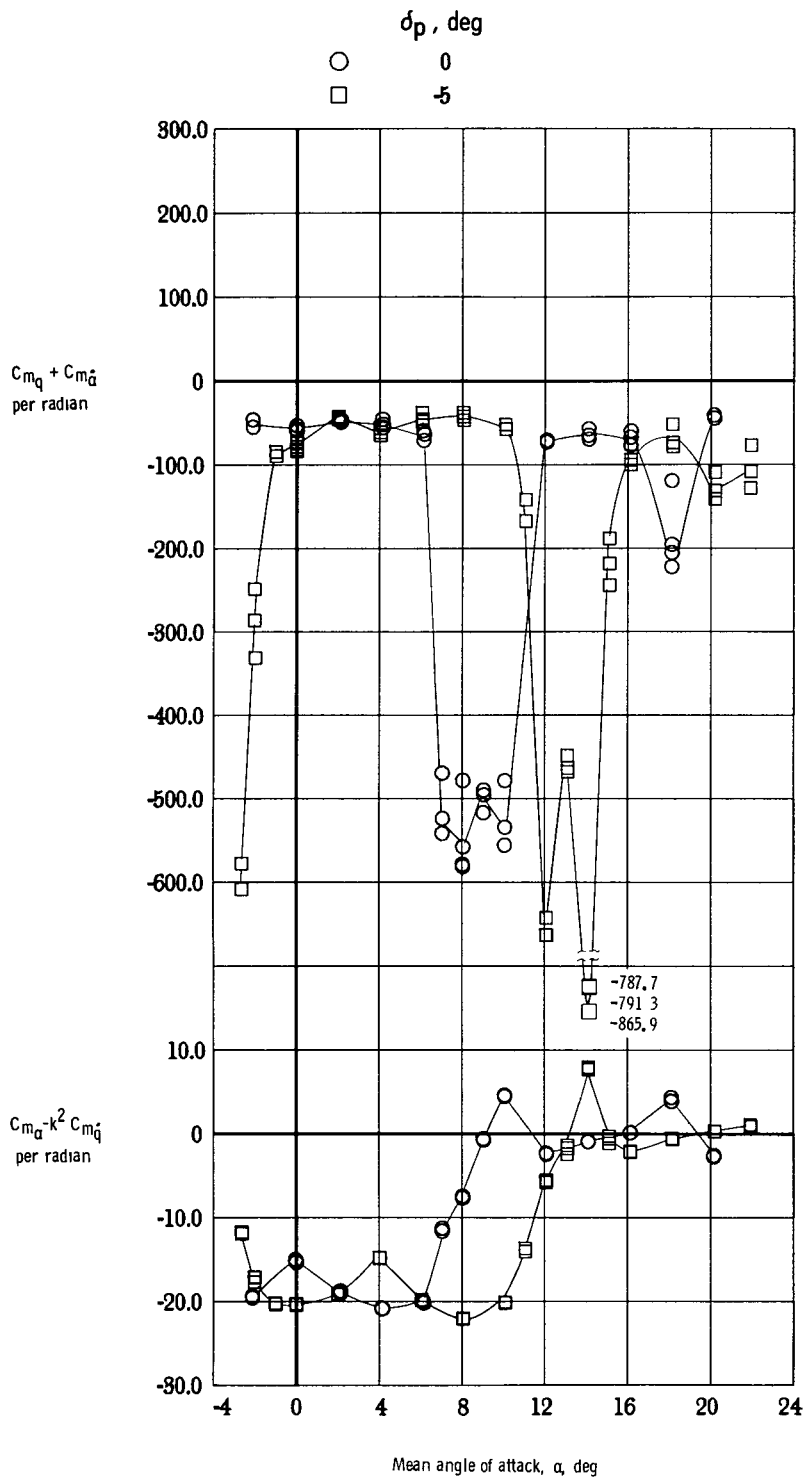
(b) $M_\infty = 0.9$.

Figure 13.- Continued.

δ_p, deg

○   0
□   -5

(c) $M_\infty = 1.1$.

Figure 13.- Continued.

δ_p , deg
○   0
□   -5

(d) $M_\infty = 1.2$.

Figure 13.- Concluded.

$C_{N_q} + C_{N_{\dot\alpha}}$
per radian

$C_{N_\alpha} - k^2 C_{N_{\dot q}}$
per radian

Mean angle of attack, α, deg
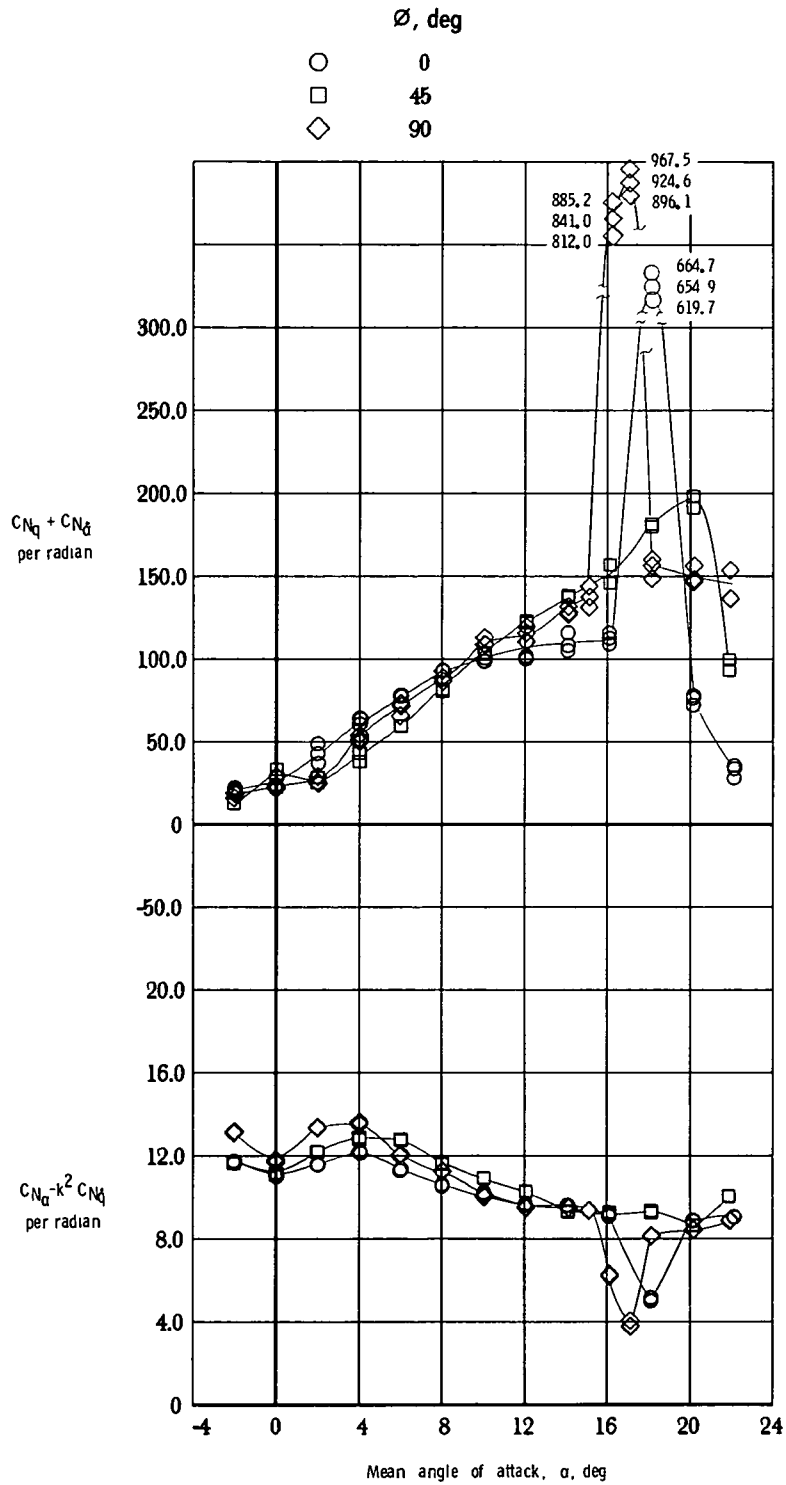
(a) $M_\infty = 0.7$.

Figure 14.- Effect of tail fins on normal force due to pitch rate parameter and on normal force due to pitch displacement parameter. $\phi = 0^\circ$; $\delta_p = 0^\circ$; $\delta_y = 0^\circ$.

55

FINS
○   ON
□   OFF

$C_{N_q} + C_{N_{\dot{\alpha}}}$ per radian

$C_{N_\alpha} - k^2 C_{N_{\dot{q}}}$ per radian

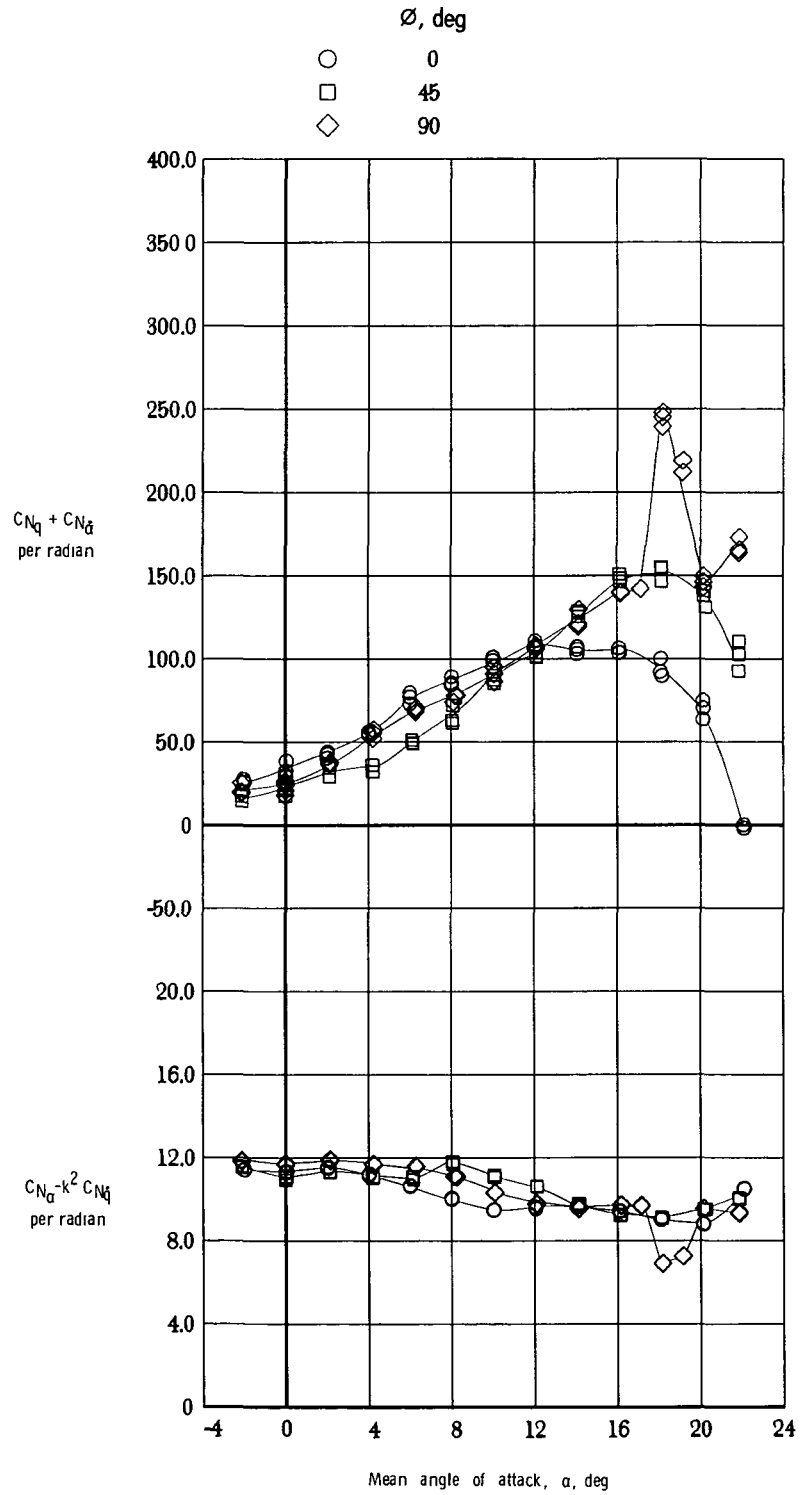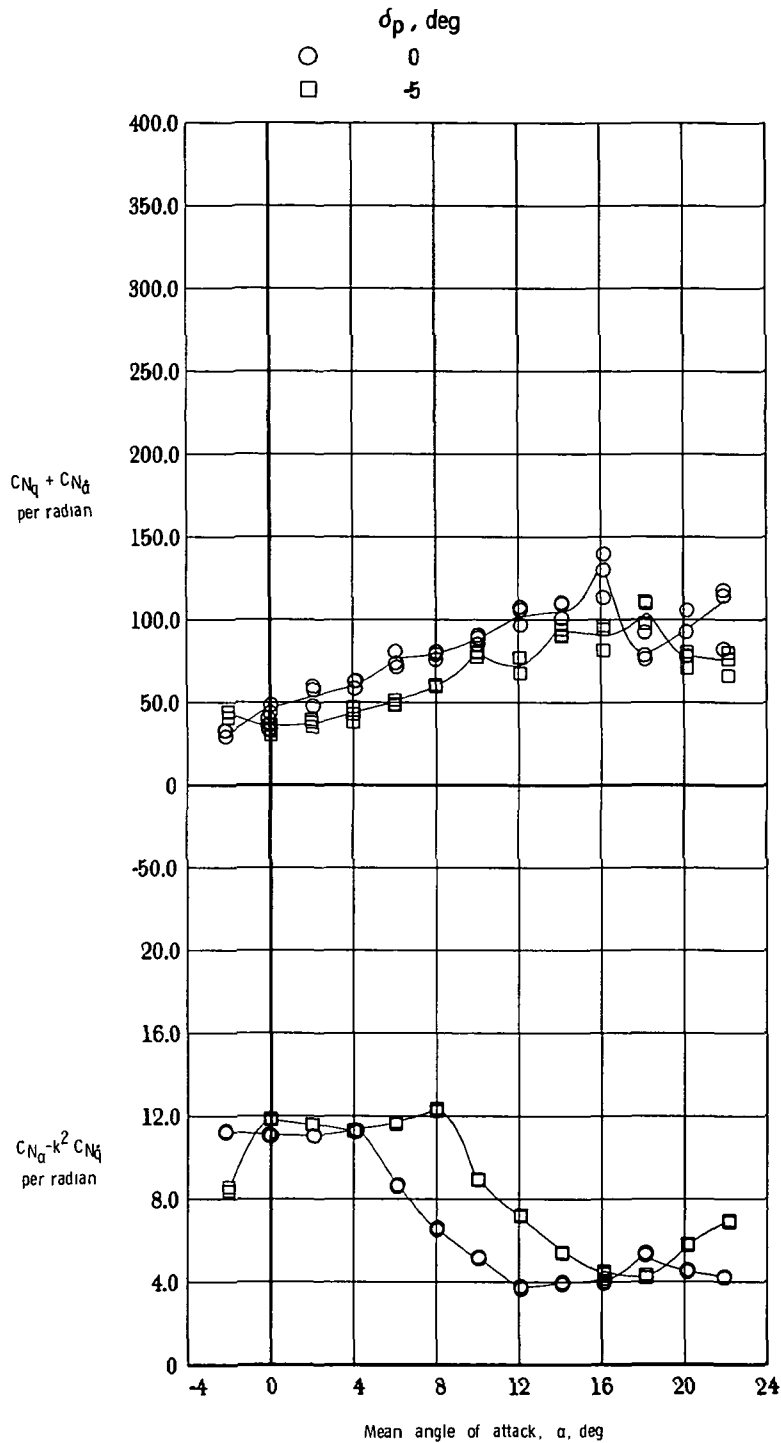Mean angle of attack, α, deg

(b) $M_\infty = 0.9$.

Figure 14.- Continued.

(c) $M_\infty = 1.1$.

Figure 14.- Continued.

(d) $M_\infty = 1.2$.

Figure 14.- Concluded.

(a) $M_\infty = 0.7$.

Figure 15.- Effect of configuration roll angle on normal force due to pitch rate parameter and on normal force due to pitch displacement parameter. $\delta_p = 0^\circ$; $\delta_y = 0^\circ$.
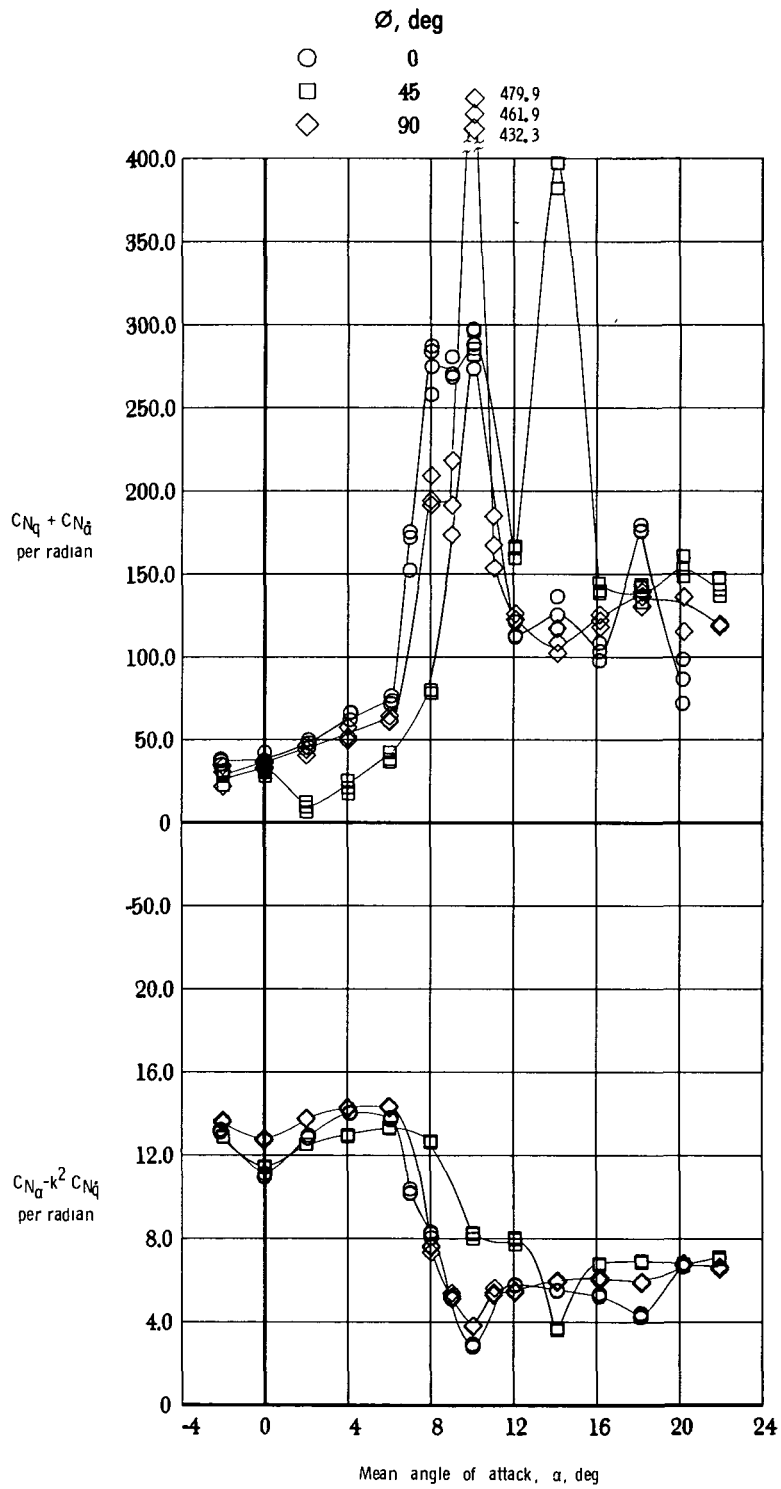
(b) $M_{\infty} = 0.9$.

Figure 15.- Continued.

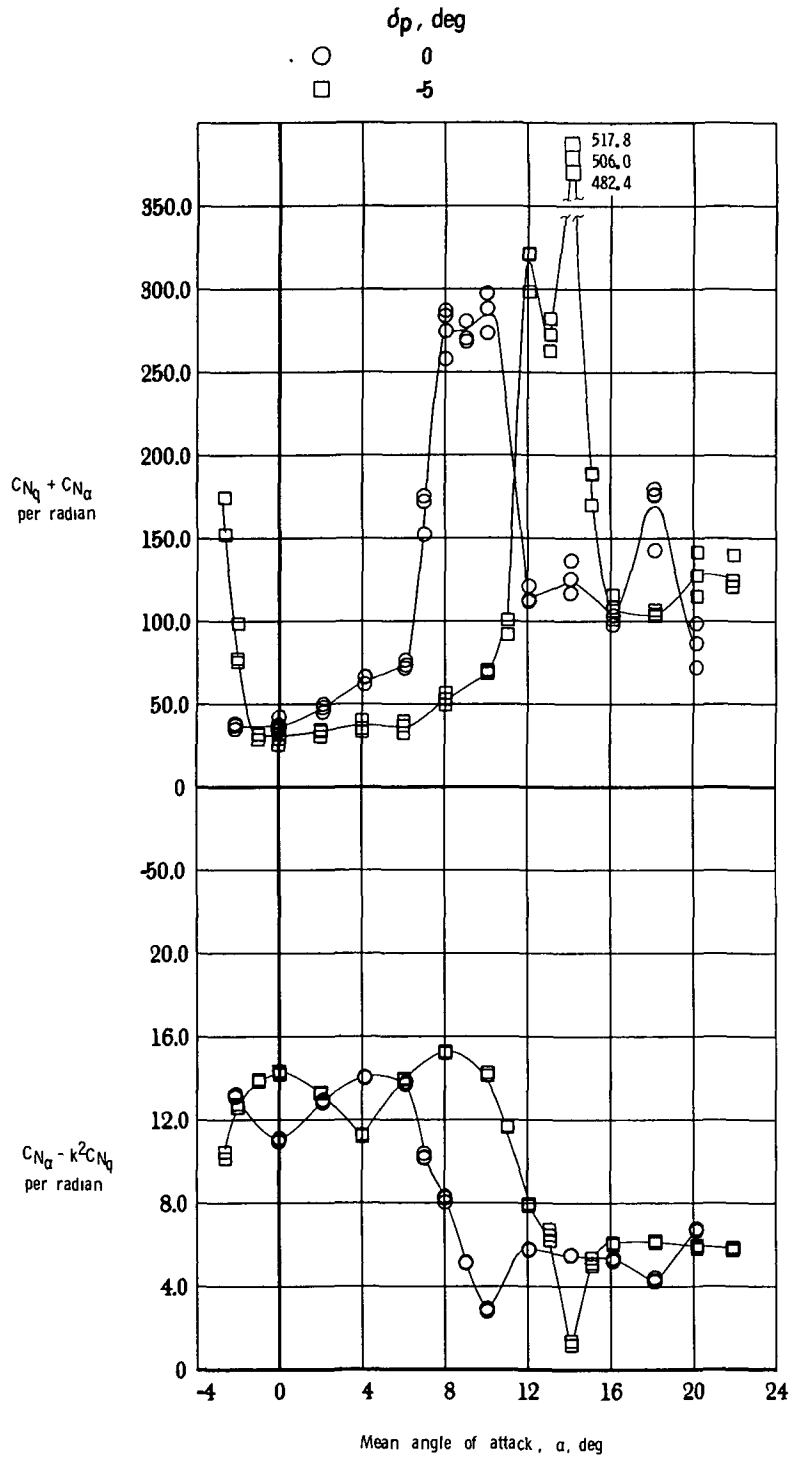(c) $M_\infty = 1.1$.

Figure 15.- Continued.

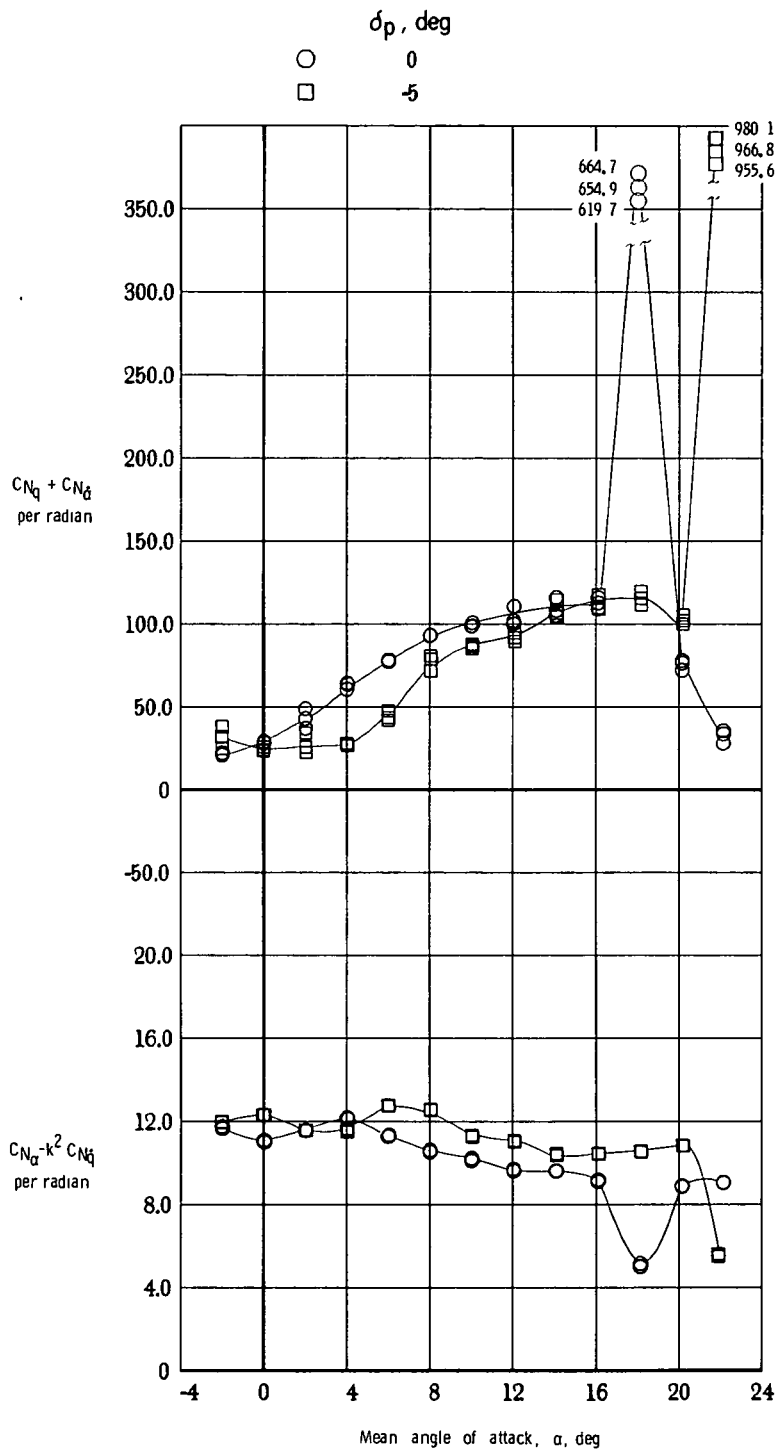(d) $M_\infty = 1.2$.

Figure 15.- Concluded.

(a) $M_\infty = 0.7$.

Figure 16.- Effect of pitch fin deflection on normal force due to pitch rate parameter and on normal force due to pitch displacement parameter. $\phi = 0^o$; $\delta_y = 0^o$.

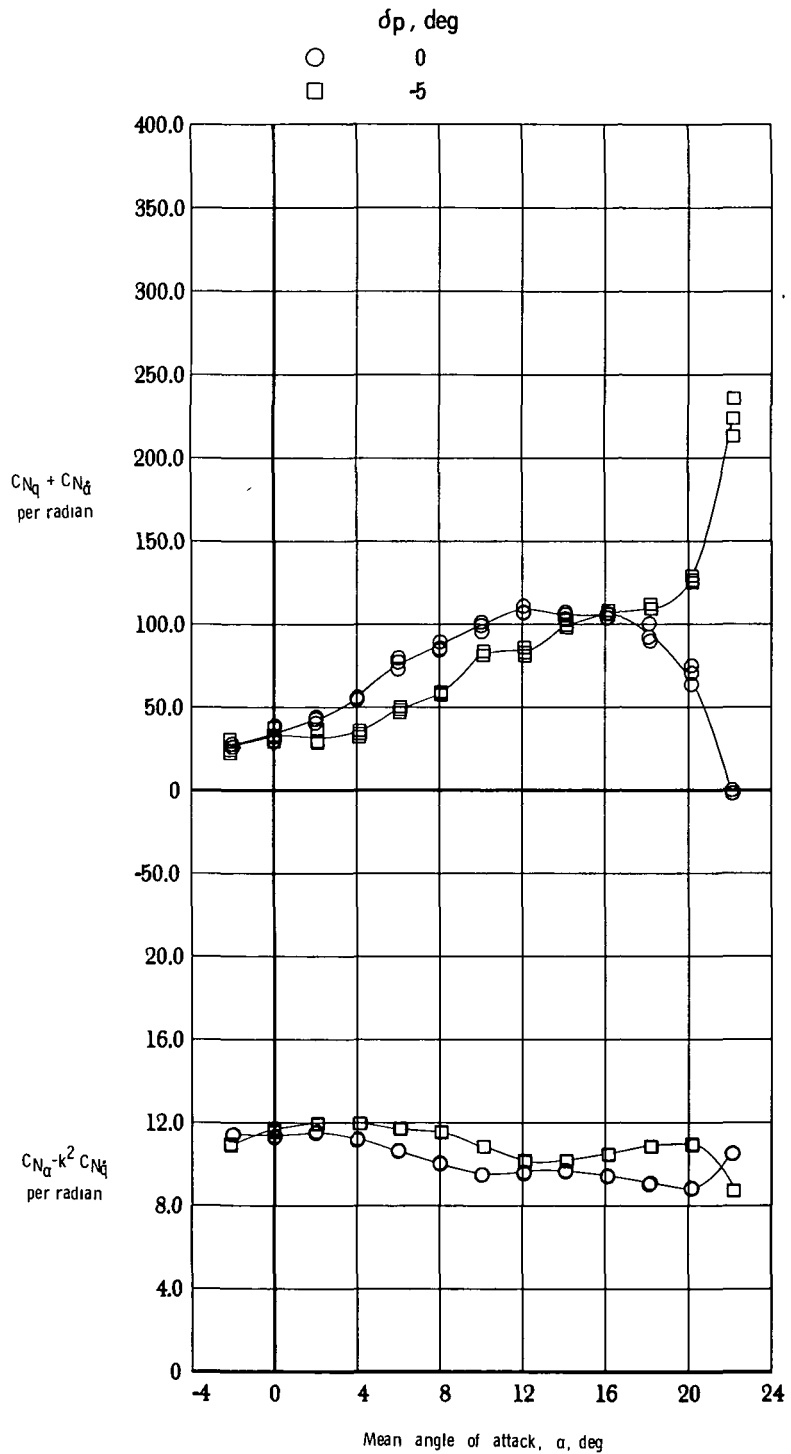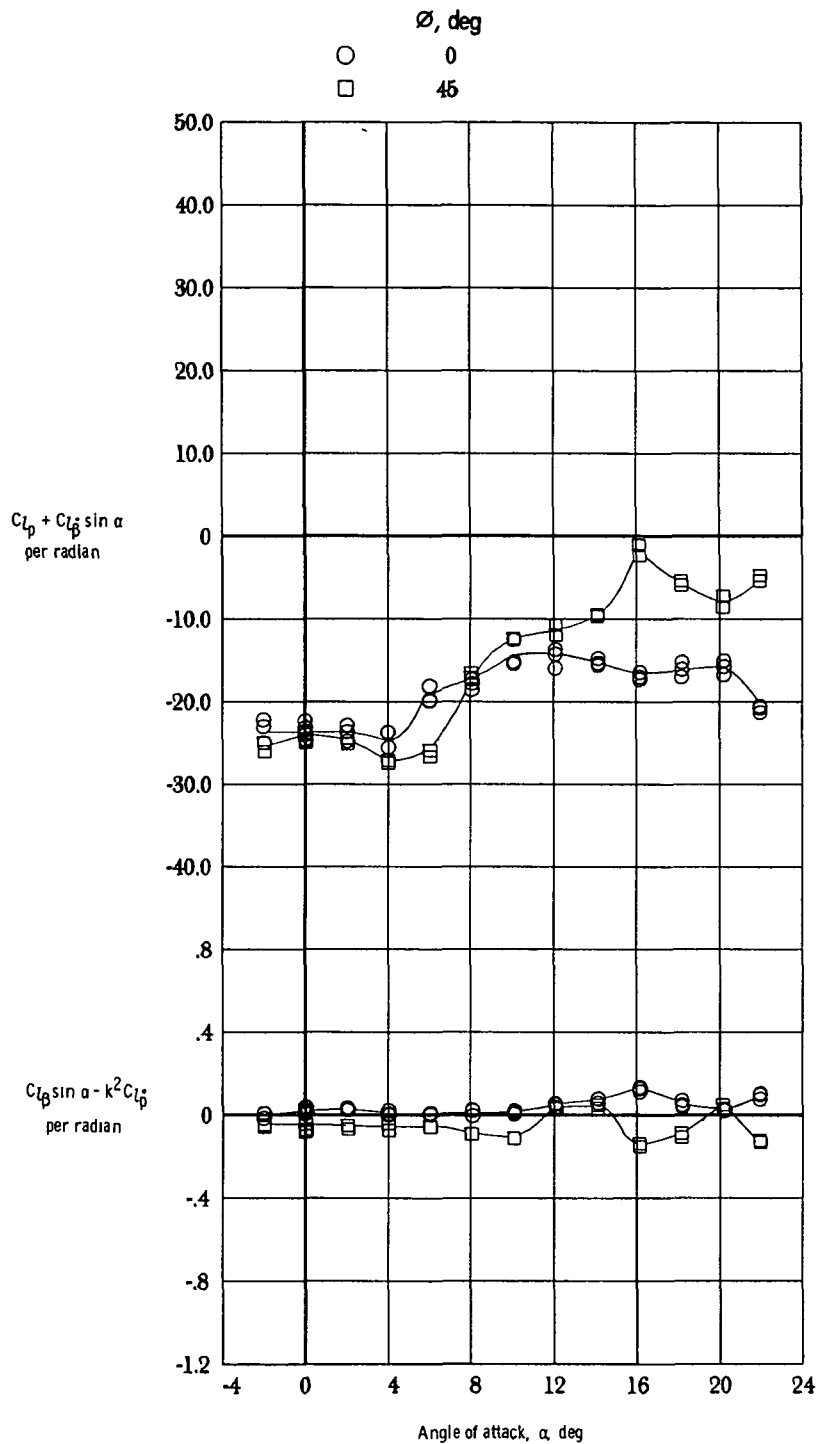δ_p, deg

○   0
□   -5

517.8
506.0
482.4

350.0
300.0
250.0
200.0
$C_{N_q} + C_{N_{\dot\alpha}}$
per radian
150.0
100.0
50.0
0
-50.0

20.0
16.0
$C_{N_\alpha} - k^2 C_{N_q}$
per radian
12.0
8.0
4.0
0

-4   0   4   8   12   16   20   24

Mean angle of attack, α, deg

(b) $M_\infty = 0.9$.

Figure 16.- Continued.

64

(c) M_∞ = 1.1.

Figure 16.- Continued.

(d) $M_\infty = 1.2$.

Figure 16.- Concluded.

$C_{l_p} + C_{l_{\dot{\beta}}} \sin \alpha$
per radian

$C_{l_\beta} \sin \alpha - k^2 C_{l_{\dot{p}}}$
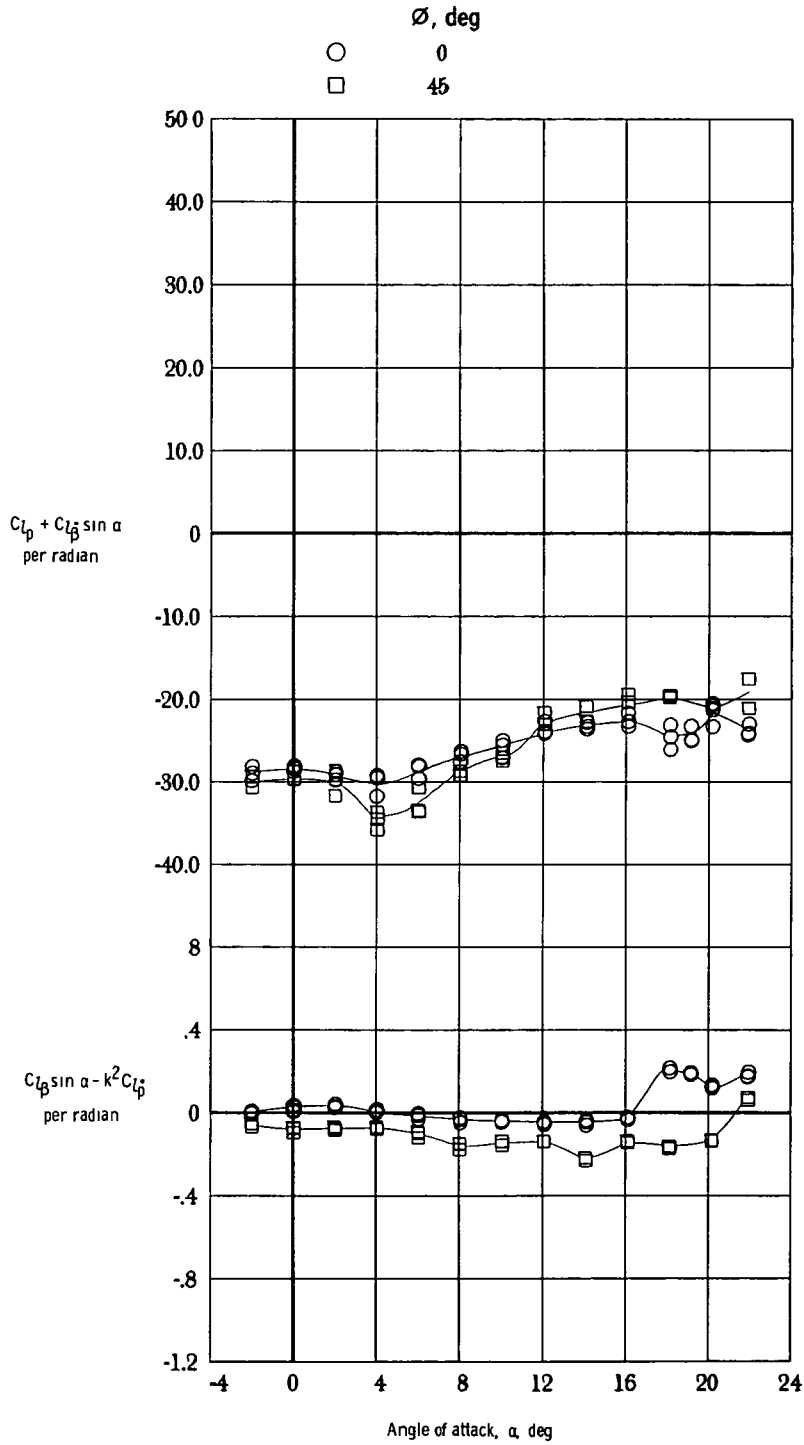per radian

Angle of attack, α, deg

(a) $M_\infty = 0.7$.

Figure 17.- Effect of configuration roll angle on damping in roll parameter and on rolling moment due to roll displacement parameter. $\delta_p = 0^\circ$; $\delta_y = 0^\circ$.
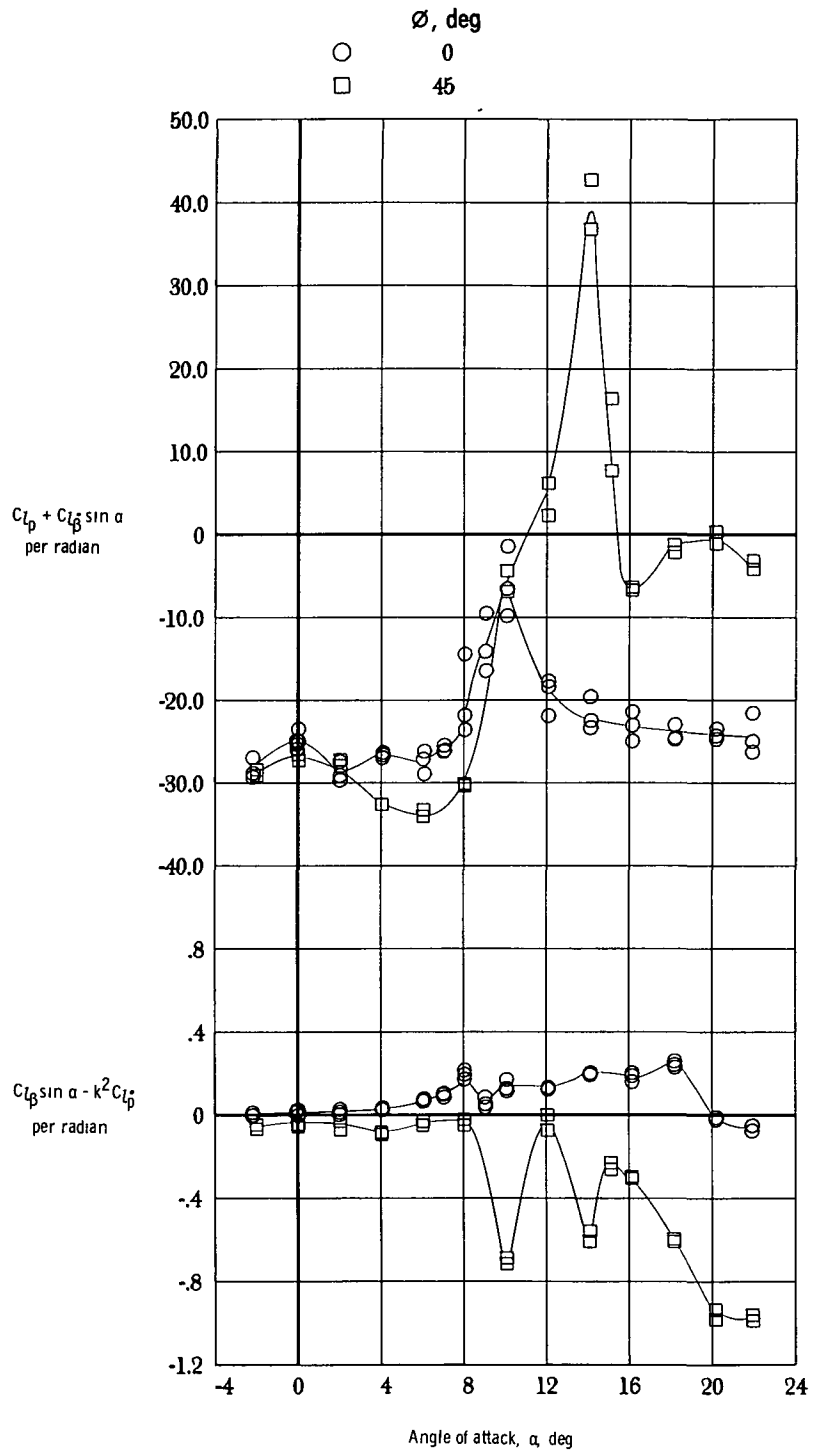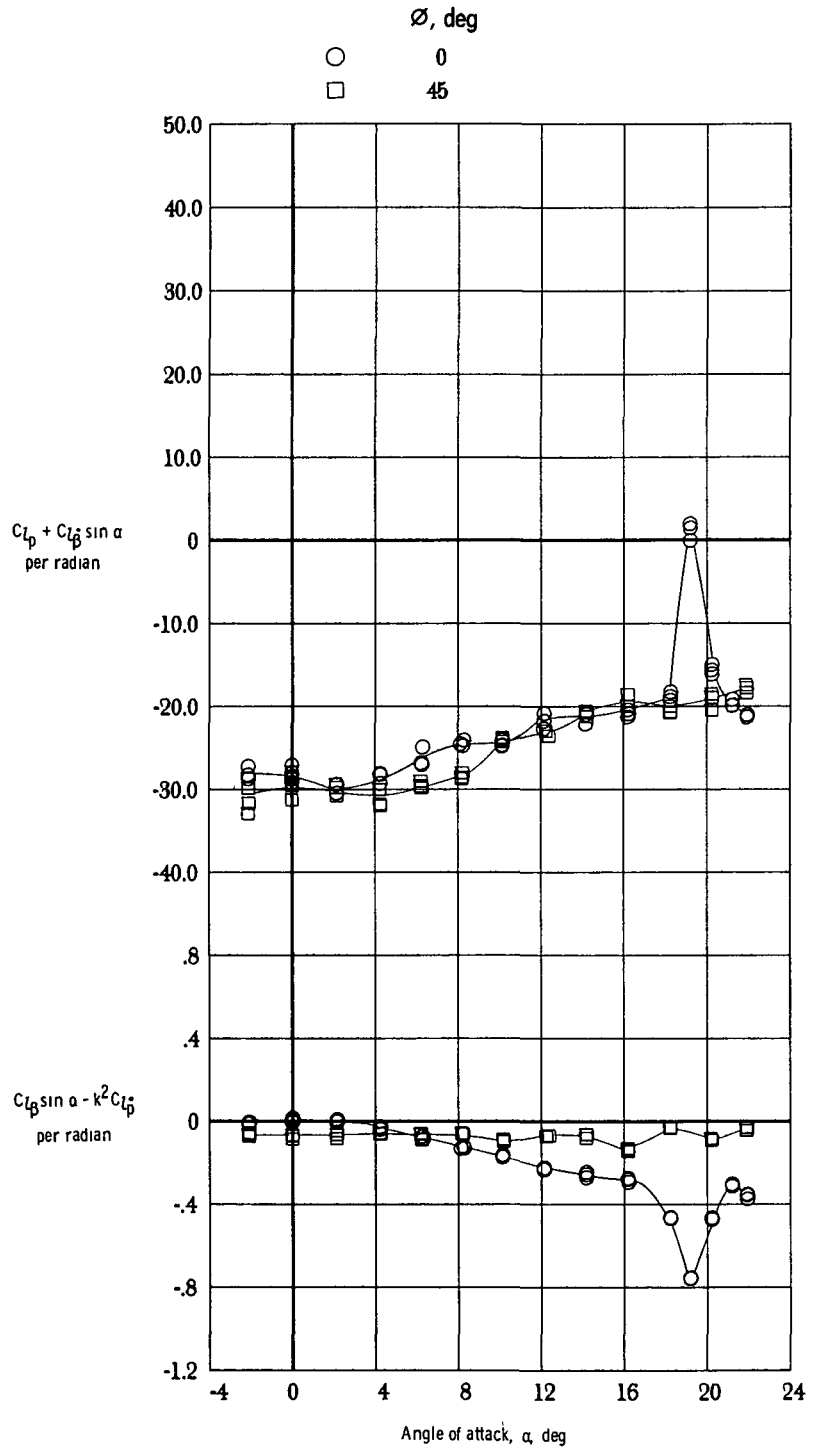
(b) $M_\infty = 0.9$.

Figure 17.- Continued.

(c) $M_{\infty} = 1.1$.

Figure 17.- Continued.

Figure 17.- Concluded.
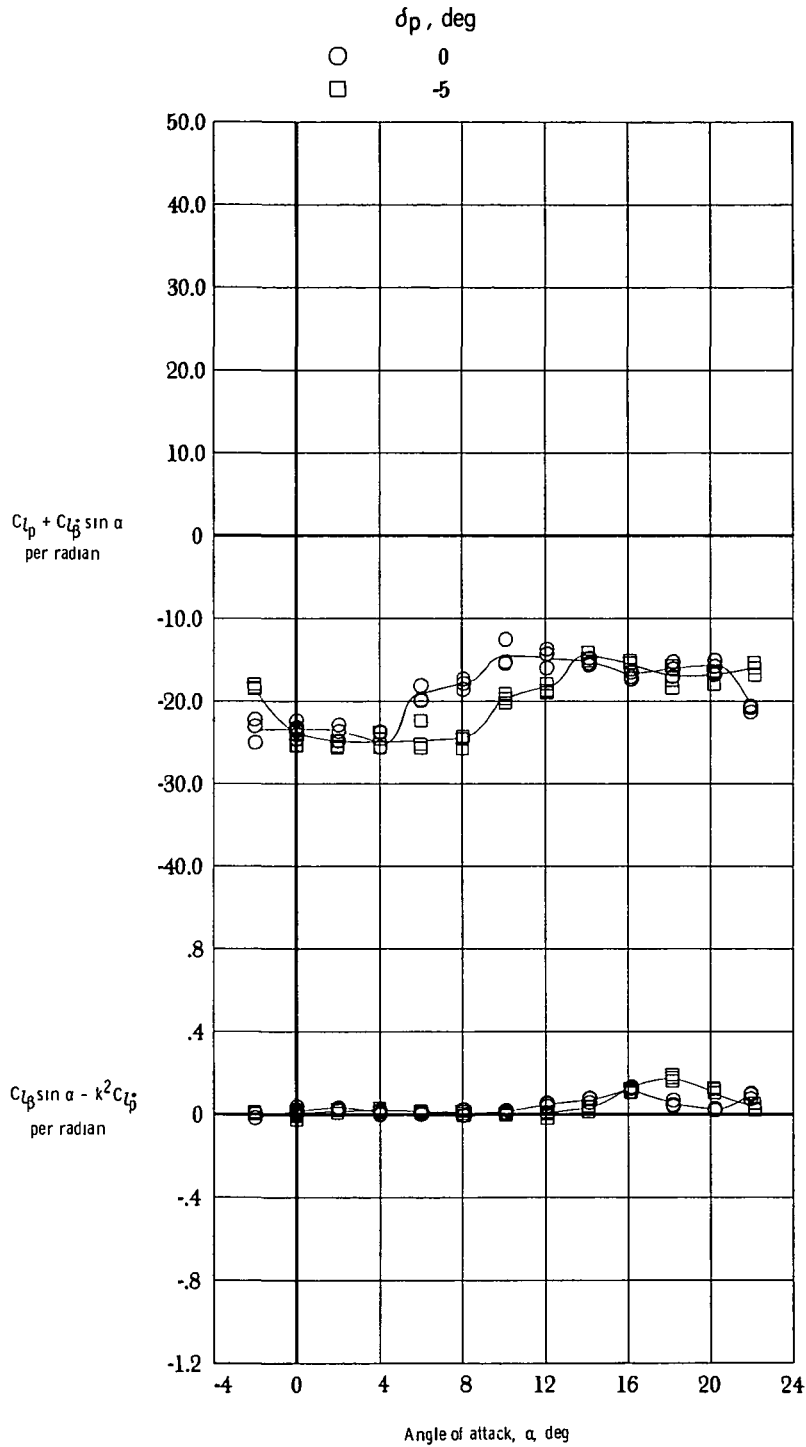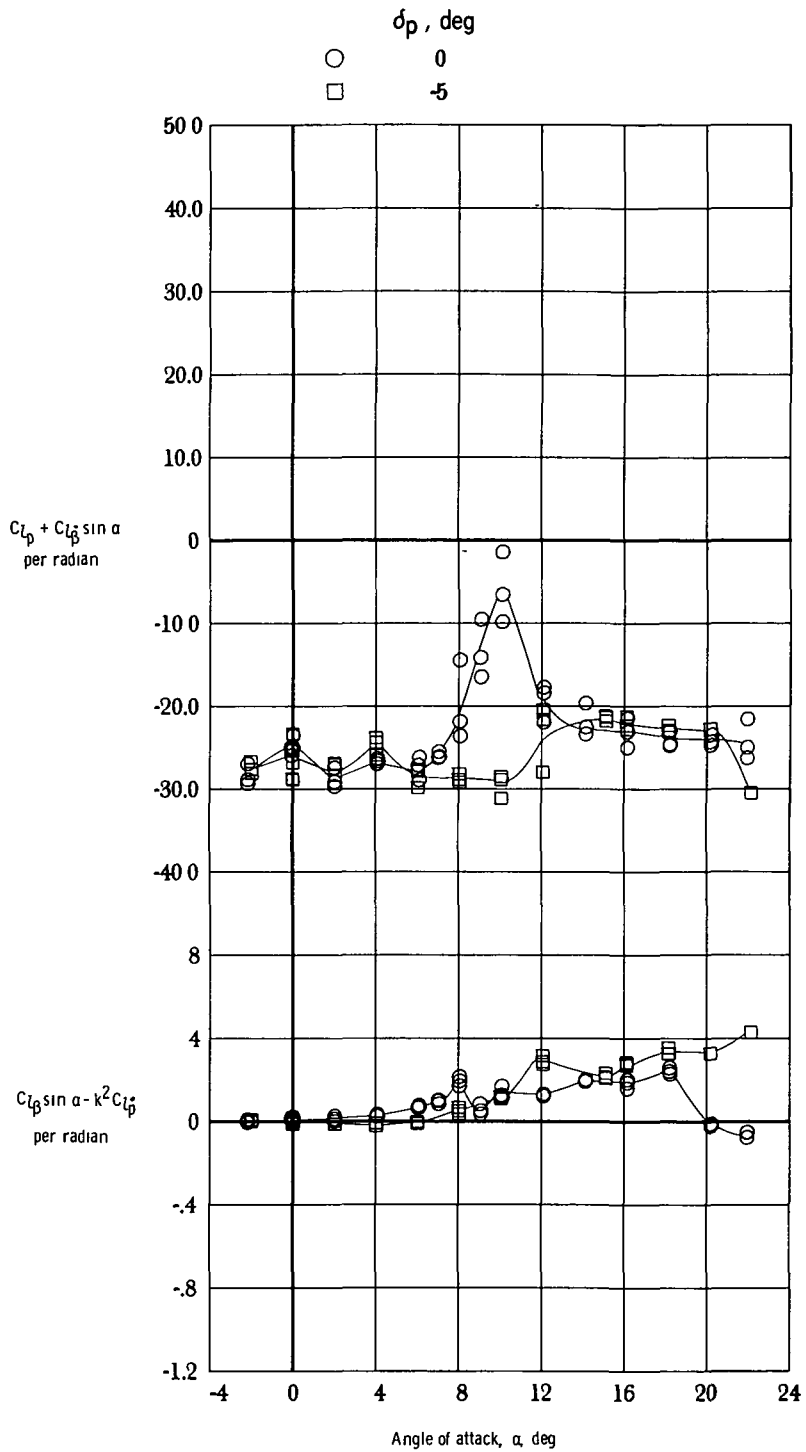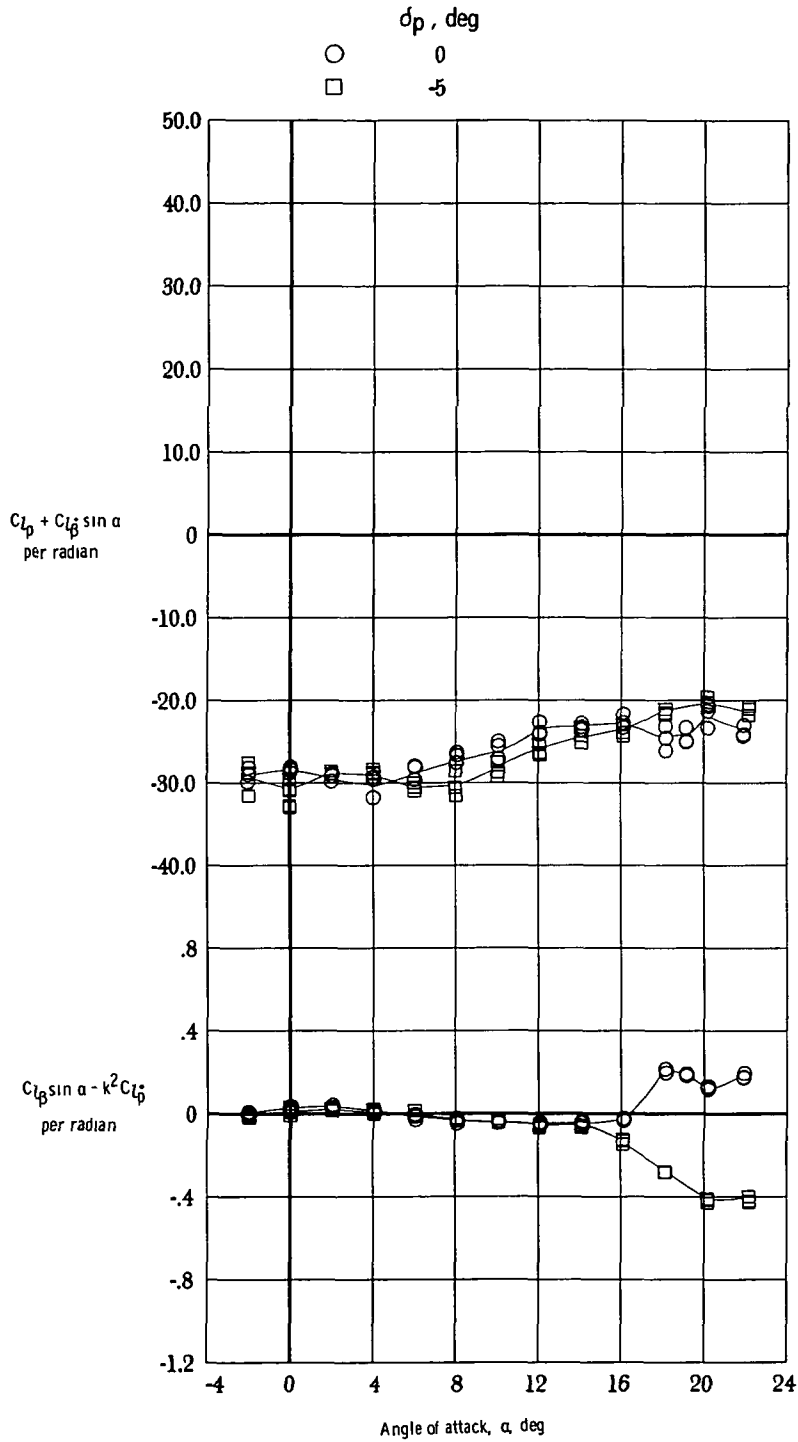
(a) $M_\infty = 0.7$.

Figure 18.- Effect of pitch fin deflection on damping-in-roll parameter and on rolling moment due to roll displacement parameter. $\phi = 0^\circ$; $\delta_y = 0^\circ$.

(b) $M_{\infty} = 0.9$.

Figure 18.- Continued.

(c) $M_\infty = 1.1.$

Figure 18.- Continued.

(d) M_∞ = 1.2.

Figure 18.- Concluded.

(a) $M_\infty = 0.7$.

Figure 19.- Effect of yaw fin deflection on damping-in-roll parameter and on rolling moment due to roll displacement parameter. $\phi = 0^\circ$; $\delta_p = 0^\circ$.

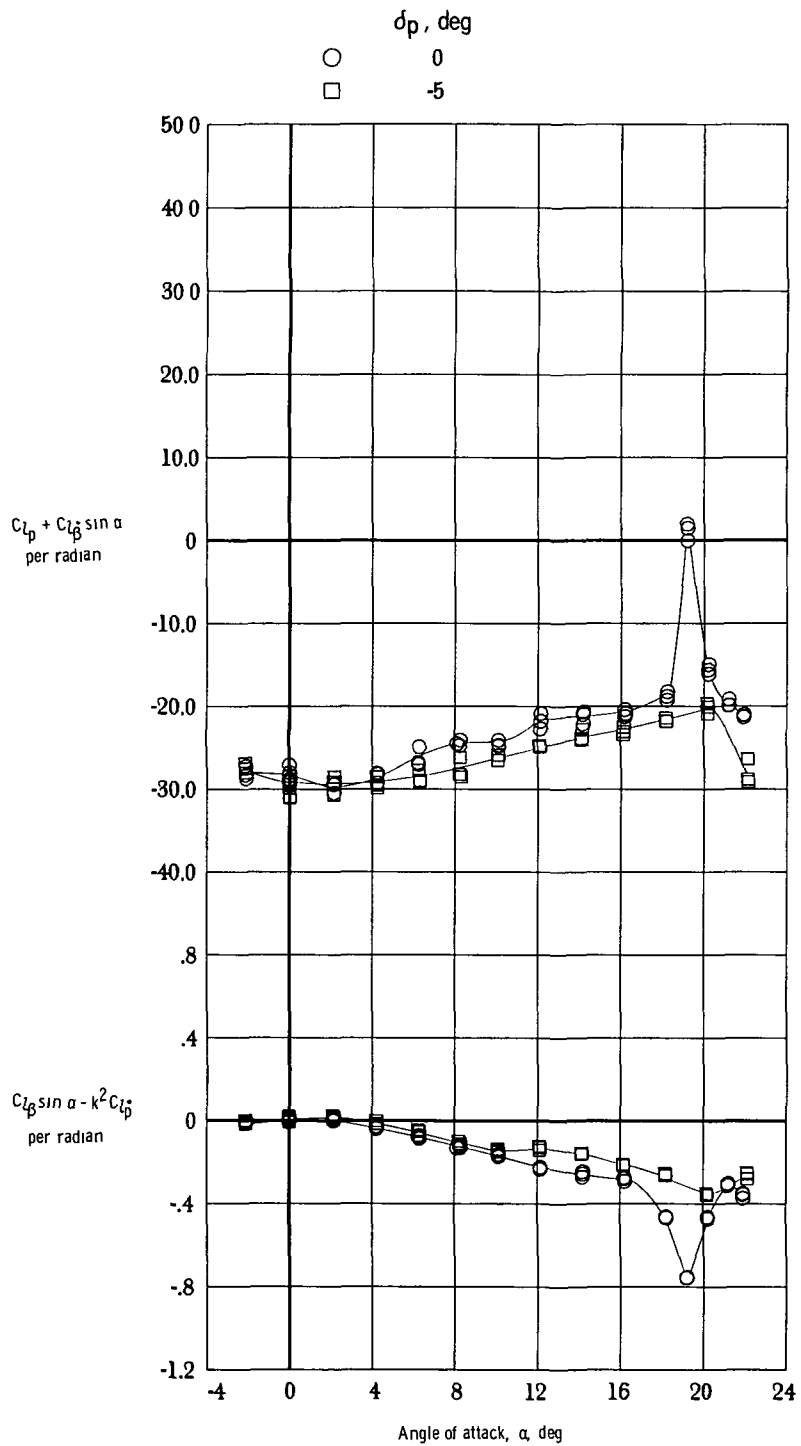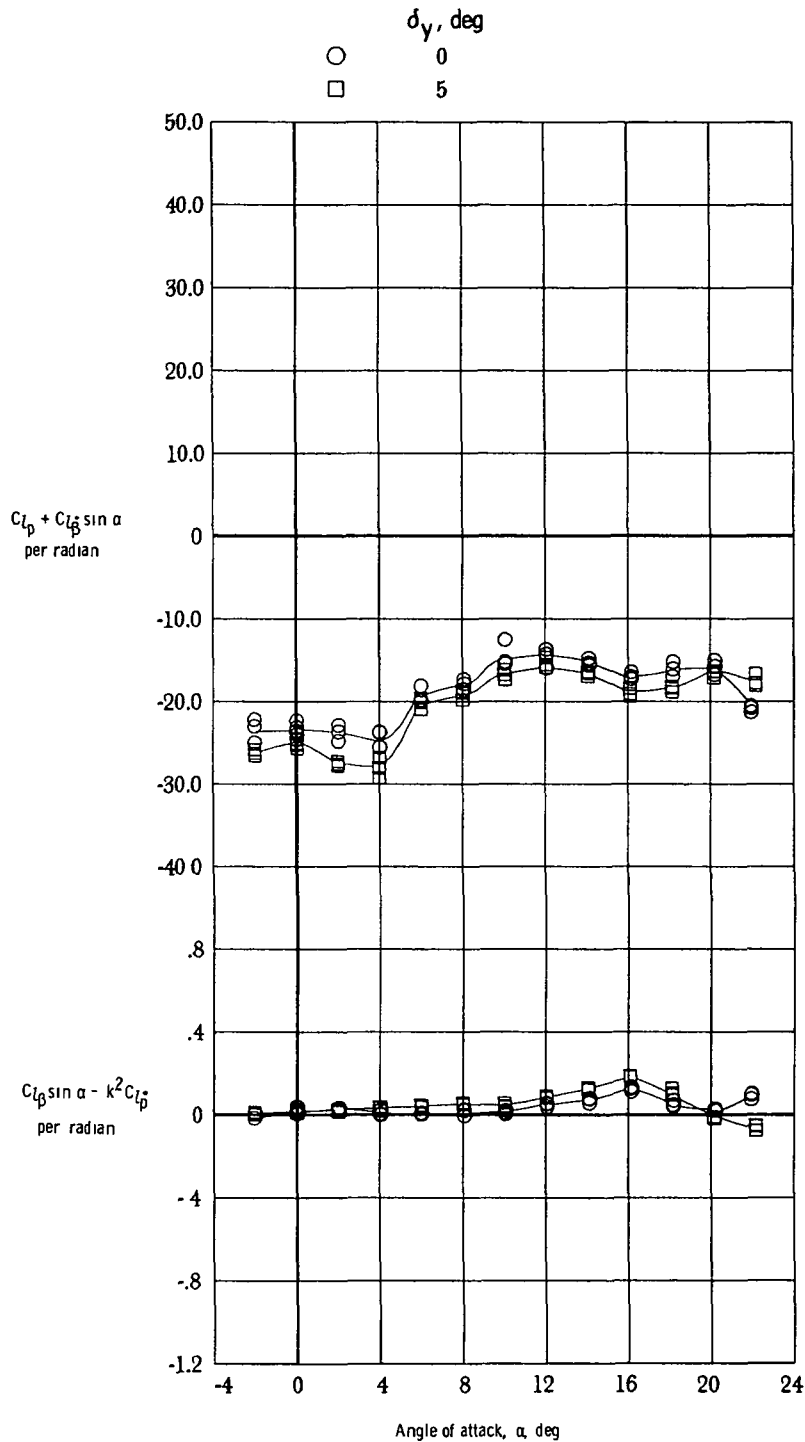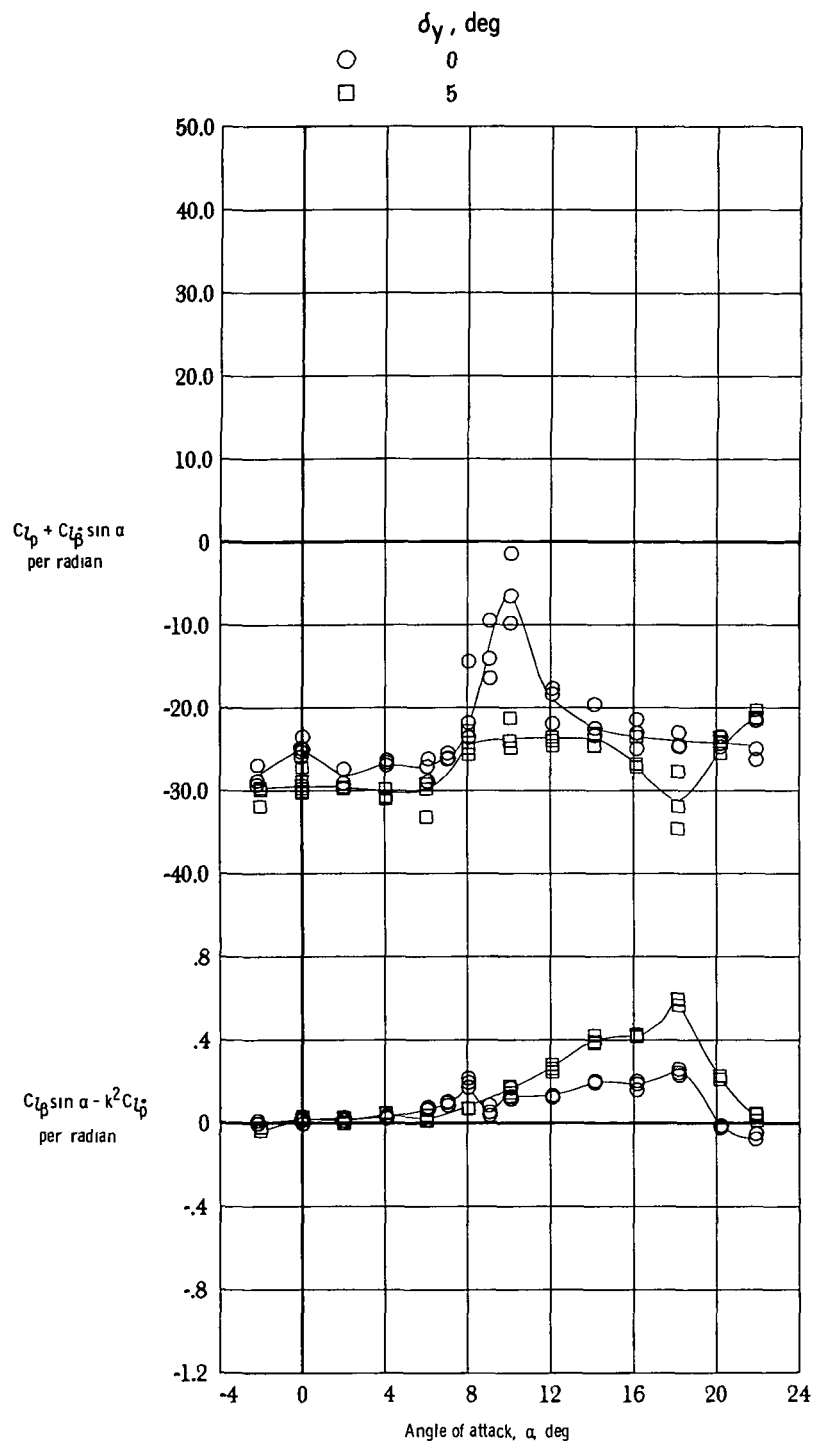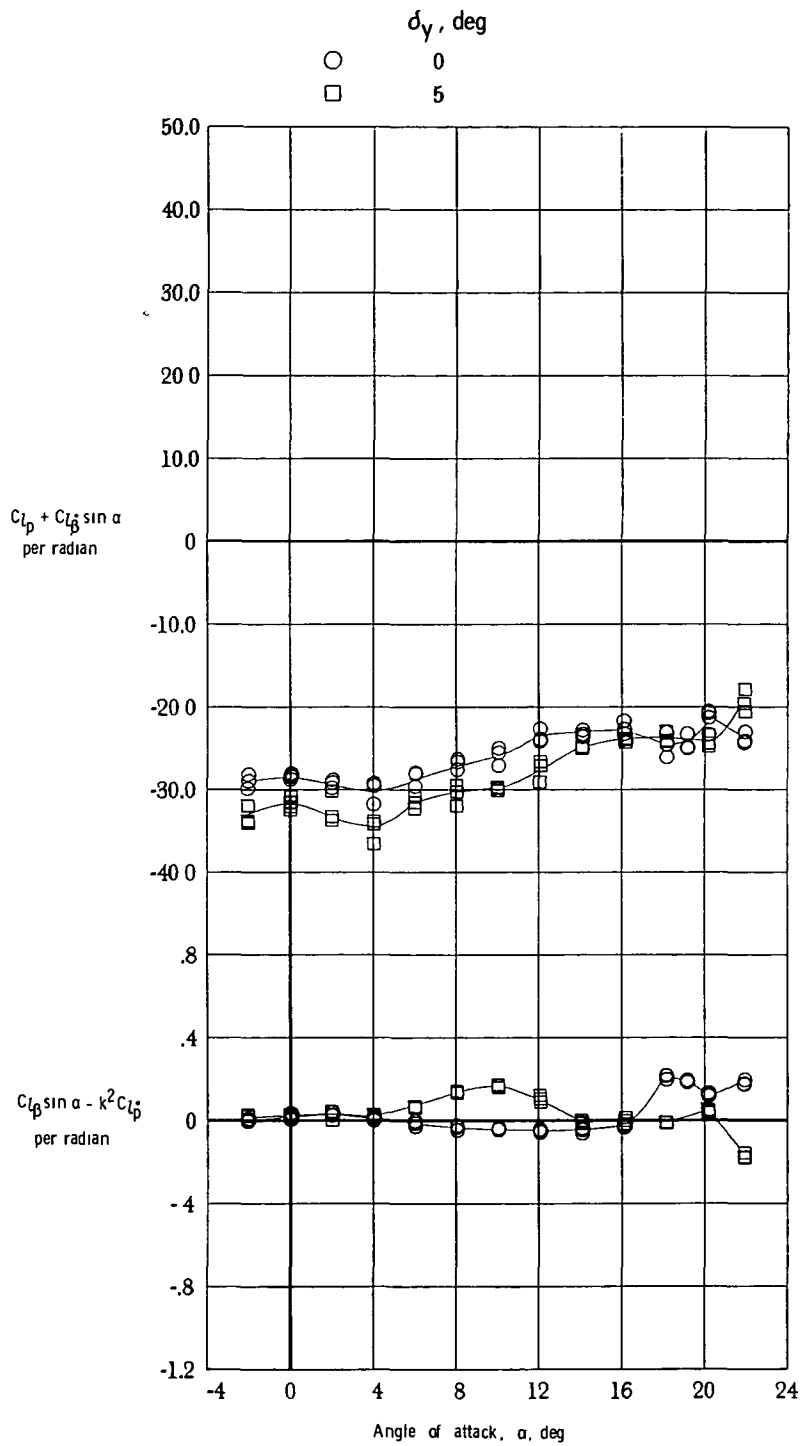(b) $M_\infty = 0.9$.

Figure 19.- Continued.

○   0
□   5

50.0

40.0

30.0

20 0

10.0

$C_{l_p} + C_{l_{\dot{\beta}}} \sin \alpha$
per radian

0

-10.0

-20 0

-30.0

-40 0

.8

.4

$C_{l_\beta} \sin \alpha - k^2 C_{l_{\dot{p}}}$
per radian

0

- 4

-.8

-1.2

-4   0   4   8   12   16   20   24

Angle of attack, α, deg

(c) $M_\infty = 1.1$.

Figure 19.- Continued.
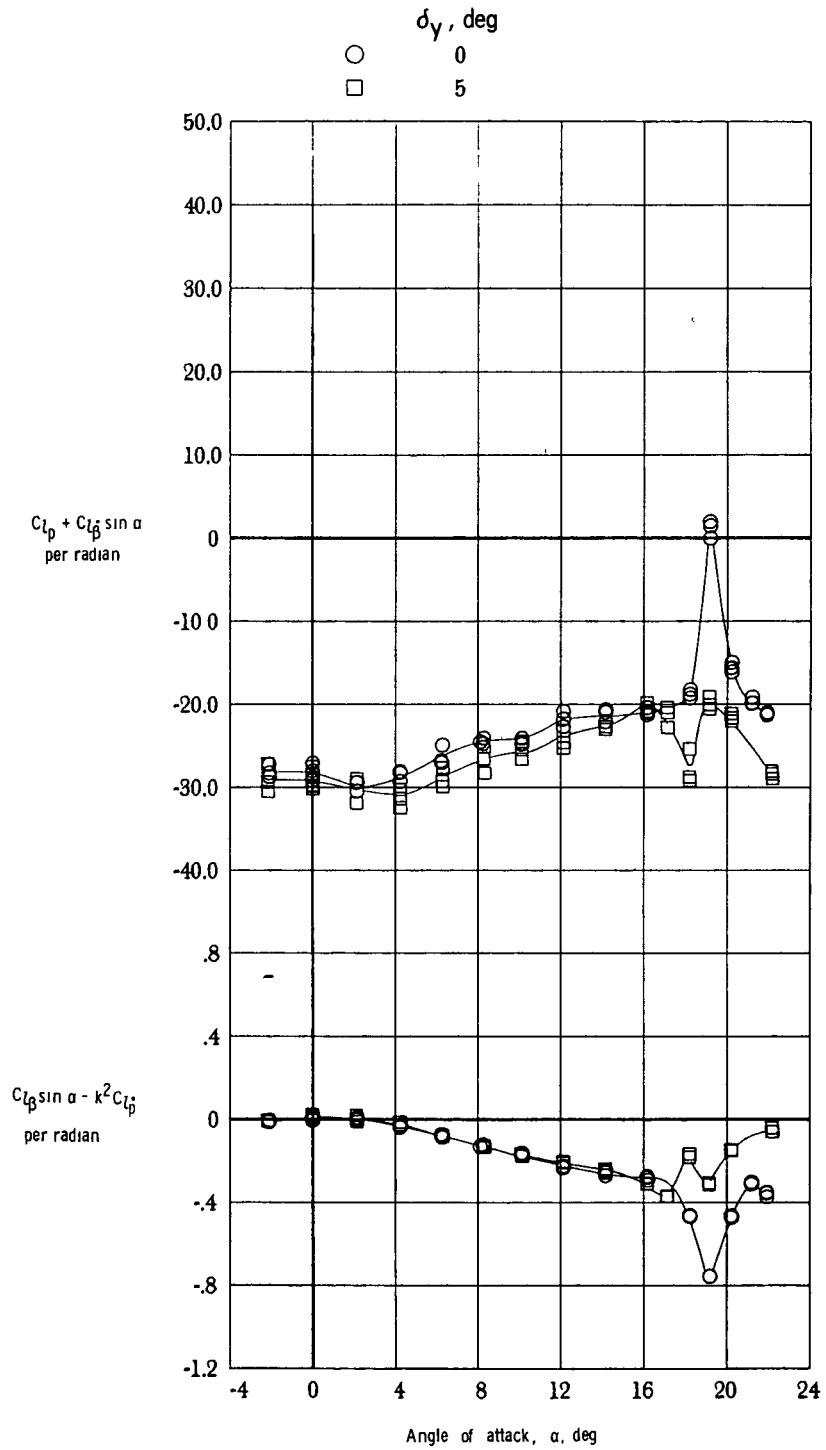
(d) $M_\infty = 1.2$.

Figure 19.- Concluded.

Configuration	Vortex lattice C_{m_q} C_{m_α}	Static test C_{m_α}	Dynamic test $C_{m_q} + C_{m_{\dot\alpha}}$ $C_{m_\alpha} - k^2 C_{m_{\dot q}}$
$\phi = 0°$	$- - - - -$	$\bigcirc$	$\square$
$\phi = 45°$	$——\,-\,——$	$\diamondsuit$	$\triangle$

C_{m_q} ,

$C_{m_q} + C_{m_{\dot\alpha}}$
per radian

C_{m_α} ,

$C_{m_\alpha} - k^2 C_{m_{\dot q}}$
per radian

Mach number
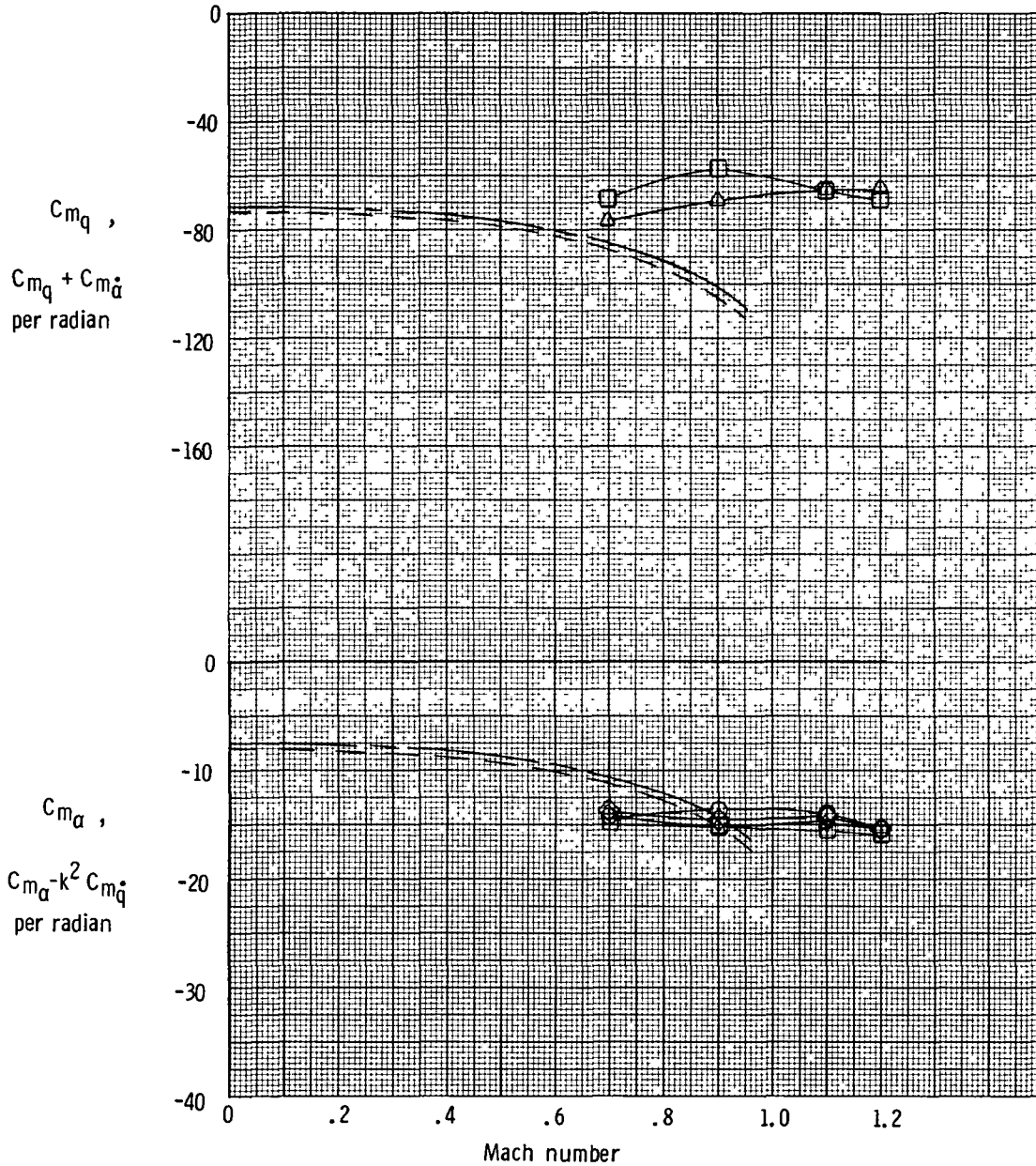
(a) Damping in pitch and longitudinal stability.

Figure 20.- Comparison of static and dynamic experimental results with vortex-lattice theoretical estimates. $\alpha = 0°$; fins on.

79

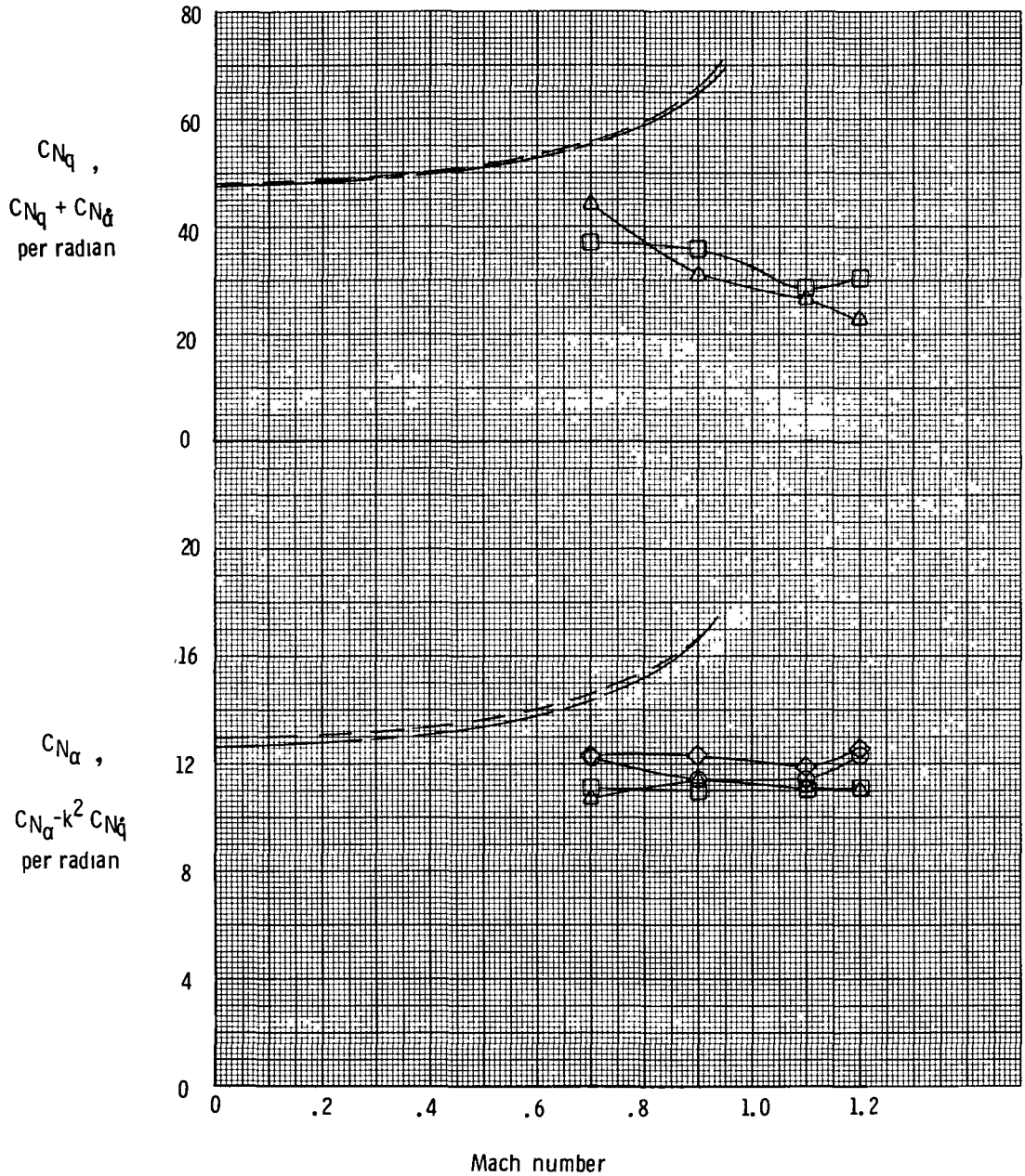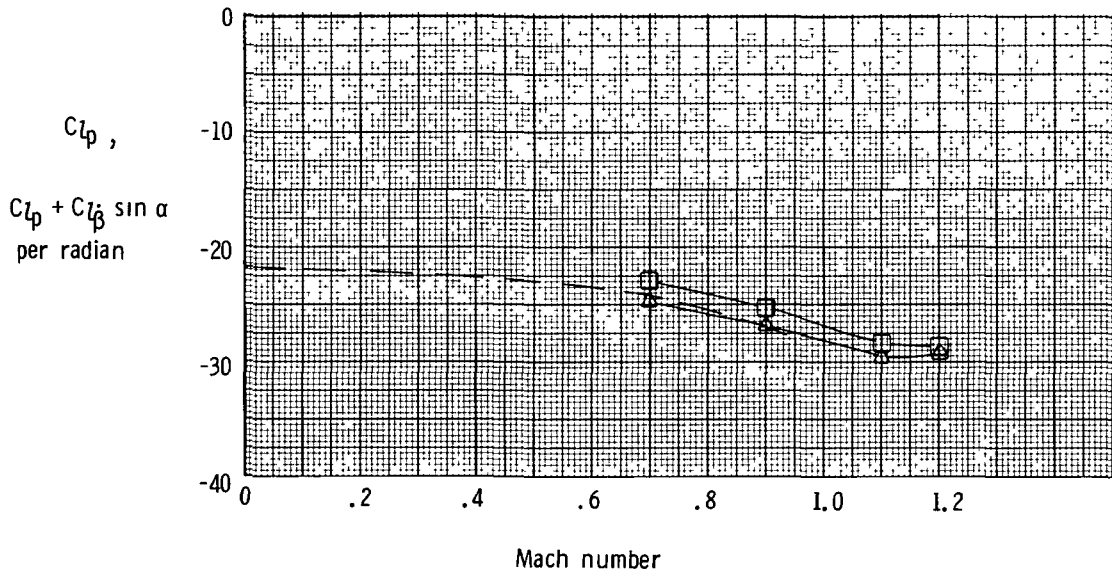| Configuration	Vortex lattice C_{N_q} C_{N_α}	Static test C_{N_α}	Dynamic test $C_{N_q} + C_{N_{\dot\alpha}}$ $C_{N_\alpha} - k^2 C_{N_{\dot q}}$
$\phi = 0°$	– – – – –	○	▢
$\phi = 45°$	—— – ——	◇	△

(b) Normal force due to pitch rate and normal force
due to pitch displacement.

Figure 20.- Continued.

Configuration	Vortex lattice C_{l_p}	Dynamic test $C_{l_p} + C_{l_{\dot{\beta}}} \sin \alpha$
$\phi = 0°$	-----	□
$\phi = 45°$	-----	△

(c) Damping in roll.

Figure 20.- Concluded.

1 Report No NASA TM-74058	2 Government Accession No	3 Recipient's Catalog No
4 Title and Subtitle TRANSONIC STATIC AND DYNAMIC STABILITY CHARACTERISTICS OF A FINNED PROJECTILE CONFIGURATION		5 Report Date April 1978
		6 Performing Organization Code
7 Author(s) Richmond P. Boyden, Cuyler W. Brooks, Jr., and Edwin E. Davenport		8 Performing Organization Report No L-11966
9 Performing Organization Name and Address NASA Langley Research Center Hampton, VA 23665		10 Work Unit No 505-11-23-13
		11 Contract or Grant No
12 Sponsoring Agency Name and Address National Aeronautics and Space Administration Washington, DC 20546		13 Type of Report and Period Covered Technical Memorandum
		14 Sponsoring Agency Code

15 Supplementary Notes

16 Abstract

Static and dynamic stability tests were made of a finned projectile configuration with the aft-mounted fins arranged in a cruciform pattern. The tests were made at free-stream Mach numbers of 0.7, 0.9, 1.1, and 1.2 in the Langley 8-foot transonic pressure tunnel. Some of the parameters measured during the tests were lift, drag, pitching moment, pitch damping, and roll damping. Configurations tested included the body with undeflected fins, the body with various fin deflections for control, and the body with fins removed. Theoretical estimates of the stability derivatives were made for the fins-on configuration.

17 Key Words (Suggested by Author(s)) Projectile Static stability Dynamic stability	18 Distribution Statement Unclassified - Unlimited Subject Category 02

19 Security Classif (of this report) Unclassified	20 Security Classif (of this page) Unclassified	21 No of Pages 81	22 Price* $6.00

11/28/91, Kevin Bruns - 106 9609

THIRD-CLASS BULK RATE

U.S.MAIL

```
     3     2 1U,A,        032178 S90844BU
MCDONNELL DOUGLAS CORP
ATTN: PUBLICATIONS GROUP PR 15246-A
P O BOX 516
ST LOUIS MO 63166
```

POSTMASTER

NASA